ALK1 ligand requirements for prevention of arteriovenous malformations

by

Teresa Lynn Rosato

Bachelor's of Science, University of Pittsburgh, 2014

Submitted to the Graduate Faculty of the

Graduate School of Public Health in partial fulfillment

of the requirements for the degree of

Doctor of Philosophy

University of Pittsburgh

2022

UNIVERSITY OF PITTSBURGH

GRADUATE SCHOOL OF PUBLIC HEALTH

This dissertation was presented

by

Teresa Lynn Rosato

It was defended on

January 26, 2022

and approved by

Zsolt Urban, Associate Professor, Department of Human Genetics, Graduate School of Public Health, University of Pittsburgh

Jeffrey Gross, Professor, Department of Ophthalmology, School of Medicine, University of Pittsburgh

Andrew Hinck, Professor, Department of Structural Biology, School of Medicine, University of Pittsburgh

Dissertation Advisor: Beth Roman, Associate Professor, Human Genetics, Graduate School of Public Health, University of Pittsburgh

ALK1 ligand requirements for prevention of arteriovenous malformations

Teresa Lynn Rosato, PhD

University of Pittsburgh, 2022

Arteriovenous malformations (AVMs) are direct connections between arteries and veins that may cause bleeding, anemia, hypoxemia, stroke, and heart failure. To understand how AVMs develop, we study the autosomal dominant disease, hereditary hemorrhagic telangiectasia (HHT). HHT-associated AVMs are caused by defective bone morphogenetic protein (BMP) signaling through the endothelial cell receptor, ALK1. BMP ligands are generated as proproteins that require furin processing to release the N-terminal prodomain from the C-terminal growth factor (GF) domain. Although BMP9 and BMP10 GF domain homodimers and heterodimers similarly activate ALK1 in vitro, the genetic requirements for *BMP9* and *BMP10* with respect to AVM prevention are unclear, and the precise molecular nature of circulating ALK1 ligands is not known.

Using zebrafish genetic models, I identified Bmp10 as the only Alk1 ligand required for vascular homeostasis and AVM prevention throughout life: with age, zebrafish *bmp10* mutants develop skin and liver vascular malformations and heart failure, similar to HHT patients. Moreover, I found that the predominant form of BMP10 in human plasma is unprocessed, full-length proBMP10, and that the physiologically relevant form of circulating proBMP10 may be a monomer or heterodimer with BMP9 GF.

Because BMP9 and BMP10 are liver-derived circulating proteins, we reasoned that these ligands may compose the "hepatic factor," found in high concentrations in hepatic venous effluent, that is required to prevent development of lung AVMs after the Glenn procedure. This palliative surgery performed in single-ventricle patients excludes inferior vena cava flow from pulmonary

circulation. Although my results fail to support BMP9 and BMP10 as "hepatic factor," per se, they suggest that decreased ALK1 signaling may play some role in lung AVM development in this population.

Improving quality of life for HHT and Glenn patients is an unmet public health need. Despite our understanding of the signaling pathway affected, there are no pharmacological therapies that restore ALK1 signaling flux in these patients. In HHT, therapeutic strategies currently focus on general inhibition of angiogenesis or administration of recombinant GF dimers. My work suggests that development of targeted therapeutics for HHT should focus on proBMP10.

Table of Contents

List of Tables

List of Figures

Preface

To begin, I would like to thank Dr. Beth Roman, who has been an exceptional mentor during my time in the lab. First as a technician, then as a graduate student, her support has been outstanding; she has shown me how to be a systematic and thorough scientist, taught me how to ask important scientific questions, and has demonstrated resilience in the face of obstacles. She has always believed in my abilities, even when I was in doubt, and has always encouraged me to push my skills and try new things. I know that, wherever I go in my career, she has prepared me for success. Her contributions to vascular biology and the underlying mechanisms of HHT are outstanding and I am eager to see where her research goes next.

I would also like to thank my committee, Dr. Zsolt Urban, Dr. Andy Hinck, and Dr. Jeff Gross, who have guided me through my graduate career. Their feedback on my projects has been instrumental for my success.

I would like to sincerely thank all of our collaborators who made this work possible, especially the Hinck lab members for their hard work generating recombinant proteins: Andy Hinck, PhD, Cindy Hinck, PhD, and Tristin Schwartze; Flordeliza Villanueva, MD and the Kim lab for their ultrasound expertise: Kang Kim, PhD, Harry Volek, and Waqas Khalid, PhD; and Sarah Trucco, MD and Morgan Hindes for their collection and preparation of the pediatric plasma samples.

Many thanks to everyone in the Roman lab that I had the pleasure to work with over the past years. You all have made this journey a wonderful experience. A special thanks to Liz Rochon, PhD, my good friend who inspired me to pursue a career in science. To Bijun Li, MS, for all of

her hard work with the *bmp10* fish. And to Selvi Anbalagan MS, Stef Morosky, and Jack Fiore, for their excellent contributions to these projects.

And lastly, I would like to thank my family, especially my parents and my husband, Bryan, who have supported me every step of the way, I could not have done it without you. And to my son, Leonardo, for being my writing buddy and filling my life with so much joy.

Abbreviations

ACVRLI	activin a receptor like type 1
AVM	arteriovenous malformation
BA	basilar artery
BAVM	brain arteriovenous malformation
BCA	basal communicating artery
BMP	bone morphogenetic protein
CV	cardinal vein
DA	dorsal aorta
ECM	extracellular matrix
ELISA	enzyme linked immunosorbent assay
GF	growth factor
GFD	growth factor dimer
HAVM	hepatic arteriovenous malformation
HHT	hereditary hemorrhagic telangiectasia
HOHF	high-output heart failure
nAb	neutralizing antibody
PAVM	pulmonary arteriovenous malformation
PD	prodomain
PHBC	primordial hindbrain channel
PMBC	primordial midbrain channel

SMAD	small mothers against decapentaplegic
SMC	smooth muscle cell
TGF-β	transforming growth factor beta

1.0 Introduction

1.1 Vascular development

The vascular system is a branched network of endothelial-lined tubes that function to transport oxygen and nutrients to all tissues in the body, and organized vascular development is critical during embryogenesis [1]. Blood vessels first emerge by vasculogenesis, during which endothelial cell progenitors differentiate from the mesoderm and form a primitive vascular network that includes honeycomb-like plexuses and largely unbranched tubes. Once the heart starts beating and blood flow begins, the primitive network remodels into a hierarchical structure of arteries, branched capillaries, and veins that is supported by mural cells, including pericytes and smooth muscle cells [2, 3]. To accommodate embryonic growth, the vascular network must continuously expand via sprouting angiogenesis, in which new vessels arise from pre-existing vessels. In response to environmental cues such as hypoxia or chemokine signals, endothelial cells remodel cell-cell junctions and degrade the extracellular matrix (ECM), mural cells detach, and a leading endothelial "tip cell" migrates away from the parent vessel, while the trailing "stalk cells" proliferate to lengthen the new blood vessel [2]. Once distal connections with existing vessels are made, the resolution phase begins, during which junctions, matrix, and mural cell interactions are restored.

1.1.1 Arteries, veins, and capillaries

The architecture of the blood vessels varies with the distance of the vessel from the heart [4]. Arteries, the blood vessels closest to the heart, carry oxygenated blood away from the heart and feed into smaller diameter arterioles, then into even smaller capillaries that allow for gas and nutrient exchange with surrounding tissues [4]. Venules then carry blood away from the capillaries, which feed into large veins and transport de-oxygenated blood back to the heart [4].

Arteries, arterioles, venules and veins consist of three layers—the tunica intima, tunica media, and the tunica adventitia—though the thickness and composition varies among the blood vessels [5]. The tunica intima is the inner-most layer that faces the vessel lumen and is a continuous monolayer of endothelial cells. The endothelial cell apical surface faces the lumen, and the basal surface sits on an endothelial-derived basal lamina [5]. The middle layer, the tunica media, is made up of smooth muscle cells (SMCs) that function to control the diameter of the blood vessel [6]. Arteries must withstand high velocity pulsatile blood flow and therefore have a thicker medial layer compared to other vessels [4, 5]. The medial layer of arteries also functions to dampen pulsatility to allow continuous laminar flow in the rest of the vasculature. The outermost layer, the tunica adventitia, consists mainly of ECM deposited by fibroblasts and functions to stabilize the blood vessels and allow attachment to surrounding tissues [5].

Capillaries differ from other vessels in three important ways. First, their tunica intima may be continuous, fenestrated, or discontinuous [4]. The fenestrated and discontinuous capillaries contain small openings in or gaps between the endothelium that allow for the enhanced exchange of oxygen, carbon dioxide, and nutrients [4]. Second, the medial layer consists of pericytes and not smooth muscle cells. Pericytes are important for endothelial cell support, maintenance of the blood-brain barrier, control of vessel diameter, and communication with surrounding tissue.

Moreover, the thin, discontinuous nature of this layer is also critical for efficient gas and nutrient exchange [5]. And third, capillaries form a highly branched network that slows blood flow and increases efficiency of exchange.

1.1.2 Arteriovenous malformations

An arteriovenous malformation (AVM) is a direct connection between an artery and a vein that likely develops via enlargement of a pre-existing capillary segment. These shunts allow blood to flow at high velocity from arteries into veins. In an effort to resist high-magnitude hemodynamic forces, shunts may muscularize and thereby eliminate gas exchange. Alternatively, shunts may rupture.

AVMs can lead to various clinical outcomes depending on their size and location. Telangiectasias are small AVMs that form in the skin and mucous membranes; they are prone to rupture, leading to epistaxis (recurrent nosebleeds), GI bleeding, and anemia [7]. Brain AVMs (BAVMs) may also rupture, leading to hemorrhagic stroke [8]. Pulmonary AVMs (PAVMs) rarely rupture. Instead, shunting through these lesions impairs gas exchange and filtration, leading to dyspnea, embolic stroke, or brain abscess [9]. Hepatic AVMs (HAVMs) may dramatically decrease systemic vascular resistance, leading to volume overload and high-output heart failure (HOHF) [7, 10].

1.2 Hereditary hemorrhagic telangiectasia

Hereditary hemorrhagic telangiectasia (HHT) is an autosomal dominant vascular disorder that presents with variable age of onset and expressivity. The disease phenotype is characterized by development of AVMs and is associated with decreased quality of life and may be associated with decreased life expectancy [11-13]. In HHT patients, telangiectasias, PAVMs, HAVMs, and BAVMs have been observed. While cautery, resection, or embolization can be effective treatments for telangiectasias or PAVMs, the primary treatment option for HHT patients with severe liver involvement and HOHF is liver transplantation [14]. Intravenous administration of antiangiogenic agents has shown some therapeutic value in HHT patients [15-17], but these therapies globally depress angiogenesis. As such, there is an unmet need for therapeutics that directly target the molecular defect that underlies HHT-associated AVMs.

1.2.1 Genetics of HHT

Mutations in genes encoding proteins in the ALK1 signaling pathway lead to HHT [18]. *ENG* (endoglin) mutations lead to HHT1, *ACVRL1* (activin A receptor like type 1, encoding ALK1) mutations lead to HHT2, and *SMAD4* (small mothers against decapentaplegic 4) mutations lead to a combined syndrome of HHT and juvenile polyposis (HHT-JP) [19-21]. Historically, HHT has been considered a disease of haploinsufficiency, though recent evidence suggests the presence of somatic second hits in telangiectasias [22]. Mutations in *ENG* and *ACVRL1* together account for approximately 90% of HHT, with *SMAD4* mutations accounting for less than 5% of disease [23]. Additionally, mutations in *GDF2 (*also known as *BMP9)* have been identified in patients with an HHT-like phenotype [24, 25].

Though *ENG* and *ACVRL1* encode proteins that are believed to act in the same signaling pathway, genotype-phenotype correlations have been observed in HHT [26-28]. While both *ENG* and *ACVRL1* patients develop telangiectasias at similar frequencies, *ENG* patients develop epistaxis with earlier age of onset [26]. PAVMs are more frequently observed in *ENG* patients and PAVMs tend to be larger and more symptomatic than those observed in *ACVRL1* patients [26-28]. Similarly, BAVMs are more frequently associated with *ENG* patients and rarely observed in *ACVRL1* patients. By contrast, HAVMs are more often found in *ACVRL1* patients than *ENG* patients [26-28]. The mechanistic basis of these genotype/phenotype correlations is unknown.

1.2.2 ALK1 Signaling

ALK1 is an endothelial cell-specific transforming growth factor (TGF)-β type I transmembrane receptor serine/threonine kinase [29]. Signaling occurs when circulating bone morphogenetic protein (BMP) ligands BMP9, BMP10, or BMP9/10, bind to the lumen-facing extracellular domains of a heterotetrameric complex of two ALK1 receptors and two TGF-β type II receptors—BMPRII, ActRIIA, or ActRIIB—which are also transmembrane receptor serine/threonine kinases (Figure 1) [30, 31]. Binding of ligand to the type I and II receptors brings the type II receptors into close proximity with ALK1, allowing the type II receptor to phosphorylate the intracellular GS (Glycine-Serine rich) domain of ALK1 [32]. ALK1 then phosphorylates an intracellular receptor-specific (r)SMAD: SMAD1, SMAD5, or SMAD9 (previously called SMAD8), collectively referred to SMAD1/5/9. rSMAD dimers recruit the co-SMAD, SMAD4. This trimeric SMAD complex translocates to the nucleus and binds to DNA to regulate gene expression.

The role of endoglin in ALK1 signaling is not fully understood. ENG is a non-signaling TGF-β type III receptor that, like ALK1, is strongly expressed in endothelial cells and binds to BMP9 and BMP10 with very high affinity [33, 34]. The BMP9/ENG binding interface overlaps with the BMP9/type II receptor binding interface, but not the BMP9/ALK1 binding interface [18, 35]. Therefore, it has been suggested that ENG may help to capture circulating ligand and present it to ALK1 before being displaced by the type II receptor in the active signaling complex. While ENG can enhance ligand-mediated ALK1 signaling, it is not required for ALK1 activity [36].

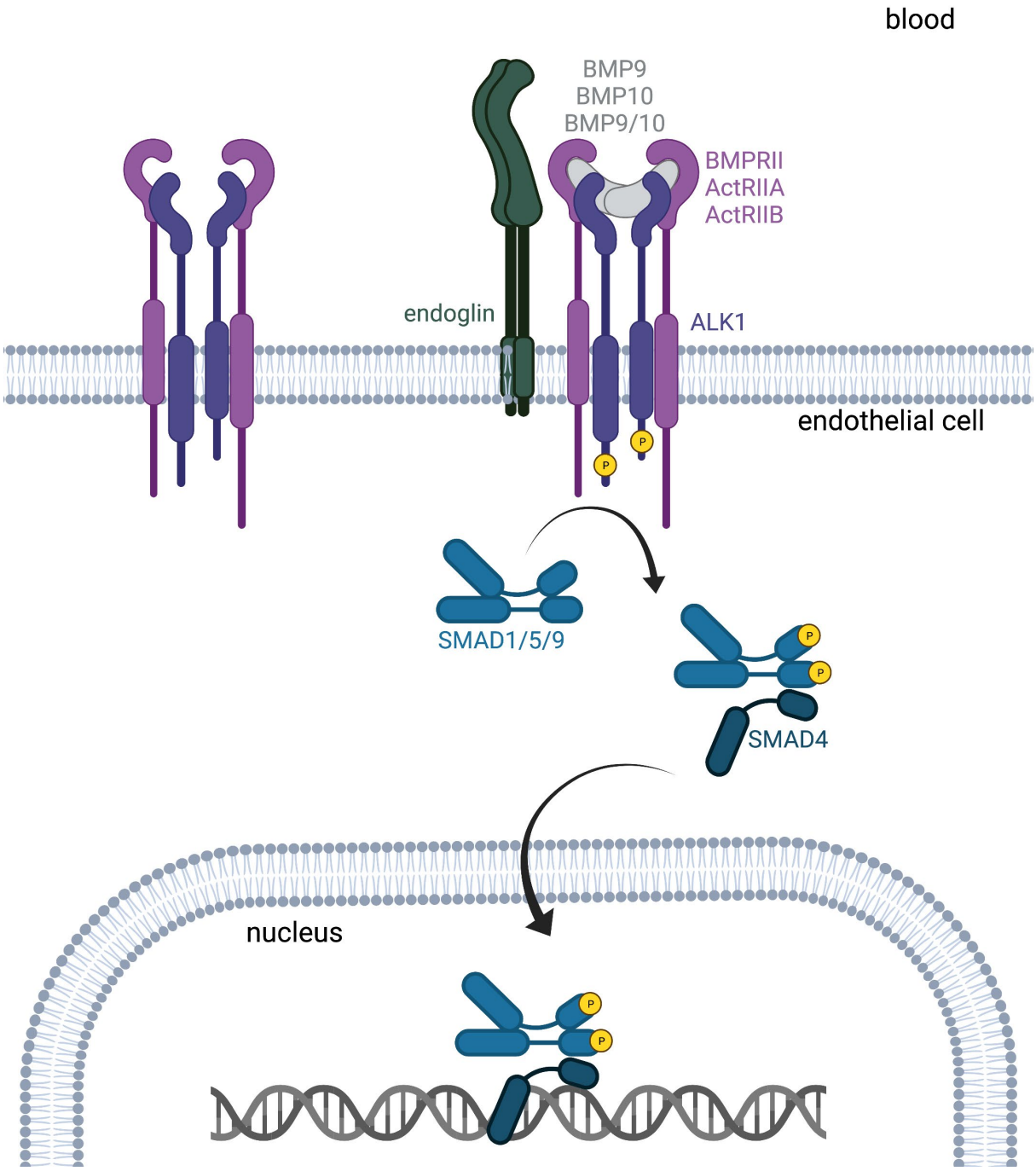

Figure 1 ALK1 Signaling

Circulating ligands BMP9, BMP10, or BMP9/10 bind to ALK1 and a type II receptor with the assistance of endoglin. This leads to the phosphorylation of ALK1, which then phosphorylates SMAD1/5/9 that then recruits SMAD4. This SMAD complex then translocates to the nucleus to regulate gene expression. Created with BioRender.com

1.2.2.1 TGF-β family ligands

In canonical TGF-β ligand synthesis, two proprotein monomers, each containing an N-terminal prodomain (PD) and a C-terminal growth factor (GF) domain, dimerize in the rough endoplasmic reticulum via single unpaired cysteines in their GF domains. Dimers are then cleaved between the PD and the GF domain by furin-like proprotein convertases that reside in the Golgi apparatus. After cleavage, the PDs remain non-covalently associated with the GF domain dimer (GFD). The structure of the 2:1 PD:GFD complex ranges from "open-armed" (PDs extending away from each other) to cross-armed (PDs extended toward each other). The open-armed structure is associated with low PD:GFD affinity and no latency, whereas the cross-armed structure is associated with higher PD:GFD affinity and latency [37, 38]. That is, the PD of non-latent complexes will readily dissociate upon GFD binding to the receptor, whereas the PD of latent complexes requires active removal from the GFD before binding to the BMP receptors.

While cleavage between the PD and GF domain is required for activation of all TGF-β family ligands, some ligands are secreted in an unprocessed form (Figure 2). For example, glial cell line-derived neurotrophic factor (GDNF), growth and differentiation factor 15 (GDF15), and Nodal may be secreted unprocessed and cleaved extracellularly by plasma membrane-associated or soluble furin-like proprotein convertases [39]. Additionally, some BMP family proteins undergo multiple and/or alternative prodomain cleavages by proprotein convertases or metalloproteinases [39]. For example, BMP4 and *Drosophila* Dpp, Gbb, and Scw have additional proprotein convertase cleavage sites in the PD that may control tissue-specific activation or signaling range, and GDF8/myostatin and GDF11 PDs may be cleaved by BMP1/Tolloid to allow release of mature GFD [39].

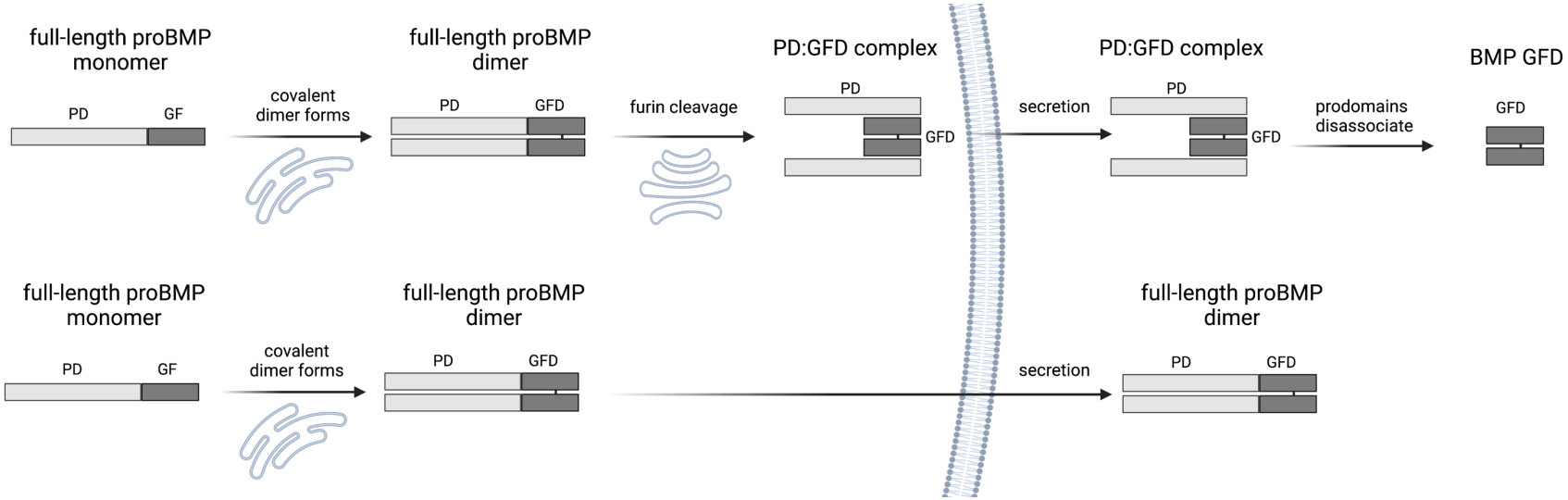

Figure 2 BMP processing and secretion

TOP: canonical BMP processing and secretion. Full-length proBMP monomers are dimerized in the endoplasmic reticulum, cleaved by proprotein convertases such as furin in the golgi, then secreted as 2:1 PD:GFD complexes. **Bottom:** alternative BMP processing and secretion. Full-length proBMP monomers are dimerized in the endoplasmic reticulum and secreted as full-length proBMP dimer.

1.2.2.2 Circulating ALK1 ligands: BMP9 and BMP10

BMP9 and BMP10 are high-affinity ligands for ALK1 and ENG that similarly induce expression of downstream target genes [30, 34, 40-43]. *BMP9* and *BMP10* are both transcribed in hepatic stellate cells [31]; however, *BMP10* expression predominates in cardiomyocytes, with postnatal expression restricted to the right atrium. While these growth factors may have some local activity, presumed homodimers as well as BMP9/10 heterodimers have been detected in blood in mice and humans [31]. Although the furin-processed BMP10 PD:GFD complex was initially described as latent [44], more recent studies show that both BMP9 and BMP10 PD:GFD complexes bind ALK1 with similar high affinity when compared to each other and to free GFDs, and that cognate PDs fail to confer latency in bioactivity assays [45-47].

Despite the numerous similarities between BMP9 and BMP10, whether these ligands are fully redundant with respect to endothelial cell ALK1 signaling remains controversial. Moreover, the circulating forms of BMP9 and BMP10 homodimers and heterodimers have not been fully described. As such, it is unclear whether these ligands are furin-processed intracellularly or post-secretion and whether additional PD cleavage sites are required for GFD release and receptor activation.

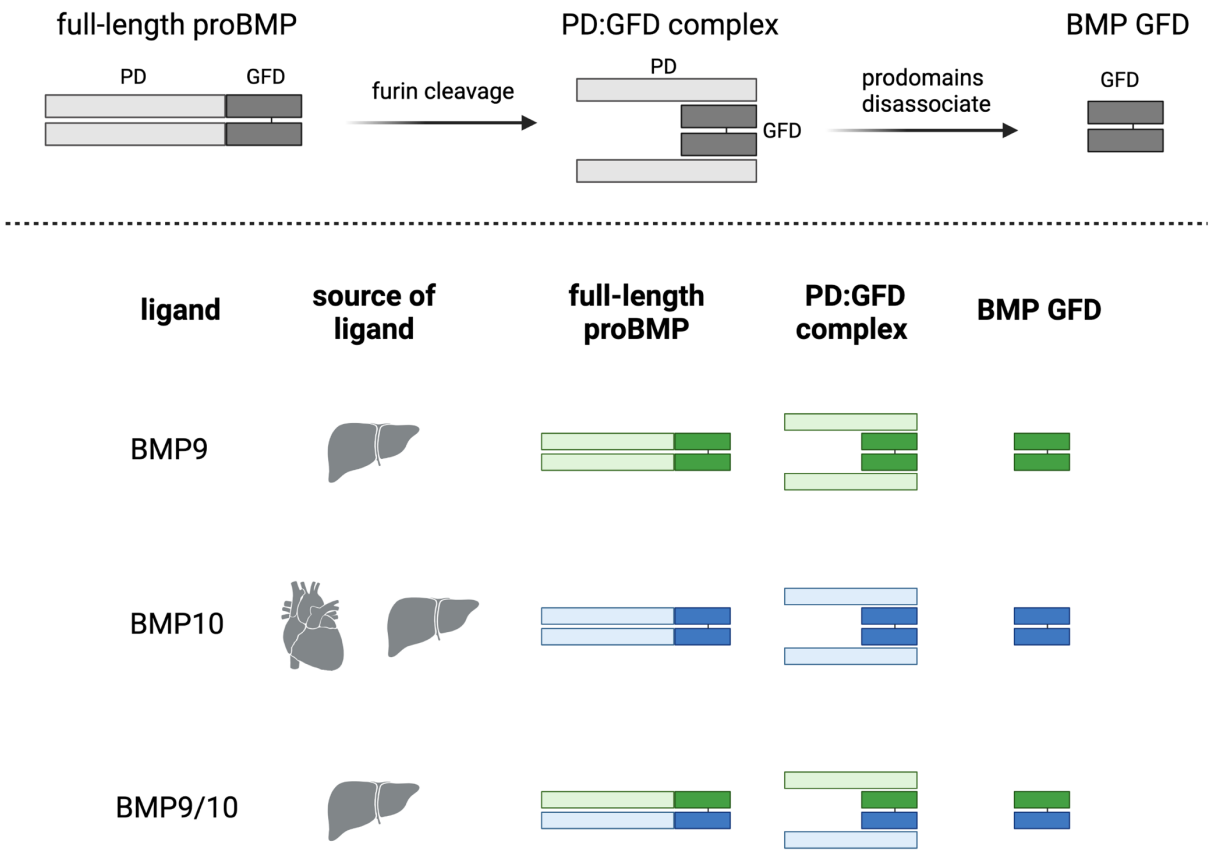

Figure 3 Processing and secretion of BMP9, BMP10, and BMP9/10

Full-length proBMP dimers are cleaved by furin between the PD and GF domain to form furin processed BMP PD:GFD complexes where the PDs non-covalently associate with the GFD. Signaling occurs when the PDs disassociate from the GFD. BMP9 is synthesized in the liver, BMP10 is synthesized in the heart and liver. Created with BioRender.com

1.2.3 Animal Models of HHT

Mouse and zebrafish models have been useful in elucidating the mechanism by which loss of ALK1 signaling leads to the development of AVMs (Table 1).

1.2.3.1 *ACVRL1* models

In mice and zebrafish, homozygous loss of *Acvrl1* leads to the development of an embryonic lethal AVM. In mice, an AVM develops between the aorta (DA) and the cardinal vein (CV) at E9.0 [48], while in zebrafish an AVM develops between the basal communicating artery (BCA) and the primordial midbrain channel (PMBC) or the basilar artery (BA) and the primordial hindbrain channel (PHBC) beginning at ~34 hours post-fertilization (hpf) [49]. In mice, endothelial cell-specific deletion of *Acvrl1* during embryogenesis phenocopies global nulls, whereas postnatal endothelial cell-specific deletion also results in AVMs and rapid lethality [50, 51]. Surprisingly, despite the fact that *Acvrl1* expression predominates in arterial endothelial cells, deletion using capillary or venous but not arterial Cre-drivers phenocopies pan-endothelial deletion [52]. Vascular phenotypes in adult heterozygous mice have been reported, but only on a background, 129/Ola, which is predisposed to vascular abnormalities [53]. Together, these data support a conserved role for ALK1 in endothelial cells in fish, mice, and humans. Moreover, they suggest that heterozygosity is insufficient for lesion development and support the idea that lesion development requires a second somatic hit or environmental insult.

1.2.3.2 ENG models

In mice, homozygous loss of *Eng* leads to abnormal yolk sac vasculature, enlarged skin vessels, and cardiac defects, which are embryonic lethal by day E10.5 [54, 55]. In zebrafish, however, homozygous loss of *eng* is not embryonic lethal though the DA and PCV are enlarged

by 72 hpf, and adult *eng* mutants develop enlarged vessels in the brain and AVMs in a fin amputation model [56] . In postnatal mice, pan-endothelial or venous-capillary deletion of *Eng* leads to AVMs in the retinal vasculature [57, 58], suggesting arterial *Eng* is not sufficient to prevent AVMs. And, global deletion in adults leads to AVMs in a wound model and is lethal by 4 to 10 days post-deletion [59]. Heterozygous loss of *Eng* leads to skin telangiectasias/AVMs and nosebleeds in adult mice, but only in 129/Ola, as observed with *Acvrl1* heterozygotes [54, 60]. As with *Acvrl1*, knockout studies suggest a conserved role for *ENG* in mice, zebrafish, and humans, and that a second somatic hit may be required for the development of AVMs in HHT patients.

1.2.3.3 BMP9 and BMP10 models

To determine whether BMP9 and BMP10 are redundant ALK1 ligands, several studies have investigated whether loss of each ligand phenocopies loss of *Acvrl1*. In mice, homozygous loss of *Bmp9* does not phenocopy the loss of *Acvrl1* [61], but instead leads to modest lymphatic valve defects [62] and impaired closure of the ductus arteriosus with no effect on viability [63] . Similarly, in zebrafish, morpholino knockdown of *bmp9* does not phenocopy loss of *acvrl1,* but leads to mild tail vasculature defects [24, 64]. By contrast, embryonic loss of *Bmp10* phenocopies the loss of *Acvrl1*. In *Bmp10* null mice, an AVM develops between the DA and the CV [65] and hearts fail to trabeculate at E9.5 [66], leading to lethality by E10.5. Similarly, in zebrafish, morpholino knockdown of *BMP10* paralogs, *bmp10* and *bmp10-like*, phenocopies the loss of *acvrl1* and an AVM forms between the BCA and PMBC or BA and PHBC [64].

In mice, the post-embryonic requirements for BMP9 and BMP10 have been assessed by neutralizing antibody (nAb) injection. Intravenous injection of BMP9 nAb leads to increased density of the retinal vasculature, though BMP10 nAb has no effect [61], while the transmammary

delivery of BMP9 and BMP10 nAbs together leads to retinal AVMs [67]. And BMP10 nAb injected into *Bmp9* knockouts lead to abnormal retinal vasculature [61, 65] and impaired closure of the ductus arteriosus [63]. Post-embryonic requirements of *bmp9, bmp10,* and *bmp10-like* in zebrafish have yet to be assessed. These data suggest that BMP10 is a required ALK1 ligand embryonically, though thorough characterization of ligands in adulthood is necessary to develop ligand based therapeutics.

Table 1 Animal Models of HHT

mouse		
model	**phenotype**	**reference**
Acvrl1$^{+/-}$	AVMs and abnormal vessels (129/Ola)	[53]
Acvrl1$^{-/-}$	AVM between DA and CV: embryonic lethal	[48]
Eng$^{+/-}$	telangiectasias and nosebleeds (129/Ola) AVMs and abnormal vessels in skin	[54] [60]
Eng$^{-/-}$	enlarged skin vessels cardiac defects abnormal yolk sac vasculature embryonic lethal	[55] [54, 55] [54, 55]
Bmp9$^{-/-}$	lymphatic valve defects mild ductus arteriosus closure defects	[62] [63]
Bmp9$^{-/-}$ + BMP10 nAb	impaired angiogenesis in retinal vasculature improper closure of ductus arteriosus	[61, 65] [63]
BMP9 nAb	increased retinal vascular density	[61]
Bmp10$^{-/-}$	improper cardiac trabeculation; embryonic lethal AVM between DA and CV; embryonic lethal	[66] [65]
BMP10 nAb	no effect	[61]
BMP9 nAb + BMP10 nAb (transmammary)	increased retinal vascular density retinal AVMs	[67]
zebrafish		
model	**phenotype**	**reference**
acvrl1$^{-/-}$	AVM between BCA and PMBC or BA and PHBC; embryonic lethal	[49, 68]
eng$^{-/-}$	enlarged DA and PCV embryonically enlarged vessels in brain in adult vascular malformations in amputated fin in adult	[56]
bmp9 MO	no embryonic phenotype	[64]
bmp10 MO	no embryonic phenotype	[64]
bmp10-like MO	no embryonic phenotype	[64]
bmp10 MO *;bmp10-like* MO	AVM between BCA and PMBC or BA and PHBC; embryonic lethal	[64]

CV = cardinal vein, BCA = basal communicating artery, DA = dorsal aorta, PCV = posterior cardinal vein, PHBC = primordial hindbrain channel PMBC = primordial midbrain channel. MO = morpholino

1.3 Hepatic dysfunction and PAVMs

Although 70-80% of PAVMs are associated with HHT, PAVMs are also associated with conditions of hepatic dysfunction. In hepatopulmonary syndrome (HPS), liver dysfunction is associated with hypoxemia secondary to PAVMs, and PAVMs are reversed by liver transplantation [69]. Additionally, portosystemic shunts that allow gut venous effluent to bypass the liver lead to PAVMs, which resolve when the shunt is closed [70]. Further evidence comes from single-ventricle patients who undergo a three-staged surgery to relieve hemodynamic burden on the heart and correct oxygen desaturation. The second-stage surgery, the bidirectional Glenn, directs passively draining venous return from the superior vena cava (SVC) to the pulmonary circulation, with venous return from the inferior vena cava (IVC) pumped to the systemic circulation. Although the Glenn effectively decreases ventricular hemodynamic stress, intrapulmonary arteriovenous shunting is pervasive, and up to 25% develop clinically significant hypoxemia secondary to diffuse PAVMs [71, 72]. While early theories of PAVM development focused on the absence of pulsatile flow or increased lower lobe perfusion [71], later evidence implicated the exclusion of a liver-derived substance from the pulmonary vasculature. This "hepatic factor" was postulated based on correlation between the laterality of PAVMs and the laterality of exclusion of hepatic venous effluent [73], and its existence is strongly supported by evidence that the third-stage Fontan procedure (completion of the total cavopulmonary anastomosis), which reroutes IVC flow to the lungs without restoring pulsatility, is strongly associated with PAVM regression [74]. Despite the strong evidence for hepatic factor, its identity remains unknown. Based on the close association with HHT and PAVMs, and the fact that *BMP9* and *BMP10* are transcribed in the liver, these ALK1 ligands may be the hepatic factor responsible for preventing PAVMs.

2.0 Summary and Dissertation Aims

Current therapeutic options for AVM treatment in HHT patients are limited to interventional approaches such as cautery, resection, or embolization or pharmacological approaches that enhance clotting or inhibit angiogenesis. These approaches do not target disease mechanism and have unwanted side effects. As such, there is a critical unmet need to develop pharmaceuticals that enhance ALK1 signaling to overcome deficiencies and prevent AVMs in HHT.

Ligands that activate ALK1 signaling may be useful as biopharmaceuticals in the treatment of HHT. This approach is being pursued for the related disease, pulmonary arterial hypertension, with promising preclinical results [75]. However, while biochemical and biophysical assays identify BMP9, BMP10, and BMP9/10 growth factor dimers as potent, high-affinity ALK1 ligands, genetic requirements for *BMP9* and *BMP10* are unclear. Moreover, the physiologically relevant molecular forms of these ligands – whether processed growth factors or unprocessed, full length proproteins, or whether monomers, homodimers, or heterodimers — remain unknown. The overarching goal of my dissertation research has been to fill these gaps in knowledge, with the long-term goal of applying my findings to development of HHT therapeutics.

To this end, I used zebrafish mutants to assess genetic requirements for *bmp9* and *bmp10* in vascular homeostasis and AVM prevention. Surprisingly, I found no requirement for *bmp9.* By contrast, I found that *BMP10* paralogs, *bmp10* and *bmp10-like*, encode redundant Alk1 ligands during embryogenesis, but that *bmp10* is the only required gene after the embryonic period. Zebrafish *bmp10* mutants develop skin and liver vascular lesions in juvenile to adult stages and high-output heart failure with variable age of onset and expressivity, similar to HHT patients.

bmp10 is expressed in the liver stellate cells and endocardium, whereas *bmp10-like* is expressed in cardiomyocytes. Taken together, these data suggest that the former cell types generate circulating Bmp10, which is required to act on endothelial Alk1.

Next, I applied ELISAs to define ALK1 ligands in human plasma. Results strongly suggested that BMP10 circulates predominantly, if not exclusively, in an unprocessed, full-length form, with the PD remaining covalently attached to the GF domain via a peptide bond. Whether this ligand exists in plasma primarily as a proBMP10 homodimer or a proBMP10 monomer could not be discerned. However, recombinant proBMP10 homodimer fails to activate ALK1 signaling when applied to cultured human endothelial cells, whereas injection of mRNA encoding human BMP10 into zebrafish embryos results in production of fully monomeric proBMP10 that robustly induces pSMAD1/5/9. Together with the genetic requirement for *bmp10*, these data suggest that the proBMP10 monomer may be an important circulating ALK1 ligand.

Finally, I tested the hypothesis that liver-derived ALK1 ligands may be the "hepatic factor' required to prevent development of PAVMs in single ventricle patients who undergo the Glenn procedure. I measured ALK1 ligand concentrations in plasma from five different vascular sites, anticipating highest concentrations in hepatic venous effluent. Although ALK1 ligand concentrations were unchanged across all sites, they were significantly lower in Glenn cases compared to controls. These data fail to support the hypothesis that BMP9/BMP10 are hepatic factor, but suggest that decreased ALK1 signaling may play some role in lung AVM development in this population.

3.0 BMP10-mediated ALK1 signaling is continuously required for vascular development and maintenance

The work presented in this chapter has been published: Capasso, T. L., B. Li, H. J. Volek, W. Khalid, E. R. Rochon, A. Anbalagan, C. Herdman, H. J. Yost, F. S. Villanueva, K. Kim and B. L. Roman (2020). "BMP10-mediated ALK1 signaling is continuously required for vascular development and maintenance." Angiogenesis **23**(2): 203-220. I performed all of the experiments and data analysis except: ultrasound imaging and analysis (Harry Volek, Waqas Khalid, Flordeliza Villanueva and Kang Kim, University of Pittsburgh); fish handling for ultrasound imaging and/or adult heart histology (Bijun Li and Su Diler, University of Pittsburgh); and single cell RNAseq analysis (Chelsea Herdman and Joe Yost, University of Utah).

3.1 Abstract

HHT is an autosomal dominant vascular disorder characterized by development of high-flow AVMs that can lead to stroke or high-output heart failure. HHT2 is caused by heterozygous mutations in *ACVRL1*, which encodes an endothelial cell BMP receptor, ALK1. BMP9 and BMP10 are established ALK1 ligands. However, the unique and overlapping roles of these ligands remain poorly understood. To define the physiologically relevant ALK1 ligand(s) required for vascular development and maintenance, we generated zebrafish harboring mutations in *bmp9* and duplicate *BMP10* paralogs, *bmp10* and *bmp10-like*. *bmp9* mutants survive to adulthood with no overt phenotype. By contrast, combined loss of *bmp10* and *bmp10-like* results in embryonic lethal cranial AVMs indistinguishable from *acvrl1* mutants. However, despite embryonic functional redundancy of *bmp10* and *bmp10-like*, *bmp10* encodes the only required Alk1 ligand in the juvenile-to-adult period. *bmp10* mutants exhibit blood vessel abnormalities in anterior skin and liver, heart dysmorphology, and premature death, and vascular defects correlate with increased cardiac output. Together, our findings support a unique role for Bmp10 as a non-redundant Alk1 ligand required to maintain the post-embryonic vasculature and establish zebrafish *bmp10* mutants as a model for AVM-associated high-output heart failure, which is an increasingly recognized complication of severe liver involvement in HHT2.

3.2 Introduction

BMP9 and BMP10 are high affinity ligands for ALK1 and ENG that similarly induce expression of downstream target genes [30, 34, 40-43]. In mice, *Bmp9* is synthesized in the liver by embryonic day (E) 9.75-10, with expression localized to stellate cells in the adult [31, 65, 76-78]. *Bmp10* predominates in the heart, with expression restricted to ventricular trabecular myocardium at E8.0, atrial myocardium by E16.5, and right atrial myocardium in adults [66, 79]. Both proteins are detected in mouse and human peripheral blood [45, 61, 65, 77, 80], suggesting that they might act redundantly as endocrine ligands for endothelial ALK1. Yet, whereas *Bmp9* null mice have no overt embryonic blood vessel phenotype and live to adulthood [61, 65], *Bmp10* nulls develop embryonic lethal AVMs, phenocopying *Acvrl1* mutants [65]. These observations suggest a unique embryonic requirement for Bmp10 as the critical Alk1 ligand. However, there is a short developmental window (E8.0-E9.75) during which only *Bmp10* and not *Bmp9* is expressed, which could mask functional redundancy. In fact, functional redundancy is supported by observations that embryonic AVMs in *Bmp10* nulls are rescued by inserting *Bmp9* into the *Bmp10* locus [65], and that neonatal retinal AVMs develop upon simultaneous blockade of Bmp9 and Bmp10 [67, 81, 82]. However, post-embryonic ligand requirements outside of the retina have not been explored.

3.3 Materials and Methods

3.3.1 Zebrafish maintenance

All zebrafish (*Danio rerio*) experiments conformed to NIH guidelines and were approved by the University of Pittsburgh Institutional Animal Care and Use Committee. Adults were maintained and bred and embryos reared according to standard protocols [83]. For experiments requiring analysis of adult phenotypes, fish were reared at a density of 40 fish/2.8 L tank from 5 days post-fertilization (dpf) until 5-6 weeks, at which time density was decreased to 20 fish/2.8L tank, or ~7 fish/L. To monitor phenotype progression, phenotypic fish were transferred to a new tank upon onset of phenotype and supplemented with fluorescent age-matched "Starfire Red" fish to maintain density at 7 fish/L.

3.3.2 Zebrafish lines

Mutant lines *acvrl1*^{ft09e} and *acvrl1*^{y6} [68] and transgenic lines *Tg(kdrl:GFP)*^{la116} (endothelial cells) [84]; *Tg(acta2:mCherry)*^{ca8} (smooth muscle cells) [85]; *Tg(flt1:tdTomato)*^{hu5333} (arterial endothelial cells) [86]; *Tg(flt4:Citrine)*^{hu7135} (venous endothelial cells) [87]; *Tg(myl7:actn3b-EGFP)*^{sd10} (α-actinin 3B-EGFP fusion; marks sarcomeric Z-discs) and *Tg(myl7:mKATE-CAAX)*^{sd11} (cardiomyocyte membranes) [88]; *Tg(myl7:EGFP)*^{twu34} (cardiomyocytes) [89]; and *Tg(myl7:DsRed2-NLS)*^{f2} (cardiomyocyte nuclei) [90] have been described. *bmp10-like*^{sa11654} was obtained from the Sanger Institute Zebrafish Mutation Project [91].

Genome editing was used to target *bmp9* (also known as *gdf2;* chromosome 12; ENSDARG00000059173; ENSDART00000082220.5/NM_01171586 (1170 bp); F1QWZ4/NP_001165057 (389 amino acids)), *bmp10* (chromosome 5; ENSDARG00000061769; ENSDART00000088492.5/NM_001130600 (1458 bp); A2BGK2/NP_001124072 (485 amino acids)), and *bmp10-like* (chromosome 10; ENSDARG00000109233, ENSDART00000192123.1 (1221 bp), A0A2R8RLC3 (406 amino acids)). To generate *bmp9/gdf2* (*pt533*, *pt536*) and *bmp10* (*pt527, pt543*) mutants, 250 pg capped, polyadenylated synthetic mRNA (mMessage mMachine T7 Ultra, Thermo Fisher, Waltham, MA USA) synthesized from pairs of TALEN-encoding plasmids was injected into 1-cell stage embryos, following established protocols [92]. Plasmids were designed and generated by Dr. Keith Joung (Harvard, Cambridge, MA USA) and deposited at Addgene (Watertown, MA USA; Table 2). To generate additional *bmp10-like* mutant alleles (*pt544, pt545*), CRISPR single guide RNA was synthesized (MegashortScript, Thermo Fisher) from a synthetic DNA template (Table 2) inserted into plasmid DR274 (Addgene) and injected along with 600 ng *Cas9* mRNA (mMessage mMachine T7 Ultra, Thermo Fisher) generated from plasmid MLM3613 (Addgene). In all cases, P0 founders were identified by outcrossing and genotyping offspring by PCR and restriction digest and/or sequencing. F1 generations were outcrossed to isolate single alleles. All genotypes were confirmed using assays provided in Table 3. Mutation nomenclature is consistent with the recommendations of the Human Genome Variation Society [93].

Table 2 TALENS and gRNAs

Gene	TALEN (Addgene #)	Target sequence (5'-3')
bmp9/gdf2	TAL3010 (36002) TAL3011 (36003)	TTGAACAAGGTGGAGAGTttcttaggctttatgaAGGAAGATTTTTTGAGGA
bmp10	TAL3032 (41206) TAL 3033 (41207)	TCAGCTCCCCGGAGAGGCaccgcactgctccagggTTGGATGATGGACATGGA
Gene	gRNA name	Target sequence
bmp10-like	gRNA bmp10l.3	AGTGGAGGACTGCAGAATAG

Table 3 Genotyping assays

Gene	Allele	Forward primer	Reverse primer	Enzyme	Result
bmp9	pt533	CACTTAAGGAACCC CGATTTC	ACTCACCCTGAAC GACAAAGC	DdeI	WT 80+95+255 bp M 95+327 bp
bmp9	pt536	CACTTAAGGAACCC CGATTTC	ACTCACCCTGAAC GACAAAGC	DdeI	WT 80+95+255 bp M 95+328 bp
bmp10	pt527	CAAAGTAGCCCCAT CAGCTC	CTTCAGGGTCTCC ATCAAGC	NA	WT 138 bp M 130 bp*
bmp10	pt543	CAAAGTAGCCCCAT CAGCTC	CTTCAGGGTCTCC ATCAAGC	BstNI	WT 44+94 bp M 131 bp
bmp10-like	pt544	GAGTTCGGCGCAGC GCTAAAGTGAAG	TGGGGACTCTTCA GATTGAGCAGCG	MboII	WT 208 bp M 155+35 bp
bmp10-like	pt545	CGCAGCGCTAAAGT GGAGGACTGCTGA	TGGGGACTCTTCA GATTGAGCAGCG	DdeI	WT 200 bp M 168+24 bp
bmp10-like	sa11654	CAGAACTGCGCATT CACATGTTTC	GATGCCGACTTTT CTCCAGTCTC	DdeI	WT 197 bp M 176+21 bp

*Separation requires high-resolution gel e.g. 4% Metaphor agarose (Lonza, Walkersville MD USA).

For *bmp9*, TALENs targeting coding nucleotides 122-180 (exon 1) were used and two mutant lines were propagated (Figure 4a). Allele *pt533* harbors a 9-bp deletion/1-bp insertion, generating a frameshift at amino acid 52 and premature termination codon within the prodomain at amino acid 84 (c.155_163delinsC p.Phe52Serfs*33). Allele *pt536* harbors a 7-bp deletion, generating a premature termination codon within the prodomain at amino acid 54 (c.159_165del p.Gly54*). To confirm the predicted effects of these mutations and assess nonsense-mediated decay (NMD), cDNA was synthesized from pooled embryos from heterozygous incrosses, PCR

amplified across the mutation, and the PCR product was cloned and sequenced. Sequencing confirmed the presence of the predicted mutant transcripts in 4/6 (*pt533*) and 5/6 (*pt536*) cDNA clones, providing no evidence of NMD.

For *bmp10*, TALENs targeting coding nucleotides 110-162 (exon 1) were used and two mutant lines were propagated (Fig. 1a). Allele *pt527* harbors an 8-bp deletion, generating a frameshift at amino acid 45 and premature stop codon within the prodomain at amino acid 48 (c.132_139del p.Thr45Argfs*4). Allele *pt543* harbors a 7-bp deletion, generating a frameshift at amino acid 45 and a premature stop codon within the prodomain at amino acid 71 (c.del134_141insT p.Thr45Metfs*27). The presence of the predicted mutant transcripts were confirmed in 6/11 (*pt527*) and 7/14 (*pt543*) cDNA clones as described above, providing no evidence for NMD.

For *bmp10-like*, an ethylnitrosourea-induced mutant allele, *sa11654* [91], was obtained, which harbors a point mutation in exon 2 that generates a premature stop codon within the prodomain at amino acid 180 (c.538C>T p.R180*) (Fig.1a). Additional *bmp10-like* alleles were generated using CRISPR/Cas9 to target coding nucleotides 900-919 within exon 2 (Fig. 1a). Allele *pt544* harbors an 18-bp in-frame deletion within the growth factor domain (c.907_924del p.Asp303-Glu308del) that included cysteine 304, which is required for intramolecular disulfide bonding. Allele *pt545* harbors an 8-bp deletion, generating a frameshift at amino acid 306 and premature stop codon within the growth factor domain at amino acid 311 (c.916_923del p.Ile306Aspfs*6). Sequencing of RT-PCR products generated from heterozygous incrosses confirmed the presence of all predicted mutant transcripts. Because all mutations are in exon 2 of this two-exon gene, NMD was not evaluated.

3.3.3 Histology and Imaging

3.3.3.1 Adult fish and whole heart imaging and measurements

Adult fish and whole hearts were imaged using an MVX-10 MacroView microscope and DP71 camera (Olympus America, Center Valley, PA, USA). Fish length was measured (nose to base of fin) using hand-held calipers. Ventricle cross-sectional area was measured by tracing the maximal ventricle outline from images of ventricles (atrium removed) positioned in 5% methylcellulose with bulbus arteriosus to the right.

3.3.3.2 Histological staining and imaging

5 μm sections of Bouin's fixed (4°C overnight), paraffin embedded hearts were stained with Acid Fuchsin-Orange G (AFOG), Hart's elastin, and Movat's pentachrome stain, using standard protocols. Stained sections were imaged using a BX51 upright compound microscope (Olympus America) and DP71 camera. Heart samples were prepared and stained by Bijun Li and imaged by Su Diler.

3.3.3.3 Confocal imaging, live embryos

To prevent pigmentation, zebrafish embryos were transferred to 30% Danieau (17 mmol/L NaCl, 2 mmol/L KCl, 0.12 mmol/L $MgSO_4$, 1.8 mmol/L $Ca(NO_3)_2$, 1.5 mmol/L HEPES) containing 0.003% phenylthiourea (PTU; Sigma, St. Louis, MO, USA) at ~23 hours post-fertilization (hpf). Just prior to imaging, embryos were anesthetized in 30% Danieau/0.003% PTU containing 0.16 g/L tricaine methanesulfonate (Pentair, Cary, North Carolina, USA) (to arrest movement) or 0.8 g/ L tricaine (to stop heartbeat) and mounted in 1% SeaPlaque low melting temperature agarose (Lonza, Walkersville, MD USA). Z-series were collected (3 μm steps) using

a TCS SP5 or TCS SP8 upright confocal microscope (Leica Microsystems, Wetzlar, Germany) outfitted a multi-line argon laser (488 nm for EGFP; 514 nm for citrine) and 561 nm diode (for dsRed, dsRed2, mCherry, tdTomato; mKATE); an HCX IRAPO L 25x/0.95 water-dipping objective; and spectral detectors. Embryos were scanned at 400 Hz with 3x line averaging or 8000 Hz with 16x line averaging.

3.3.3.4 Confocal imaging, adults

For skin vessel imaging, fish were fixed in 4% paraformaldehyde overnight at 4˚C and skin imaged without dissection, securing the tail in 1% low-melt agarose. For liver vessel imaging, the entire gut and liver were dissected as a single entity and fixed overnight at 4˚C in 4% paraformaldehyde, then the liver was dissected away from the gut. The right liver lobe was mounted in 1% low-melt agarose and the lateral face imaged. For all imaging, Z-series (3 μm steps) were collected as described above using a Leica TCS SP5.

3.3.4 Image Analysis

Using the "measure" tool in Fiji (version: 2.0.0-rc-65/1.51u; build: 961c5f1b7f, National Institutes of Health, Bethesda, MD USA), the basal communicating artery (BCA) diameters was measured on 2D confocal projections at three sites, between and on either side of the paired middle mesencephalic central arteries [94]. Each data point represents an average value from a single embryo. For trabeculation measurements, a single 3-μm optical section was identified at the level of the AV canal, and the "polygon selections" tool and "perimeter measurement" was used in Fiji to trace both the convoluted trabecular surface (T) and the minimal chamber delineated by the tips of the trabeculae (C). From these data, trabeculation was calculated as (T-C)/C, with higher values

indicating more trabeculation. For cardiomyocyte cell counts, Imaris (x64 version 9.1.2, Bitplane, Berlin, Germany) was used to generate 3D projections and the spot tool applied, with manual correction.

3.3.5 RT-PCR

Total RNA was isolated from pooled zebrafish hearts or livers (RNeasy mini kit, Qiagen, Germantown, MD, USA), cDNA was generated (SuperScript IV, ThermoFisher), and PCR was performed with gene-specific primers (Table 4) using Amplitaq Gold (Thermo Fisher). For quantitative RT-PCR, TaqMan assays (Thermo Fisher) were run on a QuantStudio 12k Flex Real Time PCR System (Thermo Fisher). All TaqMan assays were validated using a dilution series of cDNA, according to manufacturer recommendations (amplification efficiency, 1.8-2.2). Zebrafish assays included inventoried *eef1a1l1* (Dr03432748_m1) and *acvrl1* (Dr03144495_m1), and custom assays designed to target exon-exon boundaries in *bmp9/gdf2* (ARKA3UA), *bmp10* (ARMFXD9), *bmp10-like* (ARMFXD7), *nppa* (ARKA3UF), and *nppb* (APRWFMN). Data were analyzed using the $\Delta\Delta C_t$ method and results are presented as expression normalized to *eef1a1l1*.

Table 4 PCR primers

Gene	Forward primer	Reverse primer
bmp9	CGCAGGAACACAGAAAGGTT	GTTGGGTTTTGTTGCCTTGT
bmp10	ATGCCTTCGGCAAACATCATACGC	TTGAAGAGAAGTGGGTGTCGTCTCAC
bmp10-like	GGCAGCTAACATCATCAGGAGCTTC	AGATGTTGAACTGGAGACGCTGC
acvrl1	GGGTCTCGTCTTGTGGGAGA	GTCAGAGGGCACCATGTCAA
actb2	CGTGCTGTCTTCCCATCCA	TCACCAACGTAGCTGTCTTTCTG

3.3.6 *In situ* hybridization

Riboprobes were synthesized from T7-containing, PCR-generated templates using a DIG RNA labeling kit (Sigma-Aldrich, St. Louis, MO USA). Primers for *ltbp3, nkx2.5,* and *tbx20* templates are listed in Table 5. The *cxcr4a* riboprobe has been described [49].

Table 5 Primers used to generate templates for riboprobes

Gene	Forward primer	Reverse primer (with T7 site)
ltbp3	CCTGGGGCCAAAATAAATGCTACA	TAATACGACTCACTATAGGGAGAAATGGG GACTTCCGGAGGCTTGAC
nkx2.5	CATTAACCCTCACTAAAGGGAAGTG CGGGACATACTGAACCT	TAATACGACTCACTATAGGGTGCCTCTTGC ACTTGTATCG
tbx20	AGCCGCTCATCCCGACGACTC	TAATACGACTCACTATAGGGAGAGACGCG GTGTGATCTTTCTTCTTG

3.3.7 Ultrasound imaging and analysis

Zebrafish were anesthetized in 0.12 g/L tricaine for 2 minutes, then placed in a supine position in a groove cut into a sponge saturated with 0.096 g/L tricaine and scanned after waiting for 2 minutes. Ultrasound echocardiography was performed using a high-frequency ultrasound small animal imaging system (Vevo 2100, FujiFilm VisualSonics, Toronto, Canada) outfitted with a high-frequency linear array transducer, MS 700 (bandwidth 30-70 MHz; centered at 50 MHz operating frequency). Images were acquired in two planes: the longitudinal (long) axis view, with the transducer positioned parallel to the long axis of the fish, and the short axis view, with the transducer positioned across the gills and heart orthogonally to the long axis. In each view, B-mode, color Doppler and pulsed-wave Doppler images were acquired. Image acquisition time averaged approximately 5 minutes, after which fish were transferred to fresh water to allow

recovery. All fish maintained heart rate over the course of scanning. Ultrasound was performed by Dr. Kang Kim, Harry Volek, Waqas Khalid, and Bijun Li (University of Pittsburgh).

Image analysis was performed using the manufacturer-provided software package, Vevo LAB (FujiFilm VisualSonics). Color Doppler images were used to locate the valve between the ventricle and bulbus arteriosus (ventriculobulbar (VB) valve). Long axis B-mode images were acquired at this location and used to measure the diameter of the VB valve region. VB valve diameter was used to calculate the cross-sectional area of the VB valve region, assuming circularity. Along the long axis, pulsed-wave Doppler was used to record heart rate and the ventricular outflow signal, and color Doppler was used to aid in determining the location of maximal blood flow. Velocity-time integral (VTI) was computed at the VB valve and VTI was averaged over 3 cardiac cycles. Stroke volume was calculated as the VTI at the VB valve multiplied by the cross-sectional area of the VB valve, and cardiac output was calculated as stroke volume multiplied by heart rate. Stroke volume and cardiac output were normalized to weight and data were combined from males and females [95]. Ultrasound data were analyzed by Kang Kim, Harry Volek, Waqas Khalid, and Flordeliza Villanueva (University of Pittsburgh).

3.3.8 Analysis of single cell RNAseq data from adult zebrafish heart

Cell Ranger outputs (matrix.tsv, barcodes.tsv and genes.tsv) from three adult zebrafish hearts [96] were downloaded from Gene Expression Omnibus (GSE106121). The R package Seurat (v3.1.1) was used for clustering and cell type identification [97-99]. Genes found in fewer than three cells were excluded and cells were removed that had fewer than 200 genes, greater than 4000 genes, or more than 25% mitochondrial content. The latter cut-off was not stringent because cardiomyocytes express a high percentage of mitochondrial genes. The standard workflow for

integration was followed as recommended in the Seurat vignette (https://satijalab.org/seurat/v3.1/integration.html). Each heart dataset was independently processed using log-normalization, variable genes were identified based on a variance stabilizing transformation (vst), and anchors were identified. The data from the three hearts were integrated using 4000 anchor genes, which produced an expression matrix for all cells (n=14,472). Then the data were scaled and principal component analysis was performed using the first 30 components. UMAP dimensionality reduction [100] was used to cluster and visualize the data. Using differential gene expression results from a likelihood-ratio test (Seurat FindAllMarkers function), broad cell types were identified using gene expression data from the ZFIN database (https://zfin.org/). UMAP coordinates, expression values from the integrated assay "data" slot, and metadata from the Seurat data object were exported, and data.table [101] and ggplot2 [102] were used to create UMAP figures demonstrating cluster identities. Seurat DotPlot function was used to display markers for cluster identification and FeaturePlot was used to display expression values of *bmp10* and *bmp10l* on UMAP plots, with expressing cells in the foreground. Single cell RNAseq analysis was performed by Chelsea Herdman and Joseph Yost (University of Utah).

3.3.9 Statistical analysis

All data and graphs were analyzed using Prism (version 8.0.1, GraphPad, San Diego, CA USA). Sample sizes, experimental repeats, and statistical tests are indicated in figure legends. To avoid bias, all subjective analyses and image analyses were either performed prior to genotyping or by a blinded observer. All data presented are genotypic wild type versus genotypic mutant siblings unless otherwise stated. All figures were generated using Photoshop CC 2017.1.0 release

(Adobe, San Jose, CA USA). Exposure correction was applied to some images for presentation purposes only.

3.4 Results

3.4.1 Generation of zebrafish Alk1 ligand mutants

To explore the unique and overlapping roles of Alk1 ligands in development and disease, we used genome editing to generate mutations in zebrafish *bmp9* (also known as *gdf2*), *bmp10*, and *bmp10-like*. These two-exon genes encode ligands that are generated as proproteins (Figure 4A), with a furin cleavage site separating the N-terminal prodomain from the C-terminal growth factor domain [103]. The released disulfide-bonded growth factor domain dimers are the active ligands in BMP signaling [39]. For each ligand-encoding gene, I assessed two or three mutant alleles, most of which generated frame shifts and/or premature termination codons that truncated proteins within the prodomain or the N-terminus of the growth factor domain (Figure 4A). Additional details on allele identity and verification are provided in Materials and Methods.

3.4.2 *bmp10;bmp10-like* mutants phenocopy *acvrl1* mutants

Zebrafish *acvrl1* mutants develop cranial AVMs connecting the basal communicating artery (BCA) or basilar artery to neighboring veins [49, 68, 104]. This larval lethal phenotype is detectable by 40–48 hpf and is 100% penetrant. Using morpholinos, the Roman lab previously demonstrated that the Alk1 ligands Bmp10 and Bmp10-like are redundant with respect to Alk1 signaling in embryonic vascular development, with concomitant knockdown phenocopying *acvrl1* mutants [64]. Analysis of blood flow in ligand mutants confirms these results: whereas *bmp9*, *bmp10*, and *bmp10-like* single mutants do not develop AVMs (data not shown), *bmp10;bmp10-like* double mutants develop high-flow shunts in cranial vessels (from $bmp10^{pt527/+}$;*bmp10-*

like$^{sa11654/+}$ incrosses, shunts scored in 43/45 double mutants and 1/575 non-double mutants, over 2 experiments). Via confocal microscopy, I confirmed that these shunts represent AVMs between the BCA or basilar artery and flanking veins (primordial midbrain or hindbrain channel), which are indistinguishable from AVMs in *acvrl1* mutants (Figure 4B). As in *acvrl1* mutants, this phenotype is fully penetrant and larval lethal. By contrast, I identified no shunts in embryos from *bmp9*$^{pt533/+}$*;bmp10*$^{pt527/+}$ incrosses (N = 255 embryos, 2 experiments), a *bmp9*$^{pt536/+}$*;bmp10-like*$^{sa11654/+}$ incross (N = 630 embryos, 1 experiment), or a *bmp9*$^{pt536/pt536}$*;bmp10-like*$^{sa11654/+}$ x *bmp9*$^{pt536/+}$*;bmp10-like*$^{sa11654/sa11654}$ cross (N = 54 embryos, 1 experiment). These data confirm that *bmp10* and *bmp10-like* encode functionally redundant embryonic Alk1 ligands, with no embryonic requirement for *bmp9*.

3.4.3 *bmp10* mutants die prematurely

To examine Alk1 ligand requirements post-embryonically, I monitored single-mutants through adulthood. *bmp9* and *bmp10-like* mutants develop no overt phenotype and all alleles show expected genotype ratios as adults (Figure 4C). By contrast, I recovered significantly fewer *bmp10* mutant adults than expected (Figure 4C). The lack of compensation for *bmp10* loss by other Alk1 ligands is not caused by postembryonic silencing of these genes: at 6 months, I detected *bmp9* in the liver, *bmp10-like* in the heart, and *bmp10* and *acvrl1* in both heart and liver (Figure 4D). These expression patterns concur with those of mouse *Bmp9* and *Bmp10* [31, 65, 66, 76-79]. Quantitative measurement of gene expression in adult heart and liver demonstrated no upregulation or ectopic expression of *bmp9* or *bmp10-like* and no change in *acvrl1* expression in *bmp10* mutants (Figure 4E,F), suggesting no transcriptional adaptation or genetic compensation [105]. Analysis of published single-cell RNAseq data from adult zebrafish hearts [96] revealed expression of *bmp10*

predominantly in endocardium/endothelium and *bmp10-like* predominantly in cardiomyocytes (Figure 4G; Figure 5), similar to observations in embryonic zebrafish [64]. Together, these results demonstrate distinct cellular localization and subfunctionalization of zebrafish *BMP10* paralogs in the post-embryonic period and a unique requirement only for *bmp10*. Because all *bmp10* alleles showed similar adult phenotypes, hereafter, all mutant data represent $bmp10^{pt527}$.

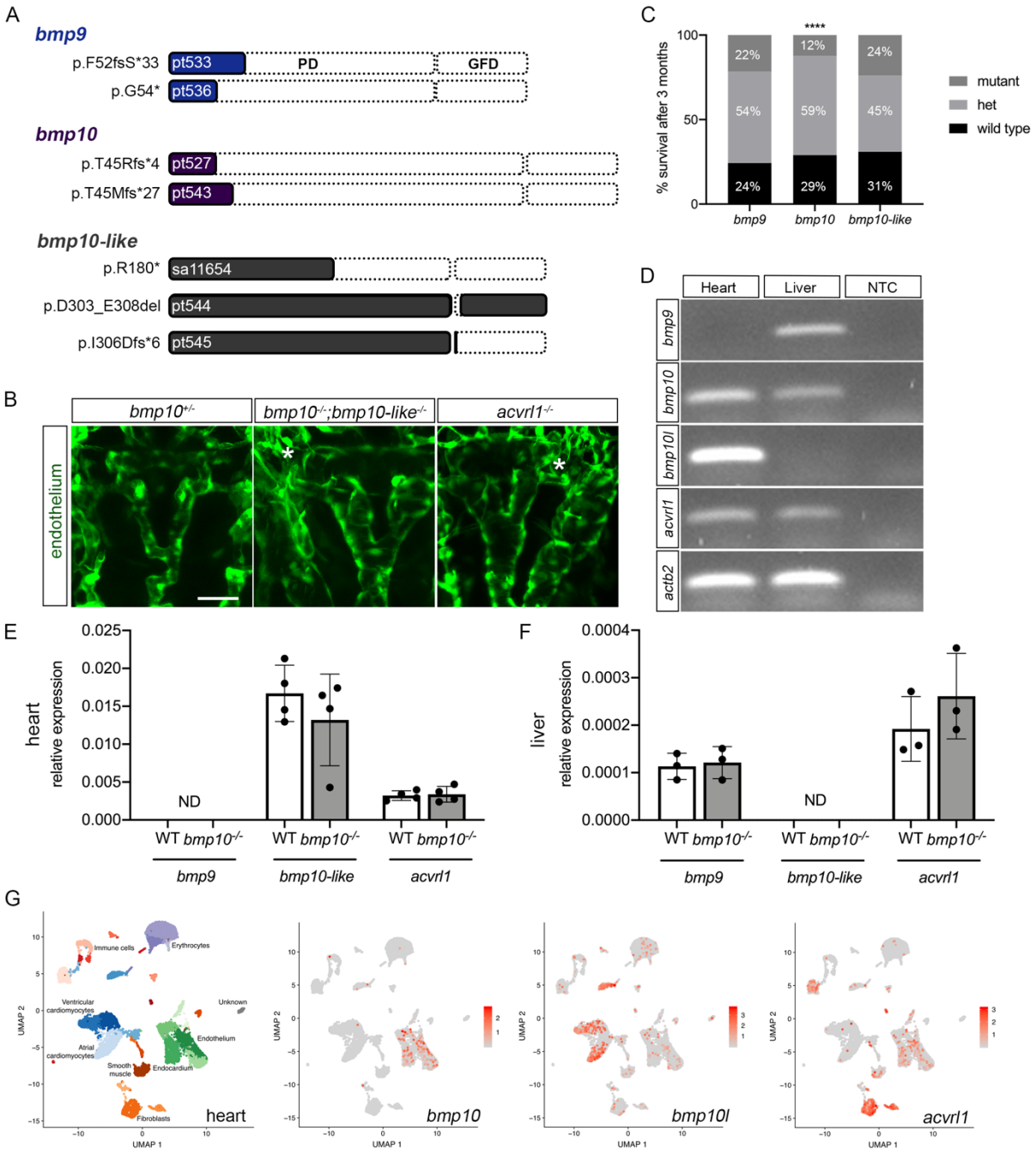

Figure 4 Duplicate *bmp10* paralogs are redundant during embryogenesis but not in adulthood

A Schematics indicating zebrafish wild type Bmp9, Bmp10, and Bmp10-like protein structures and mutant alleles. For each schematic, mutation nomenclature is indicated to the left (following conventions of the Human Genome Variation Society), allele name is indicated within the shaded region, and truncation or deletion is indicated by the unshaded region. PD, prodomain; GFD, growth factor domain; fs, frame shift; *, premature termination codon; del,

deletion. **B** Cranial vasculature in 48 hpf *Tg(kdrl:GFP)*^{la116} embryos from a *bmp10*$^{pt527/+}$;*bmp10-like*$^{sa11654/+}$ incross. "Normal" is *bmp10*$^{pt527/+}$ and representative of all genotypes except double mutants. Asterisks denote AVMs in *bmp10*$^{pt527/pt527}$;*bmp10-like*$^{sa11654/;sa11654}$ double mutants and *acvrl1*$^{y6/y6}$ mutants. Endothelial cells are green. 2D confocal projections, dorsal views, anterior up. Scale bar: 50 μm. Confocal images representative of 6 non-double mutants and 2 double mutants from a *bmp10;bmp10-like* double heterozygous incross. **C** Genotypes in adult offspring from *bmp9*, *bmp10*, and *bmp10-like* heterozygous incrosses. Data aggregated across all alleles within a single gene. *bmp9*: N = 4 clutches, 144 fish; *bmp10*: N = 25 clutches, 952 fish; *bmp10-like*: N = 6 clutches, 197 fish. Chi squared test, ****$P < 0.0001$. **D** RT-PCR from 6-month pooled wild type hearts and livers. NTC, no template control. **E**, **F** qRT-PCR, 3-month hearts (e) and livers (f), showing no transcriptional adaptation of *bmp9*, *bmp10-like*, or *acvrl1* in *bmp10* mutants. N = 3–4 pools of tissue from 4 to 10 fish. WT, wild type. Bars represent mean ± SD. Not significant by unpaired t test. ND, not detected. **G** UMAP analysis plots of single cell transcriptome of three adult zebrafish hearts (n = 14,472 cells), from published data (GSE106121). Left, cell types are annotated and subclusters within cell types are indicated by shades of the same color. Middle and right, feature plots demonstrating scaled expression values of bmp10 and bmp10-like projected on the UMAP plot. *bmp10* predominates in endocardium/endothelium, and *bmp10-like* in cardiomyocytes.

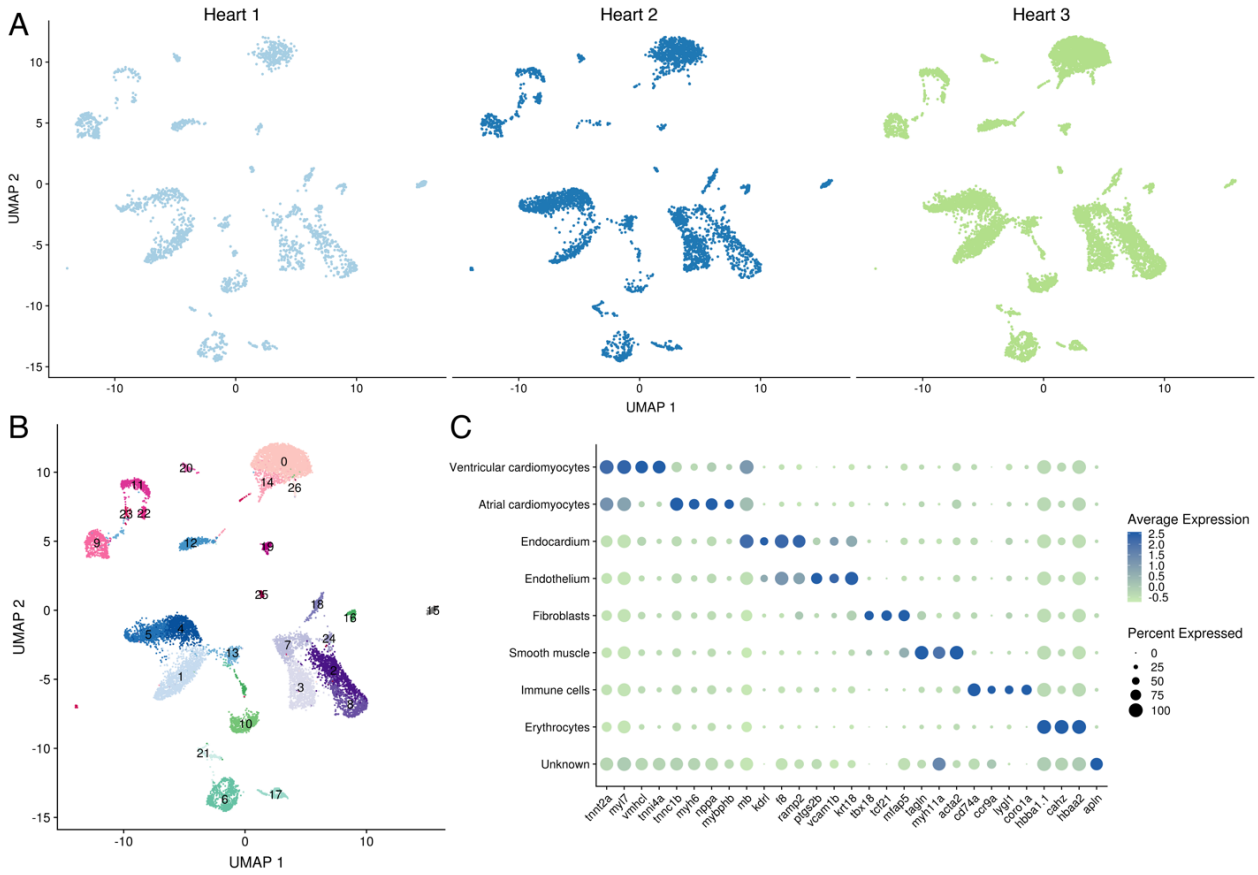

Figure 5 Analysis of single cell RNAseq data from adult zebrafish heart

a UMAP plots of individual hearts (Heart 1 = 2086 cells, Heart 2 = 3924 cells, Heart 3 = 8462 cells). **b** UMAP plot of the three integrated heart datasets. Cluster numbers correspond to the original cluster IDs from the FindClusters function (res 0.8) and colors correspond to cell type as annotated in Figure 4G. Cluster identities are as follows: 0, erythrocytes; 1, atrial cardiomyoctyes; 2, endothelium; 3, endocardium; 4, ventricular cardiomyocytes; 5, ventricular cardiomyocytes; 6, fibroblasts; 7, endocardium; 8, endothelium; 9, immune cells; 10, smooth muscle; 11, immune cells; 12, atrial cardiomyoctyes; 13, atrial cardiomyoctyes; 14, erythrocytes; 15, unknown; 16, smooth muscle; 17, fibroblasts; 18, endothelium; 19, immune cells; 20, immune cells; 21, fibroblasts; 22, immune cells; 23, immune cells; 24, endothelium; 25, immune cells; 26, erythrocytes. **c** Dotplot demonstrating the scaled expression values of select genes used to characterize the clusters. The size of each dot represents the percentage of cells within the cluster that express the gene.

3.4.4 Embryonic cranial vessels are transiently enlarged in *bmp10* mutants

To understand the cause of premature death in *bmp10* mutants, I first focused on the embryonic vasculature. Although I did not detect cranial shunts in *bmp10* mutants, confocal imaging revealed enlargement of the *acvrl1*-positive BCA at 2 days post-fertilization (dpf) (Figure 6A,B), a phenotype reminiscent of but less severe than *bmp10;bmp10-like* double mutants (Figure 4B) and *acvrl1* mutants [49, 68]. The 2 dpf BCA enlargement in *bmp10* mutants correlated with increased *cxcr4a* staining in the caudal divisions of the internal carotid arteries (CaDI), which lead directly into the BCA (Figure 6C–E). This increase in *cxcr4a* expression, characteristic of *acvrl1* mutants [49], suggests decreased Alk1 activity. However, the *bmp10* mutant cranial vascular phenotype is transient: longitudinal measurements revealed normal BCA diameter (Figure 6A,B) and smooth muscle cell investment (Figure 7) of the BCA at 5 dpf. I speculate that the transient increase in arterial caliber stems from the later onset of *bmp10-like* expression [64], leaving a short window of time (~28–36 hpf) during which Alk1 signaling is inactive in *bmp10* mutants. Based on our findings in *acvrl1* mutants [104], this transient loss of Alk1 activity may allow limited migration of endothelial cells in the direction of blood flow and modest enlargement of distal arteries in *bmp10* mutants.

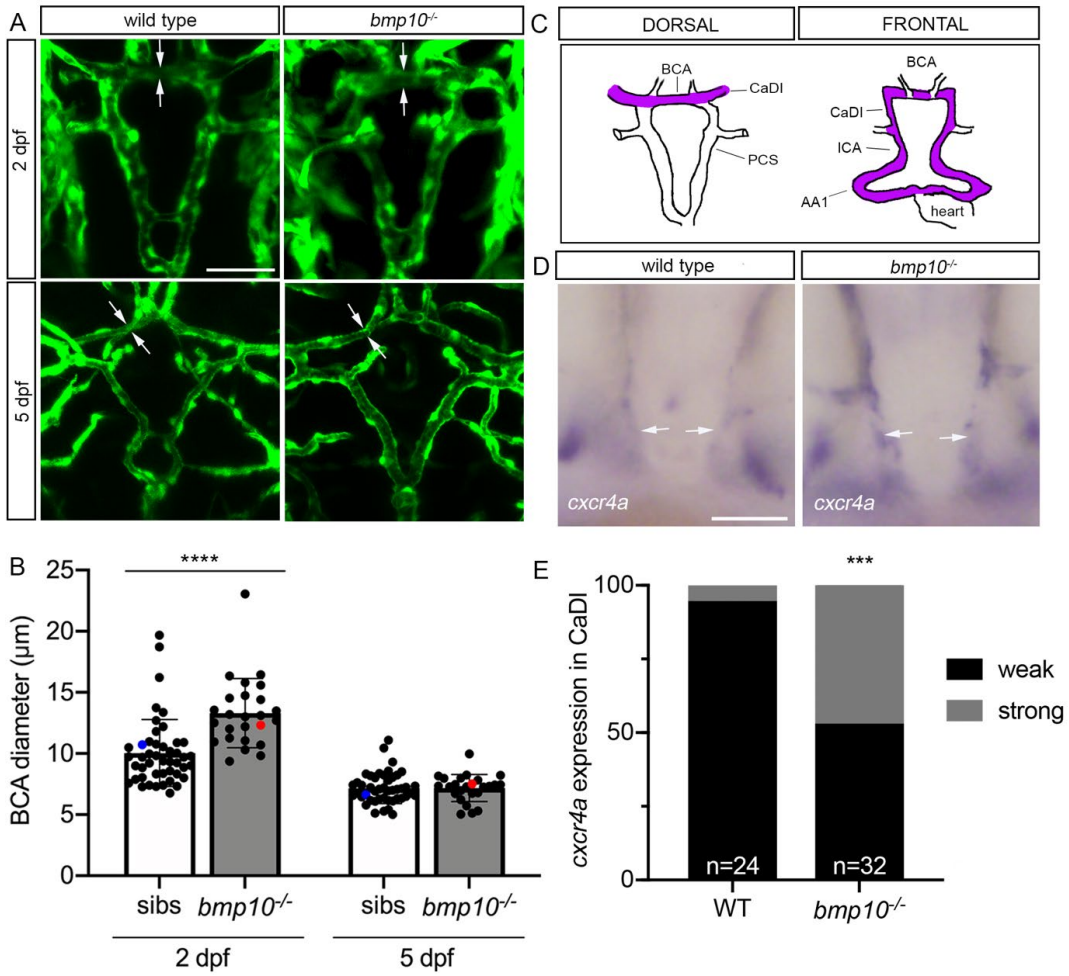

Figure 6 *bmp10* mutant embryos develop transiently enlarged cranial vessels

A Repeated imaging of cranial vessels in *bmp10*^{pt527}*;Tg(kdrl:GFP)*^{la116} mutant and wild type siblings, 2 and 5 dpf. Endothelial cells are green. Arrows delineate width of basal communicating artery (BCA). 2D confocal projections, dorsal views, anterior up. Scale bar: 50 µm. **B** Quantification of BCA diameters. Blue dot, wild type embryo shown in a; red dot, mutant embryo shown in a. N = 46 non-mutant siblings, 25 mutants over 5 experiments. Bars represent mean ± SD. Repeated measures two-way ANOVA followed by Sidak's multiple comparisons test, ****P < 0.0001. **C** Wiring diagrams of cranial vessels, dorsal and frontal views, showing acvrl1-positive vessels in purple. AA1, first aortic arch; ICA, internal carotid artery; CaDI, caudal division of internal carotid artery; PCS, posterior communicating segments. **D** Whole-mount in situ hybridization for *cxcr4a* at 2 dpf, wild type and *bmp10*^{pt527} mutant. Arrows: CaDI. Frontal views, anterior top. Scale bar: 50 µm. **E** Qualitative evaluation of *cxcr4a* expression intensity in CaDI. WT, wild type. Fisher's exact test, ***P < 0.001

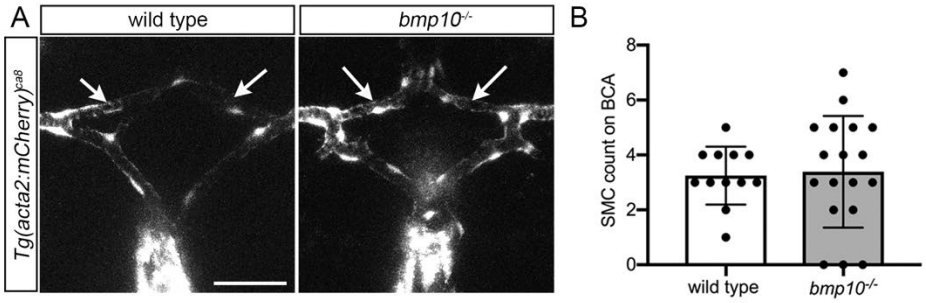

Figure 7 *bmp10* mutant embryos have normal smooth muscle cell coverage on the basal communicating artery (BCA) at 5 dpf

A Cranial vasculature in *bmp10*^{pt527}*;Tg(acta2:mcherry)*^{ca8} mutant and wild type siblings at 5 dpf. Arrows, BCA. 2D confocal projections, dorsal views, anterior top. Scale bar: 50 μm. **B** Quantification of smooth cell number on BCA. N= 12 wild types, 18 mutants over 3 experiments. Bars shown mean ± SD. Not significant by unpaired Student's *t* test.

3.4.5 Embryonic ventricular myocardium development is normal in *bmp10* mutants

Because Bmp10 reportedly plays independent roles in embryonic heart and blood vessel development in mice [65], I next asked whether *bmp10* mutants display embryonic heart defects that might contribute to post-embryonic lethality. In *bmp10* mutants, early cardiac markers and putative downstream targets of Bmp10, *tbx20* and *nkx2.5* [65, 106, 107], are unaffected at 2 dpf (Figure 8A). The second heart field marker, *ltbp3* [108], is also unaffected (Figure 8A). These observations, together with measurement of normal heart rate at 2 dpf (data not shown), suggest that the primitive heart forms and functions normally in *bmp10* mutants.

Trabeculation is the embryonic process by which the smooth heart wall generates folds that extend into the ventricle lumen and is required to generate a functionally competent, thickened ventricular wall [109]. Because mouse *Bmp10* mutants develop hypoplastic ventricular myocardium that lacks trabeculae [66, 106, 110], I asked whether trabeculation defects might contribute to lethality in zebrafish *bmp10* mutants. Zebrafish myocardium begins to trabeculate around 2.5 dpf at the outer curvature of the ventricle and by 5 dpf, a complex trabecular network is evident throughout the ventricle [111, 112]. However, I found no trabeculation defect in *bmp10* mutant zebrafish at 5 dpf (Figure 8B, C). Sarcomeric structure, as measured by distance between Z-disks (Figure 8B, D), and cardiomyocyte number (Figure 8B, E) were also unaffected, whereas ventricular outer perimeter (Figure 8B, F) was slightly increased. Together, these data suggest that zebrafish *bmp10* is not required for normal ventricular cardiomyocyte differentiation, proliferation, or trabeculation, possibly due to redundancy with *bmp10-like*.

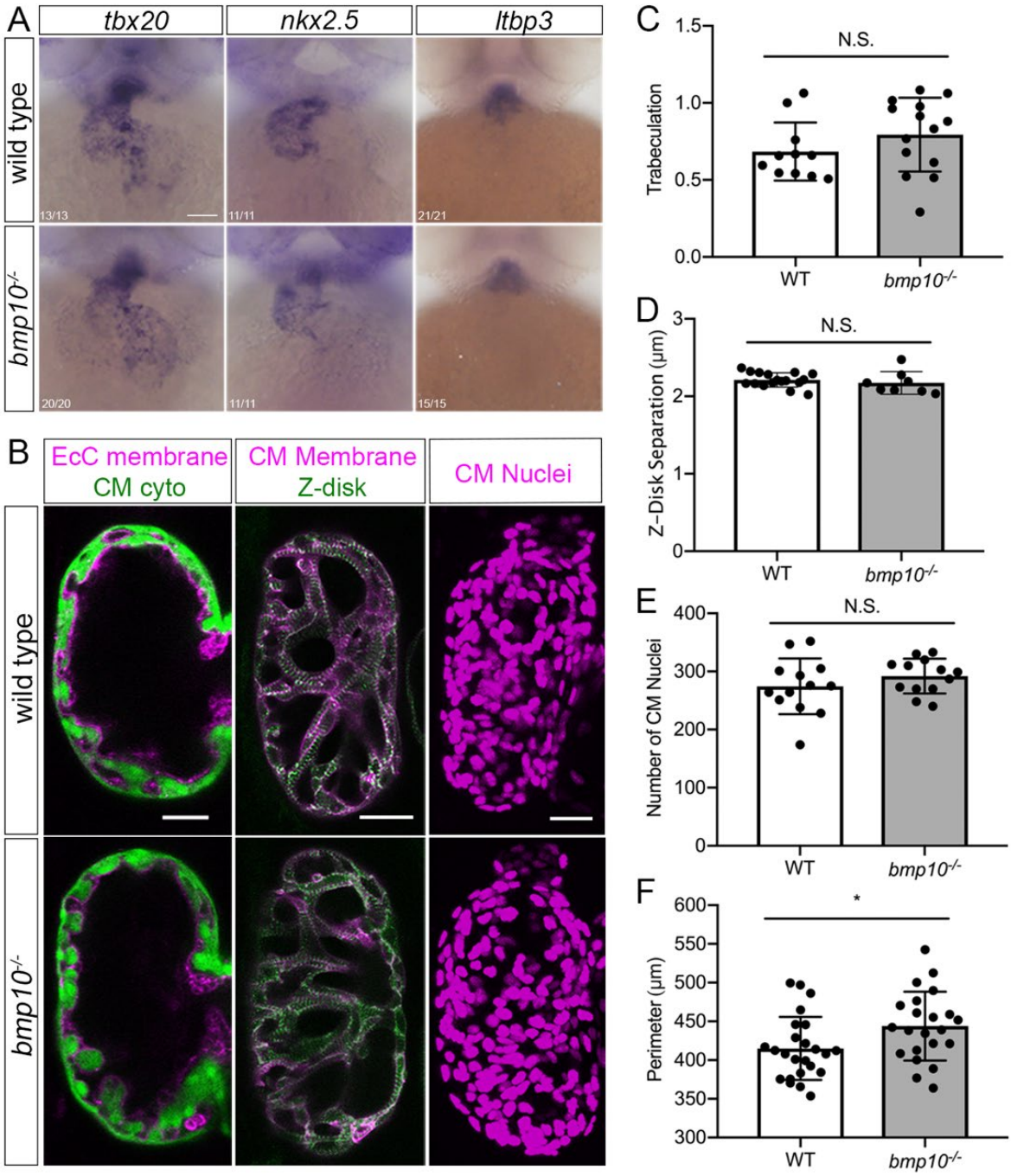

Figure 8 Embryonic ventricular myocardium development is unaffected *bmp10* mutants

A Whole-mount in situ hybridization for *tbx20, nkx2.5,* and *ltbp3* at 2 dpf, wild type and *bmp10*^{pt527} mutant siblings. Ventral views, anterior top. Numbers in left-hand corner show number of embryos with shown phenotype over total number of embryos imaged over 3 experiments. Scale bar: 100 µm. **B** Ventricle morphology at 5 dpf in wild type and

bmp10^{pt527} mutant siblings. Left panels, trabeculation: *Tg(fli1a.ep:mRFP-CAAX)*^{pt505}*;Tg(myl7:EGFP)*^{twu34}, endocardial cell (EcC) membranes magenta, cardiomyocyte (CM) cytoplasm green. Middle panels, sarcomeric architecture: *Tg(myl7:mKATE-CAAX)*^{sd11};*Tg(myl7:actn3b-EGFP)*^{sd10}; CM membranes magenta, Actn3b (Z-disks) green. Right panels, CM number: *Tg(myl7:dsRed2-NLS)*^{f2}; CM nuclei magenta. Confocal images, single planes (left, middle) or 2D projections (right). Scale bars: 25 μm. **C** Trabeculation ((trabecular trace-central chamber trace)/central chamber trace)) at 5 dpf, N = 11 wild types, 14 mutants over 4 experiments. **D** Z-disk separation, N = 17 wild types, 8 mutants over 5 experiments. **E** Number of CM nuclei, N = 13 wild types, 13 mutants over 4 experiments. **F** Ventricle outer perimeter, N = 24 wild type, 22 mutants over 8 experiments. Bars represent mean ± SD. Unpaired *t*-test, $^{*}P < 0.05$, NS = not significant.

3.4.6 *bmp10* mutants develop external vascular phenotype with variable age of onset and expressivity

Next, I monitored *bmp10* mutants for external phenotype and survival beginning at 6 weeks (juvenile period), prior to significant loss of *bmp10* mutants. Earlier onset external phenotype (6–14 weeks) is characterized by abdominal edema and enlarged and/or hemorrhagic blood vessels in skin (Figure 9A). Later onset external phenotype (15 weeks or later) is similar, but with less edema (Figure 9A). The external vascular phenotype in *bmp10* mutants predominates in anterior and ventral regions, including the face, gills, and pectoral fins (Figure 9A, B). This phenotype is reminiscent of HHT patients, who present with telangiectasias in anterior skin and mucosal membranes and on the palmar surface of the hands, with variable age of onset and expressivity [113]. *bmp10* mutants are smaller than their wild type siblings, particularly with earlier onset phenotype (Figure 9A, C).

To characterize variability in age of onset and expressivity, I tracked phenotype and survival in *bmp10* mutant and wild type siblings from 6 until 22 weeks of age. I first observed external phenotype in mutants at 6 weeks and identified on average approximately 2 newly phenotypic fish per week, with 7/30 fish (23.3%) remaining non-phenotypic at 22 weeks (Figure 9D). Only 37% of *bmp10* mutants survived until 22 weeks compared to 100% of their wild type siblings (Figure 9E). During the course of this study, I identified 3 *acvrl1*^{ft09e} heterozygous adult zebrafish that phenocopied *bmp10* mutants, with enlarged and hemorrhagic vasculature in anterior and ventral skin and gills (Figure 10). I speculate that the low penetrance of this *acvrl1* heterozygous phenotype (ascertained anecdotally) may reflect the rare acquisition of second somatic hits that drive lesion development, as recently observed in HHT patient telangiectasias

[22]. In sum, our data support the assertion that *bmp10* encodes an Alk1 ligand that is required for vessel maintenance throughout life.

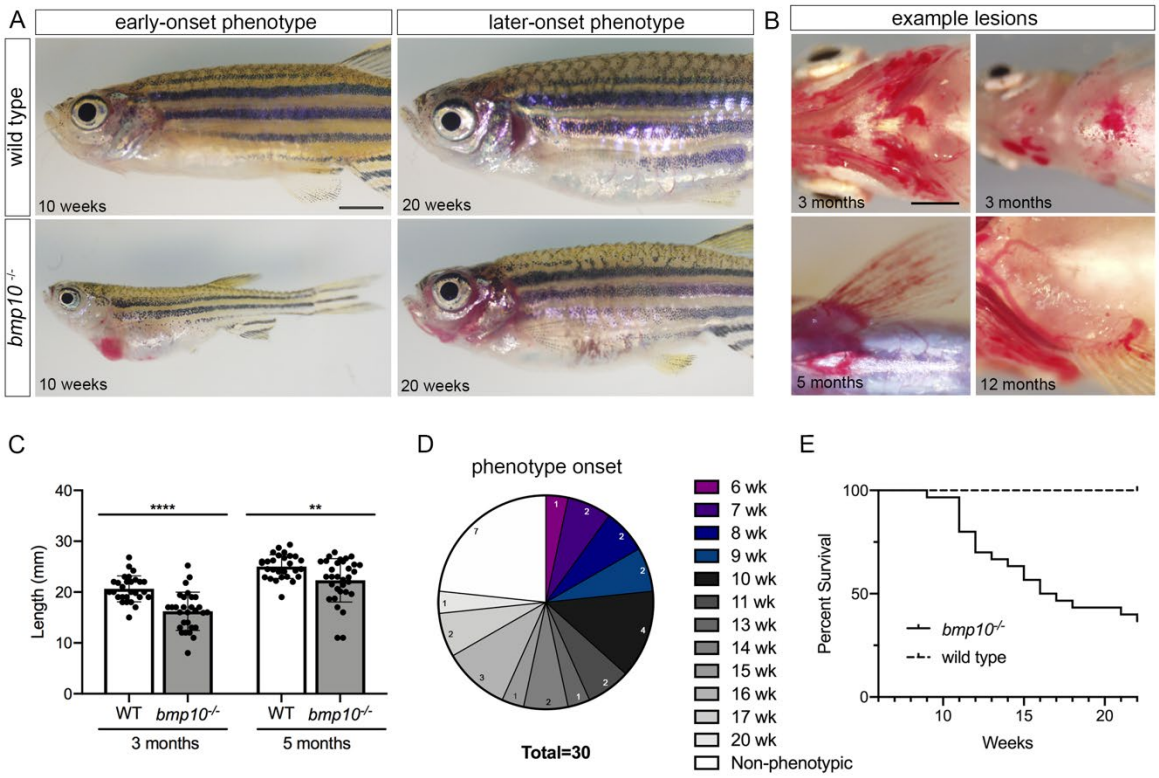

Figure 9 *bmp10* mutants develop external phenotype with variable age of onset and expressivity

A Representative examples of early-onset (6-14 weeks; left) and later-onset (≥ 15 weeks; right) external phenotype in *bmp10*^{pt527} mutants, compared to wild type siblings. Lateral views, anterior left. Scale bars: 2 mm. **B** Dilated vessels and hemorrhages in pharyngeal arch arteries (top left), anterior abdomen (top right), and pectoral fins (bottom). Ventral views, anterior left. Scale bar: 1 mm. **C** Fish lengths at 3 months (N = 28 wild types, 29 mutants from 7 independent lines) and 5 months (N = 28 wild types, 32 mutants from 6 independent lines). Data include phenotypic and non-phenotypic mutants. Bars represent mean ± SD. Unpaired *t*-test, $^{**}P < 0.01$; $^{****}P < 0.0001$. **D-E** Phenotype onset and survival in 1 clutch containing 30 *bmp10*^{pt527} mutants and 33 wild type siblings**. D** Age at onset of external phenotype. Numbers within chart indicate number of fish that became phenotypic during the indicated week, or remained non-phenotypic at 22 weeks. **E** Survival in *bmp10* mutants and sibling wild types. Log-rank (Mantel-Cox) test, $^{****}P < 0.0001$.

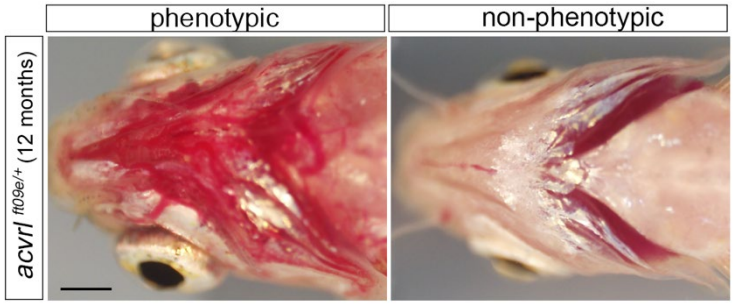

Figure 10 *acvrl1*$^{ft09e/+}$ fish phenocopy *bmp10* mutants with low penetrance

12-month fish. Scale bar: 1 mm.

3.4.7 *bmp10* mutants develop skin and liver vascular abnormalities

To further probe the architecture and location of vascular malformations in *bmp10* mutants, I used confocal microscopy to image blood vessels in a double transgenic line that differentially marks arterial and venous endothelium. Although *Tg(flt1:tdTomato)*^{hu5333} has been used primarily to mark arterial endothelial cells and *Tg(flt4:Citrine)*^{hu7135} to mark venous and lymphatic endothelial cells in embryos [114-116], these transgenes also mark heart, skin, and fin arterial endothelium and fin venous endothelium, respectively, in adults [117-119]. In wild type adult skin, I found that both transgenes are expressed, revealing an interconnected network of thin, elongated arteries and veins that meander through the tissue in a somewhat stochastic pattern (Figure 11). By contrast, in *bmp10* mutants, blood-filled vascular malformations that were visible upon gross examination manifested as enlarged arteries and plexus-like veins (Figure 11). Liver vasculature in phenotypic *bmp10* mutants was also abnormal. In wild type adults, well separated clusters of small, branching arterial vessels connect to similarly sized straight sinusoids of venous character, which then drain into a large central vein (Figure 11 and data not shown). In *bmp10* mutants with external vascular phenotype, the liver vasculature was markedly less organized, with elongated, branching arteries and large swaths of plexus-like sinusoids (Figure 11). Although I could not define liver AVMs per se, possibly because of the profoundly different, non-lobular architecture of the zebrafish liver [120, 121], this vascular phenotype is reminiscent of enlarged arteries and ectatic sinusoids that have been described in HHT patients [122, 123]. Based on a report of tortuous brain vessels in zebrafish adult *eng* mutants [56], I also examined the superficial brain vasculature in *bmp10* mutants. However, I detected no brain vessel abnormalities using bright field (N = 11; 3 experiments) or confocal (N = 8; 2 experiments) microscopy. In sum, *bmp10* mutants develop vascular malformations in skin and liver, two primary sites of AVM development in HHT. I

hypothesize that the abdominal edema and ascites fluid in *bmp10* mutants is related to liver vascular malformations and consequent liver dysfunction, as this is a common presentation of HHT with symptomatic liver involvement [124]. However, lymphatic defects may also cause edema, and Alk1 signaling has been suggested to play a role in lymphatic vessel development and function [62, 125, 126]. Evaluation of effects of *bmp10* mutation on the lymphatic vasculature will require further studies.

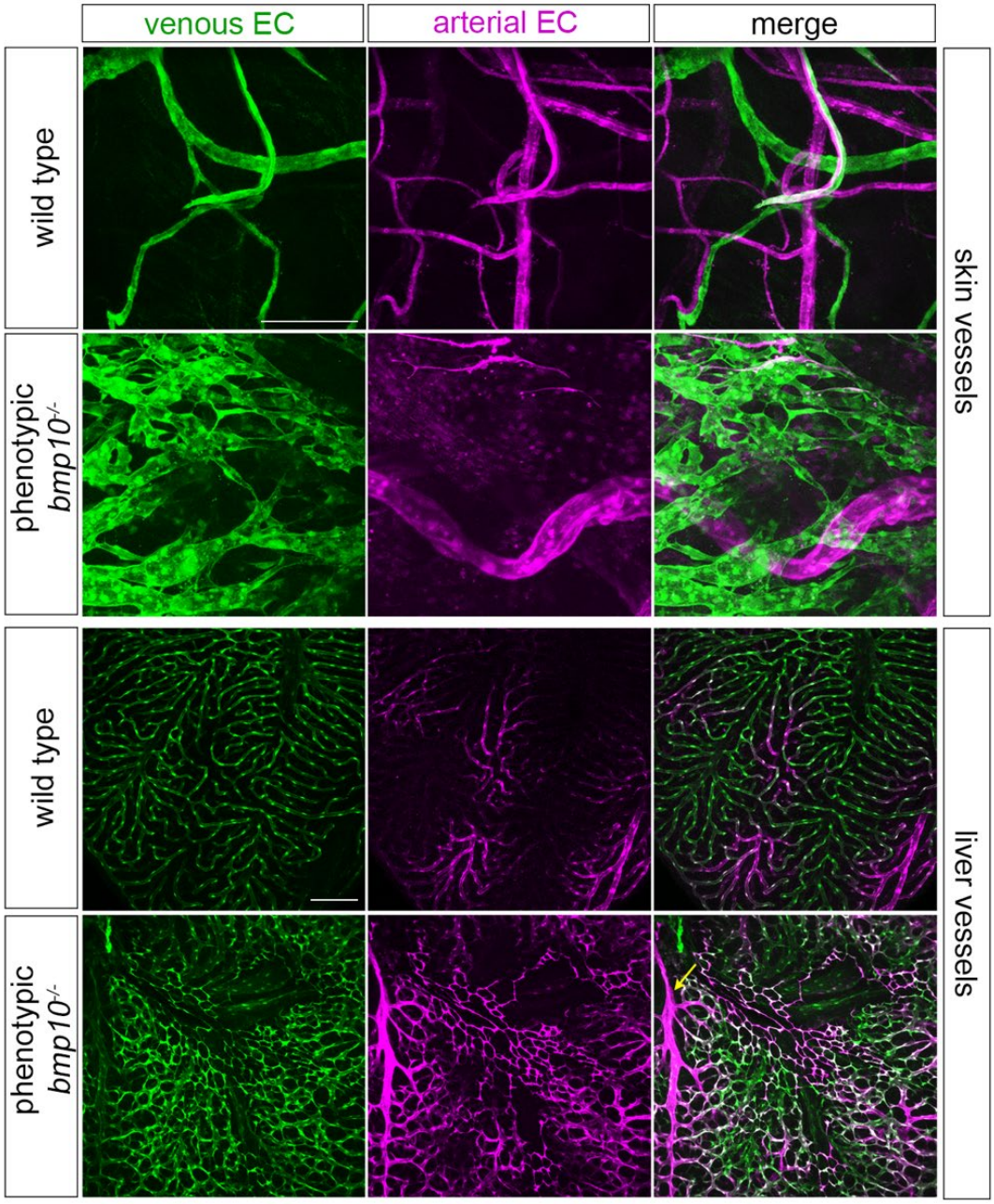

Figure 11 *bmp10* mutants develop skin and liver vascular malformations

TOP: Venous (green) and arterial (magenta) vasculature in anterior ventral skin, adult *Tg(flt4:citrine)*^{hu7135}*;Tg(flt1:tdTomato)*^{hu5333} wild type and *bmp10*^{pt527} mutant siblings. Images are from 23-month fish and representative of N = 7 wild types and 8 phenotypic mutants from 2 independent lines, ages 3-23 months. Siblings were randomly paired to match imaging site in wild types to lesion site in mutants. 2D confocal projections. Scale bar:

50 μm. **BOTTOM**: Venous (green) and arterial (magenta) vasculature in distal tip of right liver lobe from adult *Tg(flt4:citrine)*^{hu7135}*;Tg(flt1:tdTomato)*^{hu5333} wild type and *bmp10*^{pt527} mutant siblings. Images representative of N = 12 wild types and 9 phenotypic mutants from 2 independent lines, age 5 months. 2D confocal projections. Arrow, enlarged artery. Scale bar: 100 μm.

3.4.8 Vascular defects are associated with high-output heart failure in *bmp10* mutants

Because embryonic ventricular myocardium development is normal in *bmp10* mutants and liver AVMs in HHT patients are associated with low vascular resistance, volume overload, and HOHF [10], I reasoned that early lethality in *bmp10* mutants may be caused by HOHF. To test this hypothesis, our collaborator Dr. Kang Kim and his team used echocardiography to assess heart function. At 3 and 5 months, externally phenotypic mutants exhibited significantly increased normalized stroke volume and cardiac index compared to wild type siblings (Figure 12A, B), consistent with a high-output state. Additionally, I found that mutant hearts expressed increased levels of *nppa* and *nppb* (Figure 12C), both of which are elevated in high-output heart failure [127, 128]. Dissection of externally phenotypic *bmp10* mutants at 3 months and 5 months (Figure 12D-F; 3 month data not shown) revealed an enlarged heart with rounded ventricle. Qualitatively, the severity of the cardiac phenotype correlated with the severity of the external vascular phenotype. However, despite these obvious shape, size, and tissue integrity abnormalities, we failed to detect extracellular matrix remodeling or fibrosis, and elastin staining indicated normal development of the bulbus arteriosus (outflow tract) and atrioventricular valves (Figure 12E–F; figure courtesy of Bijun Li, MS). In sum, these data support the hypothesis that adult *bmp10* mutants develop vascular malformations in skin and liver that lead to low systemic vascular resistance and volume overload, precipitating HOHF without fibrosis.

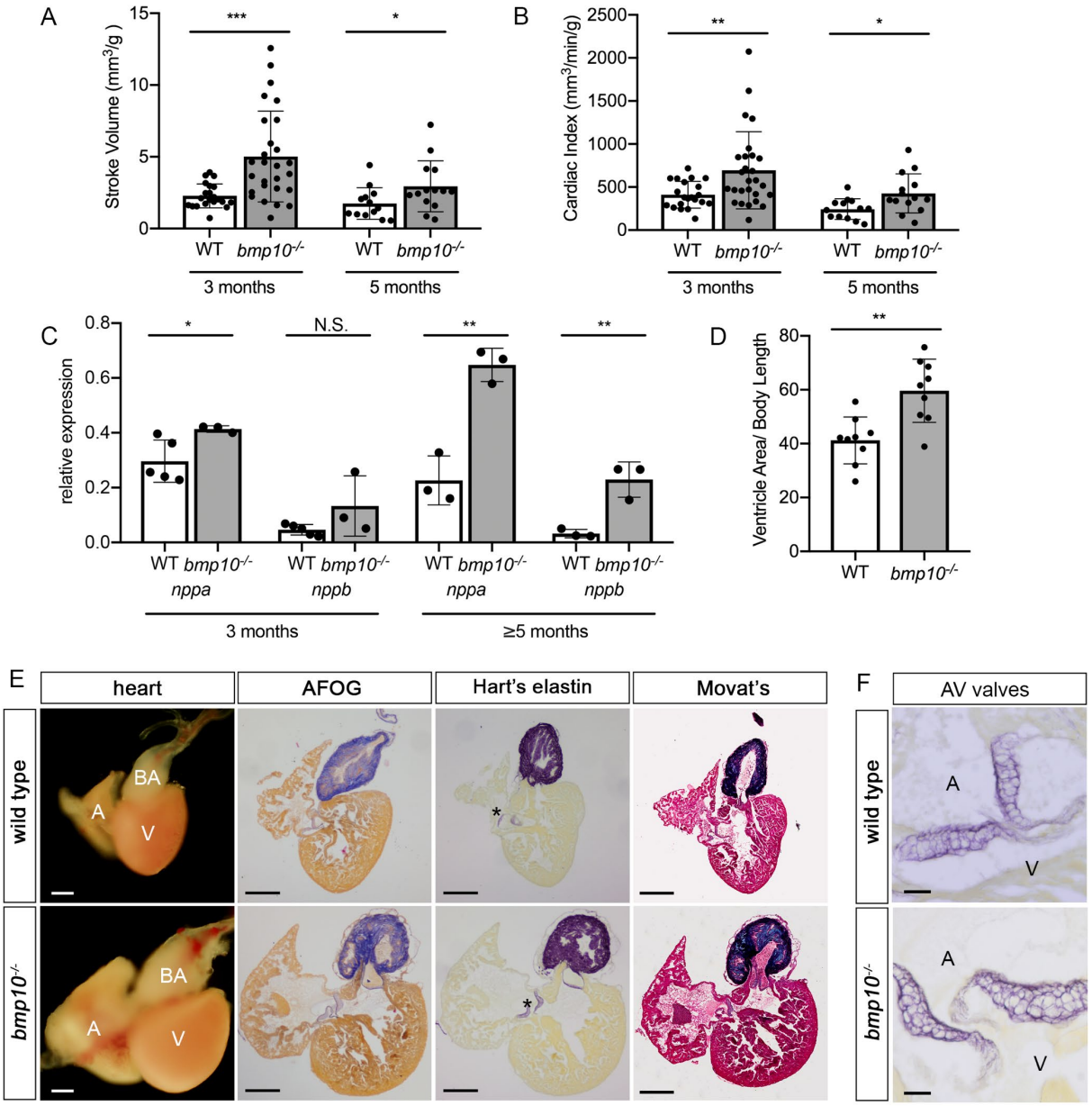

Figure 12 *bmp10* mutants develop high-output heart failure

A, **B** Normalized stroke volume (**A**) and cardiac index (**B**) at 3 months (N = 21 wild types (16 males, 5 females), 28 *bmp10*^{pt527} mutants (25 males, 3 females) over 3 experiments) and 5 months (N = 13 wild types (11 males, 2 females), 16 *bmp10*^{pt527} mutants (13 males, 3 females) over 2 experiments). **C** qRT-PCR quantification of *nppa* and *nppb* in the heart at 3 months (wild type, N= 4 pools, 6-10 hearts per pool; phenotypic *bmp10*^{pt527} mutants^{-}, N = 3 pools, 4-10 hearts per pool) or 5 months (N= 3 pools, 10 hearts per pool, for both wild type and phenotypic *bmp10*^{pt527} mutants**).** **D** Relative ventricle size at 5 months, measured as maximal cross-sectional ventricle area/body length. N = 9 hearts

(3 males, 6 females) per genotype, 1 experiment. Bars represent mean ± SD. Welch's *t*-test (**A, B**) or unpaired Student's *t*-test (**C, D**), **P*<0.05,***P*<0.01, ****P*<0.001. NS = not significant. **E** Hearts from 5-month wild type and *bmp10*^{pt527} mutant siblings, whole mount or sections stained with acid fuchsin orange G (AFOG) for collagen (blue) and fibrin (red); Hart's elastin stain (purple); or Movat's pentachrome stain for muscle (red), collagen (yellow), elastin (blue-black), and ground substance (light blue). A, atrium; V, ventricle; BA, bulbus arteriosus; asterisks, atrioventricular valves. Scale bar: 200 μm. Images representative of N = 3 hearts per genotype, males from 2 independent lines. **F** Atrioventricular valves, 5-month wild type and *bmp10*^{pt527} mutant siblings, Hart's elastin stain. A, atrium; V, ventricle; AV, atrioventricular. High magnification of different section of hearts shown in **E**. Scale bar: 20 μm.

In conclusion, our data demonstrate that Bmp10 is the only Alk1 ligand that is required for maintenance of the post-embryonic vasculature, a finding that should be taken into consideration in development of ligand-based therapies for HHT. In addition, I present zebrafish *bmp10* mutants as a valuable model to investigate cardiac adaptation and the progression to heart failure in conditions of volume overload, especially in HHT2.

3.5 Discussion

The striking vascular phenotype in juvenile-to-adult *bmp10* mutants and, rarely, *acvrl1* heterozygotes, combined with the lack of phenotype in *bmp9* and *bmp10-like* mutants, suggests that Bmp10 is the only required Alk1 ligand in post-embryonic zebrafish. The unique requirement for *bmp10* was unexpected given the embryonic redundancy of *bmp10* and *bmp10-like* [64] and the continued expression of *bmp10-like* in the adult heart. We speculate that these duplicate paralogs of mammalian *BMP10* may have subfunctionalized in zebrafish, with endocardial- or

liver-derived Bmp10 predominating over cardiomyocyte-derived Bmp10-like in circulation. We hypothesize that cardiomyocyte-derived Bmp10-like may act primarily at close range, with diminishing contribution to circulating Alk1 ligand concentration with increasing age. This explanation could account for the ability of *bmp10-like* to compensate for *bmp10* during the embryonic period but not at later times. Further studies are required to confirm this hypothesis and to understand whether differential cell type of origin influences disposition and function of these Bmp10 paralogs.

The presence of post-embryonic phenotype in *bmp10* mutants was also surprising given the continued expression of *bmp9* in adult liver and the consensus that BMP9 and BMP10 are redundant ALK1 ligands. The notion of redundancy was initially derived from observations in mice showing that 1) *Bmp9* nulls live to adulthood and do not develop AVMs; 2) *Bmp10* nulls develop embryonic lethal AVMs at E9.5, similar to *acvrl1* nulls; and 3) insertion of *Bmp9* into the *Bmp10* locus rescues embryonic AVMs in *Bmp10* mutants [61, 65]. These data, combined with the fact that *Bmp9* expression in liver begins at E9.75-E10, imply functional redundancy of BMP9 and BMP10, with respect to vascular requirements, at time points when both are expressed [65]. However, careful examination of this work reveals that rescued mice develop enlarged, hemorrhagic vessels by E17.5 [65], a phenotype that is remarkably similar to zebrafish *bmp10* mutants, albeit at a much younger age. Additional support for redundancy of BMP9 and BMP10 derives from data showing that simultaneous depletion of these ligands in neonatal mice results in vascular dysplasia and/or AVMs [61, 65, 67, 81, 82]. However, these studies focused almost exclusively on the retinal vasculature, and the few studies that presented true retinal AVMs utilized combined but not independent BMP9/BMP10 antibody blockade [67, 81, 82]. More recently, two

independent studies demonstrated that neither constitutive global *Bmp9* deletion nor inducible global or cardiomyocyte-specific *Bmp10* deletion resulted in phenotype. However, on a *Bmp9* null background, global *Bmp10* deletion resulted in vascular shunting and HOHF [129], similar to our zebrafish *bmp10* mutants, whereas cardiomyocyte-specific *Bmp10* deletion resulted in vascular dilation and decreased smooth muscle cell coverage and contraction [130]. The reported lack of phenotype in *Bmp10* conditional knockouts may reflect incomplete deletion (residual *Bmp10* mRNA in global inducible knockouts was 20-40% of wild type, and hepatic stellate cell *Bmp10* remained in the cardiomyocyte-specific model) or later-onset phenotype. However, we cannot discount the idea that *Bmp9* may be more able to compensate for *Bmp10* in mice than in fish.

The requirement for *bmp10* but not *bmp9* in vascular homeostasis in zebrafish is also surprising because heterozygous and ultra-rare homozygous mutations in *BMP9* are associated with pulmonary arterial hypertension as well as an HHT-like syndrome [24, 25, 131-134]. By contrast, while there is one report linking *BMP10* heterozygous mutations to PAH [133], there is no evidence linking *BMP10* mutations to HHT, Interestingly, the ExAC browser (exac.broadinstitute.org) calculates a probability of loss-of-function intolerance (pLI) of 0.72 for *BMP10* and 0.09 for *BMP9*. The high pLI for *BMP10* suggests that it is approaching intolerance to loss-of-function with a high likelihood of haploinsufficiency, whereas the low pLI for *BMP9* suggests that the null state may be tolerated [135], as borne out by the identification of viable *BMP9* nulls.

Because HHT is an autosomal dominant disorder, ligand-based therapies may overcome haploinsufficiency. As proof of principle, administration of recombinant BMP9 in rodent models of PAH, which is primarily caused by BMP receptor 2 (*BMPR2*) heterozygous mutation or deficiency, enhances pSMAD1/5 and improves disease phenotype [75]. Our data suggest that

BMP10, which is required for ALK1 signaling and, unlike BMP9, does not have strong osteogenic activity [136], may be the best choice for ligand-based therapy for HHT. Although we acknowledge a recent report identifying somatic second hits in some HHT telangiectasias [137], regardless of genetic mechanism of disease, this BMP10-based approach to therapy should remain a viable option for HHT1/*ENG* patients with intact ALK1.

The active form of TGF-β family ligands was originally described as disulfide-bonded homodimers, but developmental requirements for heterodimers (Bmp2/Bmp7; Gdf3/Nodal) have been reported [138, 139]. Notably, BMP9 and BMP10 can form biologically active heterodimers when co-expressed in vitro, and heterodimers, speculated to be produced by liver stellate cells, reportedly account for the large majority of ALK1-activating activity in mouse and human plasma [31]. However, BMP9/BMP10 heterodimers activate signaling with similar potency to homodimers [31], providing no clear biochemical advantage. Moreover, given the lack of a requirement for *Bmp9* in AVM prevention in both mouse [61] and zebrafish, it is unlikely that the ALK1 ligand is an obligate BMP9/BMP10 heterodimer. Parsing out the differential functions of BMP10 homodimers versus BMP9/BMP10 heterodimers requires further investigation.

In mice, *Bmp10* acts directly on embryonic ventricular cardiomyocytes to induce proliferation and trabeculation [65, 66, 106, 110, 140, 141]. However, we detected no changes in ventricular cardiomyocyte number or trabeculation in *bmp10* mutant zebrafish embryos. It is possible that *bmp10-like* may compensate for the loss of *bmp10* in zebrafish heart development. Alternatively, effects of *Bmp10* loss on trabeculation in mice may be, at least in part, secondary to AVM development: AVMs disrupt flow patterns, and normal heartbeat and shear stress are required for proper trabeculation [111, 142]. In zebrafish, the progressive loss of blood flow

subsequent to AVM development in *acvrl1* [49] and *bmp10;bmp10-like* double mutants makes it difficult to distinguish between these two possibilities.

The zebrafish *bmp10* mutant phenotype is reminiscent of the HHT patient phenotype, with variable age of onset and expressivity of vascular lesions concentrated in anterior skin (face), gill vessels (developmental origin of pulmonary arteries), pectoral fins (analogous to hands), and liver. Moreover, lesion development closely correlates with an enlarged heart and HOHF without maladaptive remodeling, similar to that reported in *Acvrl1* conditional knockout mice [143]. HOHF is increasingly recognized as a complication of HHT in aging patients and correlates with severe liver involvement [144]. There is little information regarding the progression of HOHF in humans and no therapy for this disease short of elimination of the underlying vascular problem [145]. In the case of HHT patients, this means liver transplantation. However, even liver transplantation is not a cure, as vascular malformations reappear in transplanted HHT patients with a cumulative risk of 48% over 15 years [146]. As such, *bmp10* mutants afford us an opportunity to study the progression of HOHF and to gain mechanistic insight into the factors that tip the trajectory from compensation to failure.

4.0 ALK1 ligands in circulation

4.1 Abstract

HHT is an autosomal dominant vascular disorder characterized by the development of AVMs throughout life. Though defective ALK1 signaling has been identified as causal for disease manifestation, no targeted therapies have yet been developed for HHT patients. Administration of ALK1 ligand-based therapeutics may be a logical approach to prevent the development of AVMs. However, although BMP9 and BMP10 circulate in human plasma and specifically activate ALK1, the precise molecular identity of ALK1 ligands in circulation remains unclear. Using ELISAs that distinguish full-length, unprocessed proproteins from processed, mature GFDs, we determined that BMP9 circulates in a processed form while BMP10 circulates as full-length proBMP10. These data suggest that covalently attached PD may confer stability to BMP10 and/or help to target the ligand to endothelial cells, and that ligand activity may be regulated by post-secretory processing. This new insight into the nature of endogenous ALK1 ligands may inform development of ligand-based therapeutics for HHT.

4.2 Introduction

Though BMP9 and BMP10 are functionally equivalent with respect to ALK1 and ENG binding and activation of ALK1 signaling [46] and are both present in circulation [31], our zebrafish experiments demonstrate a clear genetic requirement for *bmp10* but not *bmp9* . This finding suggests that BMP10 may be endowed with some unique characteristic that distinguishes it from BMP9 and confers necessity with respect to ALK1-dependent vascular homeostasis. BMPs are synthesized as proproteins that are cleaved by proproteins convertases, such as furin, between the N-terminal PD and C-terminal GF domain. Once cleaved, the PD associates non-covalently with the GFD to form 2:1 PD:GFD complexes. Removal of the PD is thought to be a necessary step in ligand activation because the GFD interface with the PD and the type II receptor overlap [37]. With respect to BMP9 and BMP10, noncovalently associated PDs readily dissociate and PD:GFD complexes are not latent [37, 45, 46]. However, while BMP9 and BMP9/10 reportedly circulate in processed forms with GFDs readily accessible [31, 45, 131], BMP10 is detected primarily as unprocessed, full-length proBMP10 [131]. The goal of this work is to better characterize the molecular nature and activity of ALK1 ligands in plasma.

4.3 Materials and Methods

4.3.1 Recombinant protein production

Recombinant BMPs were generated using the expi293 expression system (ThermoFisher, Waltham, MA USA) by the Hinck lab (Dr. Andrew Hinck, Dr. Cynthia Hinck, and Tristin Schwartze; Structural Biology, University of Pittsburgh). Briefly, human *BMP9* and *BMP10* sequences were codon-optimized and modified by replacing the endogenous signal sequence with the rat serum albumin signal sequence followed by a removable 8-His-tag or StrepII-tag. Additionally, in some clones, the primary furin (F) cleavage site (for BMP9, RRKRS; for BMP10, RIRR) was replaced by an enterokinase (EK) site (DDDDK) or a factor Xa (Xa) site (IEKR); these proteins were secreted and purified as fully unprocessed proteins, or were cleaved *in vitro* with EK or Xa, respectively, with subsequent purification of prodomain and GFD. To generate full-length unprocessed proBMPs containing the endogenous furin cleavage site, cells were cotransfected with α1-antitrypsin Portland (α1-PDX) to inhibit furin [147]. To generate heterodimers, Strep II-BMP9 and 8-His-BMP10 were co-transfected followed by sequential purification using Streptactin and nickel columns. A description of the cDNA constructs and derived proteins is found in Table 6.

Table 6 ALK1 ligand expression plasmids

construct	Signal peptide	N-tag	N-tag/PD cleavage site	PD	PD/GFD cleavage site	GFD	Proteins
BMP9							
BMP9-Xa	RSA	Strep II	Xa	p.G29E, R30Q	Xa	intact	proBMP9-Xa proBMP9/10-Xa BMP9 GFD BMP9/10 GFD
BMP9-F	RSA	8-His	Xa	p.G29E, R30Q	F	intact	proBMP9-F
BMP10							
BMP10-EK	RSA	8-His	Thr	Intact (?)	EK	intact	proBMP10-EK
BMP10-Xa	RSA	8-His	Xa	p.G237D, R238T	Xa	intact	proBMP9/10-Xa BMP10 GFD BMP9/10 GFD
BMP10-F	RSA	8-His	Xa	p.G237D, R238T	F	intact	proBMP10-F

RSA = rat serum albumin; Thr = thrombin; GFD = growth factor dimer

4.3.2 Enzyme linked immunosorbent assays (ELISAs)

ELISAs were developed using recombinant proteins and pooled normal adult human K_2EDTA plasma. Briefly, clear polystyrene microplates (R&D, Minneapolis, MN USA) were coated with 100 µl capture antibody diluted in PBS (see Table 7) and incubated overnight at 4ºC. After aspiration, wells were washed three times with 400 µl phosphate-buffered saline (PBS) (Corning)/0.05% tween (Sigma) then blocked in 300 µl PBS/2% bovine serum albumin (BSA) (R&D) for 2 hours at 23ºC. Standards (Table 7) and samples (30 µl) were diluted to 100 µl in reagent diluent to achieve a final concentration of 1%BSA/0.5% triton/0.2% goat serum/4.5 mM EDTA in PBS [131] and incubated for 2 hours at 23ºC. After three washes with 400 µl PBS/0.05% tween, 100 µl detection antibody (Table 7, diluted as indicated in PBS/1%BSA/0.2% goat serum) was added and incubated for 2 hours at 23ºC. After three washes with 400 µl PBS/0.05% tween, 100 µl streptavidin-HRP A (R&D; 1:200 in PBS/1%BSA) was added and incubated for 20 minutes at 23ºC, followed by three washes with 400 µl PBS/0.05% tween and incubation with 100 µl HRP substrate tetramethylbenizidine (substrate reagent pack, R&D Systems) for 5-20 minutes (as

indicated in Table 7). The color reaction was stopped by adding 50 µl 2N H_2SO_4 and plates were immediately read at 450 nm and corrected at 560 nm using a Genios Tecan plate reader. All standards and samples were run in duplicate, with a separate standard curve on each plate. Standard curves were generated using GraphPad Prism (version 8) by plotting the log_{10}-transformed GFD-equivalent concentrations on the x-axis and the absorbance replicates on the y-axis, and unknowns were interpolated using sigmoidal 4PL non-linear regression.

Table 7 ALK1 ligand ELISAs

	Capture Antibody		Detection Antibody		Standard Curve			
	Name	Working Concentration	Name	Working Concentration	Name	Top Concentration	Dilution Series	Reagent Incubation time
BMP9 GF/GF [45, 131]	Human/Mouse/ Primate BMP-9 Antibody (R&D MAB3209)	2 µg/mL	Human/Primate BMP-9 Biotinylated Antibody (R&D BAF3209)	0.4 µg/mL	BMP9 GFD	1000 pg/mL	1:1	20 minutes
BMP9 GF/PD	Human/Mouse/ Primate BMP-9 Antibody (R&D MAB3209)	2 µg/mL	Human BMP-9 Propeptide Biotinylated Antibody (R&D BAF3879)	0.4 µg/mL	proBMP9-Xa	1000 ng/mL	1:3	8 minutes
BMP10 GF/GF [131]	Human/Mouse BMP-10 DuoSet ELISA (DY2926) Capture Antibody	1 µg/mL	Human/Mouse BMP-10 DuoSet ELISA (DY2926) Detection Antibody	1 µg/mL	BMP10 GFD	1000 ng/mL	1:3	20 minutes
BMP10 GF/PD [131]	Human/Mouse BMP-10 Antibody (R&D MAB2926)	5 µg/mL	Human BMP-10 Propeptide Biotinylated Antibody (R&D BAF3956)	0.4 µg/mL	proBMP10-EK	100 ng/mL	1:3	8 minutes
BMP9/10 GF/GF	Human/Mouse/ Primate BMP-9 Antibody (R&D MAB3209)	2 µg/mL	Human/Mouse BMP-10 DuoSet ELISA (DY2926) Detection Antibody	0.4 µg/mL	BMP9/10 GFD	1000 ng/mL	1:10	8 minutes
BMP10/9 GF/GF	Human/Mouse BMP-10 Antibody (R&D MAB2926)	5 µg/mL	Human/Primate BMP-9 Biotinylated Antibody (R&D BAF3209)	0.4 µg/mL	BMP9/10 GFD	10000 pg/mL	1:3	8 minutes
BMP9/10 GF/PD	Human/Mouse/ Primate BMP-9 Antibody (R&D MAB3209)	2 µg/mL	Human BMP-10 Propeptide Biotinylated Antibody (R&D BAF3956)	0.4 µg/mL	proBMP9/10-Xa	1000 ng/mL	1:4	8 minutes
BMP10/9 GF/PD	Human/Mouse BMP-10 Antibody (R&D MAB2926)	5 µg/mL	Human BMP-9 Propeptide Biotinylated Antibody (R&D BAF3879)	0.4 µg/mL	proBMP9/10-Xa	1000 ng/mL	1:4	8 minutes

4.3.2.1 Spike and Recovery Assays

To assess protein recovery in a plasma matrix, a known amount of recombinant BMP standard was added to plasma (spiked) and spiked and un-spiked samples were evaluated by ELISA. Percent recovery (%R) was calculated by subtracting the ligand concentration in plasma ($C_{un\text{-}spiked}$) from the ligand concentration in spiked plasma ($C_{un\text{-}spiked}$) and expressed as a percentage of the added concentration (C_{added}).

$$\% R = \frac{(C_{spiked} - C_{unspiked})}{C_{added}} \times 100$$

4.3.3 Cell culture

4.3.3.1 Line Maintenance

Cells were maintained in a humidified incubator in 5% CO_2 at 37°C. Pooled primary human umbilical vein endothelial cells (HUVEC, PromoCell, Heidelberg, Germany) were grown in Endothelial Cell Growth Medium 2 (EGM2, containing 2% fetal bovine serum (FBS) and growth factors; PromoCell). Cells were passaged at 80-90% confluence and seeded at passage 6 in 6-well plates at a density of 15,625 cells/cm^2. After 2 days, cells reached 90% confluence, and EGM2 was replaced with 1 mL Endothelial Cell Basal Media 2 (EBM2, without growth factors; PromoCell) supplemented with 0.2% FBS for four hours. Ligands were diluted in EBM2/0.2% serum, media was aspirated from cells, and 1 mL of diluted ligands was added to each well for 45 minutes.

C2C12 mouse myoblast cells (ATCC, Manassas, VA USA) were maintained in Dulbecco's Modified Eagle's Medium – high glucose (DMEM, Gibco, Waltham, MA, USA) with 10% FBS (Gibco, ThermoFisher). Cells were passaged at 80% confluence and seeded in 6-well plates at a

density of 13,000 cells/cm^2 and allowed to grow to 80% confluency for two days. Media was replaced with 1 mL DMEM + 0.2% FBS for four hours, and cells stimulated with ligand as described for HUVEC.

4.3.3.2 Cell lysate preparation

To collect cell lysates, media was aspirated and cells were washed two times with one mL of cold PBS (Corning). Cells were then placed on ice and the final PBS wash was aspirated. 100 mL of RIPA+HALT protease/phosphatase inhibitor (ThermoFisher) was added to each well, cells were scraped, and lysates were transferred to microcentrifuge tube and stored at -80ºC.

4.3.3.3 RT-PCR

Total RNA was isolated from HUVEC using RNeasy Mini Kit (Qiagen) and cDNA made using Superscript IV (Invitrogen). PCR was performed using Phusion hot start II (Thermo Scientific) and gene-specific primers (Table 8).

Table 8 RT-PCR primers

Gene	Forward primer	Reverse primer
ACVRL1	TGACATCTGGGCCTTTGGCCT	AAAGCTGGGGTCATTGGGCACCA
BMP1	GTACGACTATGTGGAGGTCCGAGATG	GTCATCAGGCTTCTCATAGCCACAG
ENG	CAGCATTGTGGCATCCTTCG	CACCTTTTTCCGCTGTGGTG
FURIN	ACGGAAGCATGGGTTCCTCAACCT	ACCTGCTGTTCCAGCCACTGTA
TLL1	GCCGTAATGGATTTGTGCTACATG	GGTTTTGATTCTGCTTTCAATCGTCC
TLL2	GCCTATGACCACCTGGAAATGTATG	CGTAGGCTTCCATGTAGTCGTAG

4.3.4 Human BMP mRNA injections into zebrafish embryos

4.3.4.1 Plasmids and mRNA synthesis

Capped mRNAs encoding human BMPs were generated from NotI-digested pCS2+ expression plasmids using mMessage mMachine SP6 Transcription kit (ThermoFisher). The

human wild type *BMP9* plasmid was previously described [24]. *BMP9 C392S* (eliminates the Cys required for dimer formation so generates an obligate monomer), wild type *BMP10*, and *BMP10 C388S* (obligate monomer) were generated from synthetic DNA (Twist Biosciences, South San Francisco, CA USA) based on endogenous cDNA sequence. Wild type *BMP2* was generated from synthetic DNA (Twist Biosciences) based on codon-optimized cDNA sequence, whereas *BMP2 C360S* (obligate monomer) was generated by QuikChange site-directed mutagenesis (Agilent, Santa Clara, CA USA) using forward primer 5'-CAAGATCCCTAAGGCTA GCTGTGTGCCTACAG-3' and reverse primer 5'- CTGTAGGCACACAGCTAGCC TTAGGGATCTTG-3'. All plasmid inserts were verified by bidirectional Sanger sequencing.

4.3.4.2 mRNA injection and sample preparation

Two to four nL of a solution containing 200 pg of BMP mRNA and/or 200 pg EGFP mRNA was injected into wild type zebrafish embryos within 45 minutes of fertilization, at the one- to two-cell stage. At sphere stage (4 hpf), embryos were either fixed in 4% paraformaldehyde overnight at 4°C (for immunostaining) or manually dechorionated (for Western blotting). To generate lysates for Western blotting, the embryos were placed in 30% Danieau and the embryonic sheet of cells was removed from the yolk using sharp forceps, then cells were transferred in 2 μL 30% Danieau to RIPA buffer + HALT, 1:1 volume:volume. Lysates were combined within treatment (10-20 embryos) and stored up to a week at -80ºC.

4.3.5 SDS-PAGE and Western blotting

HUVEC and C2C12 lysates were thawed on ice and sonicated at amplitude 10 (Microson, Misonix, Farmingdale, NY, USA) for 15 seconds two times with the probe inside the sample tube.

Zebrafish embryo lysates were thawed on ice and sonicated at amplitude 10 for 30 seconds in an ice water bath, with the probe outside of the sample tube. Lysates were centrifuged at 18,506 rcf at 4ºC for 12 minutes, and supernatant was transferred to a new tube containing an appropriate volume of 4x Protein Sample Loading Buffer (LI-COR, Lincoln, NE, USA). For reducing gels, sample was added to 4x Protein Sample Loading Buffer with 10% beta mercaptoethanol and boiled at 95ºC for 5 minutes. Samples were immediately loaded on 10% Tris-Glycine SDS polyacrylamide gels, separated at 120 V for 90 minutes, and transferred to nitrocellulose at 30 V for 90 minutes. Blots were rinsed in diH_2O and dried for one hour. Membranes were rehydrated in diH_2O, blocked for one hour at RT in 3 mL Intercept (TBS) Blocking Buffer (LI-COR), then incubated in 3 mL of primary antibody as indicated in Table 9 . Blots were washed 4 x 5 minutes in TBS/0.1% tween, incubated in 3 mL of secondary antibody (Table 9), and imaged on an Odyssey CLx infrared imaging system (LI-COR). Band size and intensity were measured using Image Studio (LI-COR) and normalized to GAPDH (Table 9). Data are presented as molecular weight or as normalized intensity values, which were graphed and analyzed using GraphPad Prism.

Table 9 Western blotting conditions

Antibody	Host Species	Catalog numbers	Dilution	Incubation
BMP9 GFD	mouse	R&D MAB3209	1:500	o/n at 4ºC
BMP9 GFD	goat	R&D AF3209	1:2,000	o/n at 4ºC
BMP9 PD	goat	R&D AF3879	1:2,000	o/n at 4ºC
BMP10 GFD	mouse	R&D MAB2926	1:500	o/n at 4ºC
BMP10 PD	goat	R&D AF3956	1:2,000	o/n at 4ºC
GAPDH	mouse	Abcam AB8245	1:10,000 (Hs) 1:2,000 (Dr)	1 hr at RT (Hs) o/n at 4ºC (Dr)
pSMAD1/5/9	rabbit	CST 13820S	1:1,000	o/n at 4ºC
IRDye 800CW Donkey anti-Rabbit IgG	donkey	LI-COR 926-32213	1:12,000	1 hr at RT
IRDye 680LT Goat anti-Mouse IgG	goat	LI-COR 926-68020	1:12,000	1 hr at RT
IRDye 800CW Donkey anti-Goat IgG	donkey	LI-COR 926-32214	1:12,000	1 hr at RT
IRDye 680LT Donkey anti-Mouse IgG	donkey	LI-COR 926-68022	1:12,000	1 hr at RT

4.4 Results

4.4.1 BMP9 and BMP10 are secreted as monomer/dimer mixtures

To better understand the predominant forms of circulating ALK1 ligands and to test their activity on endothelial cells, we produced recombinant full-length proproteins, prodomains, and GFDs in HEK293 cells. As expected, proteins in which EK or Xa sites replaced the primary furin cleavage site were secreted as unprocessed proteins, and, as previously reported for BMP9 and BMP10 [47, 148], as a mixture of monomer and dimer. Because the monomeric proteins can form noncovalent dimers, the monomer and dimer were difficult to separate by size exclusion chromatography (A. Hinck, personal communication; data not shown). Therefore, some of the full-length proteins used were monomer:dimer mixtures (Table 10). After cleavage with the appropriate enzyme (Table 10) *in vitro*, the prodomain, GFD, and GFM were purified to homogeneity. The furin-cleavable constructs were also secreted as monomer:dimer mixtures. These were partially processed prior to secretion; co-transfection of α-1PDX allowed production and purification of full-length, furin-cleavable proBMP monomers and dimers (A. Hinck, personal communication).

Table 10 Recombinant Alk1 ligands

Name	Description	% dimer	Use	Schematic
proBMP9-Xa	Uncleavable full-length proBMP9	50	ELISA standard negative control for cell stimulation	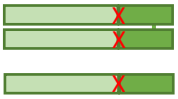
proBMP9-F	Furin-cleavable full-length proBMP9	33	Cell stimulation	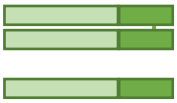
BMP9 GFD	BMP9 growth factor dimer	100	ELISA standard Positive control	
BMP9 GFM	BMP9 growth factor monomer	0	ELISA specificity	
proBMP10-EK(D)	Uncleavable full-length proBMP10 dimer	100	ELISA standard negative control for cell stimulation	
proBMP10-F(D)	Furin-cleavable full-length proBMP10 dimer	100	Cell stimulation	
proBMP10-F(M)	Furin-cleavable full-length proBMP10 monomer	0	ELISA specificity	
BMP10 GFD	BMP10 growth factor dimer	100	ELISA standard Positive control for cell stimulation	
BMP10 GFM	BMP10 growth factor monomer	0	ELISA specificity	
proBMP9/10-Xa	Uncleavable full-length proBMP9/10	~50%	ELISA standard	
BMP9/10 GFD	BMP9/10 growth factor heterodimer	100	ELISA standard	

4.4.2 ALK1 ligand ELISA development

Although it is clear that BMP9, BMP10, and BMP9/10 GFDs can similarly activate ALK1 [31], whether these ligands circulate as monomers or covalent dimers, or as full-length proproteins, processed PD:GFD complexes, or free GFDs, is unclear. To begin to answer these questions, I used sandwich ELISAs designed to detect furin processed and full-length forms of BMP9, BMP10, and BMP9/10. For each ELISA, I used a mouse monoclonal capture antibody against the GF domain and a goat polyclonal, biotinylated detection antibody against either the GF domain (assay designated as GF/GF) or the PD (assay designated as GF/PD) and the appropriate standard (Table 7). For ease of comparison, standard concentrations are expressed as GFD equivalents. Concentrations of full-length proteins that are monomer:dimer mixtures reflect total GF concentration. All assays generated sigmoidal standard curves with their cognate recombinant protein, but with differing sensitivity (Figure 13). The most sensitive assays were BMP9/10 GF/GF (detection limit 1 pg/mL) and BMP9 GF/GF (detection limit 10 pg/mL). Four assays had detection limits around 100 pg/mL (BMP10 GF/GF; BMP10/9 GF/GF; BMP9 GF/PD, BMP10 GF/PD) whereas two had detection limits around 1 ng/mL (BMP9/10 GF/PD; BMP10/9 GF/PD).

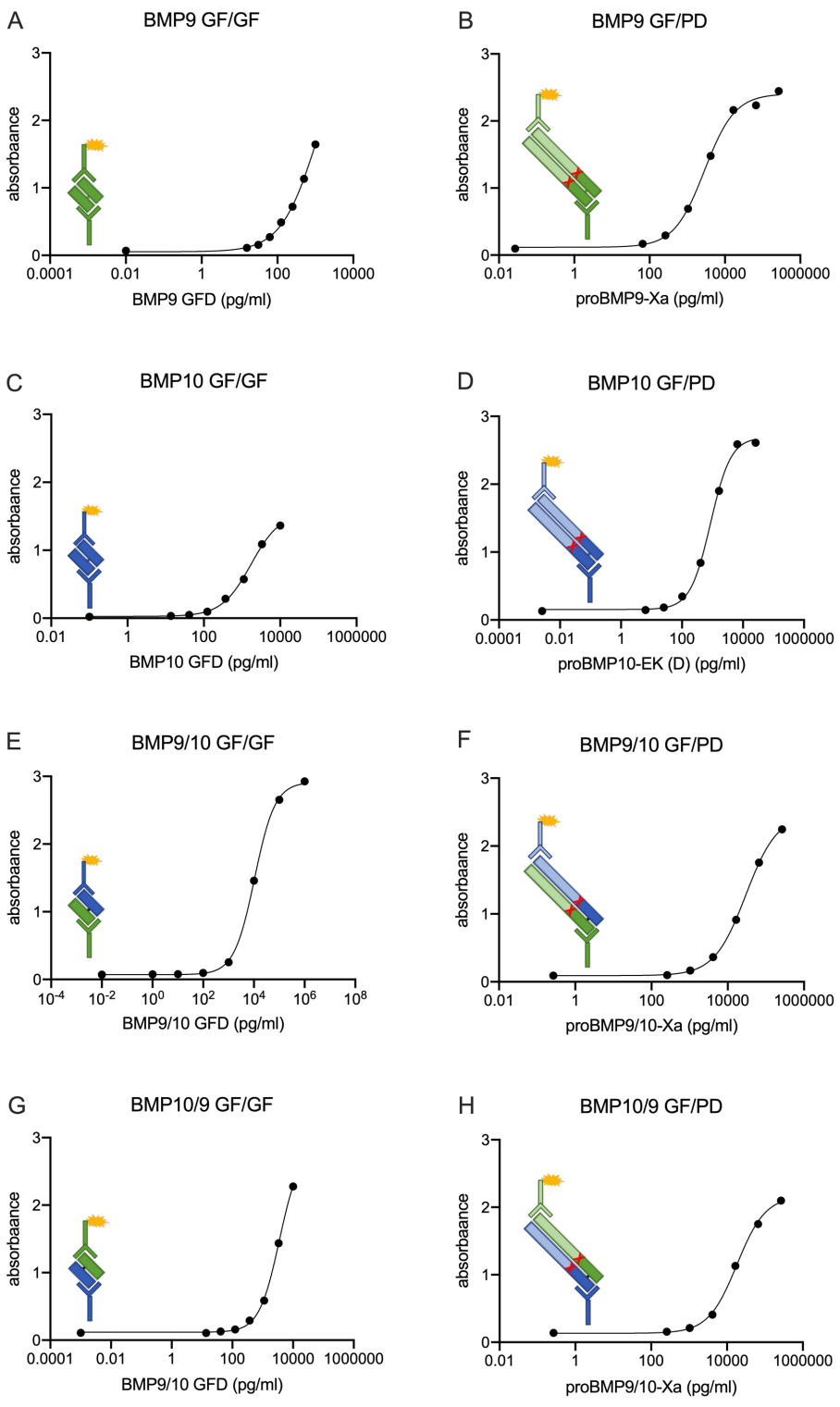

Figure 13 ALK1 ligand ELISA standard curves

Refer to Table 7 for ELISA details and Table 10 for key to schematized proteins. Y-axis: absorbance at 450 nm, corrected at 560 nm. X-axis: standard concentration $\log_{10}$ scale. Solid line is 4-PL non-linear regression.

4.4.3 BMP10 circulates as full-length proBMP10

To determine the concentrations and molecular identity of circulating ALK1 ligands, I applied the above described battery of ELISAs to pooled normal human adult plasma (N = 1 biological sample). Of the eight assays, four generated signal above background: BMP9 GF/GF; BMP10/9 GF/GF, BMP10 GF/ PD, and BMP9/10 GF/PD (Table 11). Others have reported similar results in human plasma [31, 45, 131]; however, we are the first to report signal with a BMP9/10 GF/PD assay. Strikingly, despite the relatively low sensitivity (1 ng/mL limit of detection), across 3 independent adult plasma samples, the BMP9/10 GF/PD ELISA gave the highest reading, at 29,860.1 ± 7,293.8 pg/mL. By contrast, the other assays detected ligand in the 100-2,500 pg/mL range, similar to previously reported concentrations of BMP9, BMP10, and BMP9/10 GFDs [31, 45, 131].

Next, to validate that lack of signal in some assays was not due to masking of protein epitopes in plasma, I performed spike and recovery assays in one pooled plasma sample. ELISAs are considered valid for use with plasma if the protein used to generate the standard curve is "recovered" or detected in plasma at 80 - 120% of the actual concentration, when "spiked" or added to plasma. All homodimer assays and the BMP9/10 GF/GF assay showed protein recovery within the acceptable range (Table 11). However, the BMP10/9 GF/GF and BMP9/10 GF/PD, which both returned signals in plasma, showed poor recovery, suggesting some masking of heterodimer in plasma and therefore underestimation of concentration. By contrast, the BMP10/9 GF/PD assay recovery was high, suggesting that something in plasma may increase availability of antibody binding sites to this protein.

Although previous reports suggested that a BMP10 GF/PD ELISA can detect processed BMP10 PD:GFD complexes [131], I was unable to detect reconstituted or cleaved complexes with

my BMP9 or BMP10 GF/PD assays (data not shown). Moreover, my GF/PD ELISAs gave signal with BMP9 or BMP10 GF capture antibodies paired with BMP10 PD detection antibody, but not with BMP9 PD detection antibody. Together, these results suggest that BMP9 circulates predominantly if not exclusively in a processed form, whereas BMP10 circulates predominantly if not exclusively in a full-length, unprocessed form. Moreover, because the BMP9/10 GF/PD assay detects strong signal in plasma even with relatively low recovery, these data suggest that a novel half-processed heterodimeric ligand (Figure 14), containing full-length proBMP10 dimerized with BMP9 GF, may be the predominant ligand in plasma, potentially accounting for 79-89% of total ALK1 ligand.

Table 11 ALK1 ligand ELISA characterization

ELISA					
Capture Ab	**Detection Ab**	**Standard/Spiked Recombinant Protein**	**Approximate Sensitivity**	**Detection in adult human plasma[a]**	**Recovery from adult human plasma[b]**
9 GF	9 GF	BMP9 GFD	10 pg/mL	138.61 ± 12.27 pg/mL	120.8 ± 26.9%
10 GF	10 GF	BMP10 GFD	100 pg/mL	undetected	94%
9 GF	10 GF	BMP9/10 GFD	1 pg/mL	undetected	99.20%
10 GF	9 GF	BMP9/10 GFD	100 pg/mL	1,053.7 ± 701.0 pg/mL	62.4 ± 10.3%
9 GF	9 PD	proBMP9-Xa	100 pg/mL	undetected	87-95%
10 GF	10 PD	proBMP10-EK	100 pg/mL	2,541.0± 3,0601.2 pg/mL	93.1± 61.0%
9 GF	10 PD	proBMP9/10-Xa	1 ng/mL	29,860.1 ± 7,293.8 pg/mL	106.0 ± 5.2%
10 GF	9 PD	proBMP9/10-Xa	1 ng/mL	undetected	230-445%

a: concentrations reflect mean ± SD of N = 3 samples. b: performed in duplicate N= 1 pooled plasma sample.

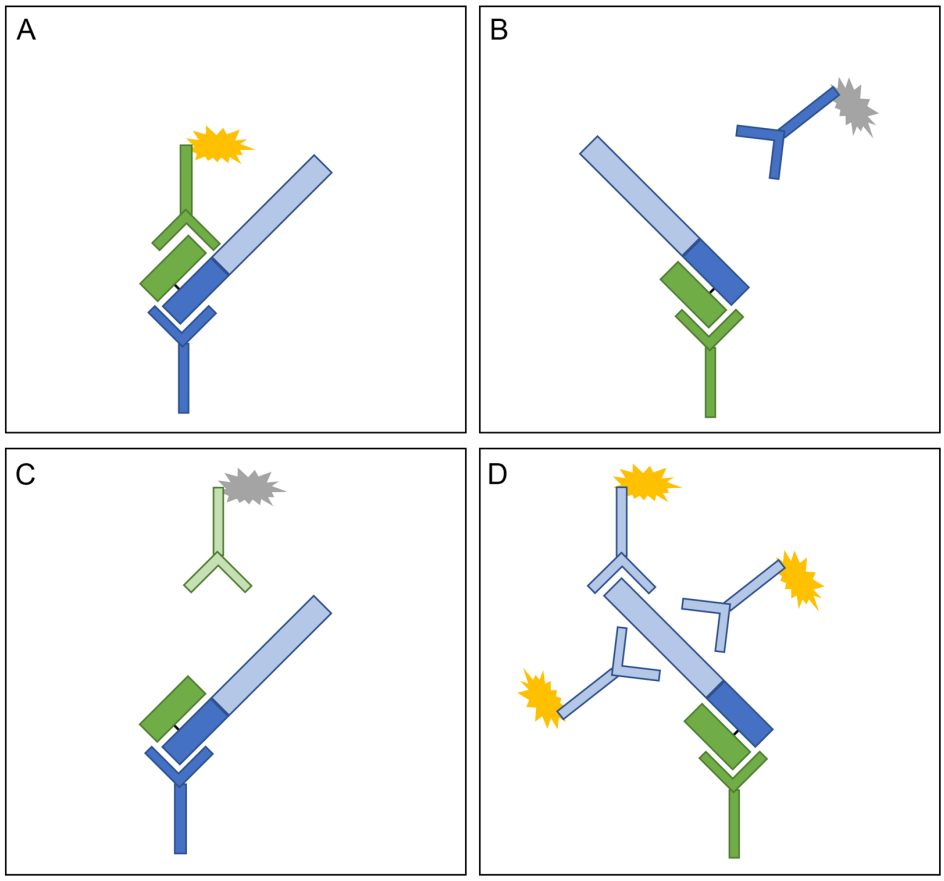

Figure 14 BMP9/10 may be circualting as "half-processed" proBMP10/BMP9 GF

A BMP10 GF capture, BMP9 GF detection gives a signal in plasma and would likely detect half-processed proBMP10/BMP9 GF. **B** BMP9 GF capture, BMP10 GF detection does not give a signal in plasma and would likely not be able to detect half-processed proBMP10/BMP9 GF. **C** BMP10 GF capture, BMP9 PD detection does not give a signal in plasma and would likely not be able to detect half-processed proBMP10/BMP9 GF. **D** BMP9 GF capture, BMP10 PD detection gives a signal in plasma and would likely be able to detect half-processed proBMP10/BMP9 GF.

4.4.4 Full-length proBMP10 dimer does not activate ALK1 in HUVEC in static culture

Because *bmp10* is the only necessary Alk1 ligand in zebrafish and because plasma from *Bmp9* null mice is entirely depleted of Alk1-activating on HUVEC [31], we hypothesized that proBMP10 detected in ELISAs is a latent circulating ligand that must be activated by prodomain cleavage at the endothelial cell surface. To test this hypothesis, we first assayed HUVEC for expression of furin and tolloid family metalloproteinases, which are implicated in BMP10 processing [44, 103]. Using RT-PCR, we detected furin, *BMP1*, *TLL1* and *TLL2* in HUVEC (Figure 15A), suggesting that they may have the ability to process proBMP10. Next, we stimulated HUVEC with 1 ng/mL GFD equivalents of BMP10 GFD, proBMP10-F(D), or proBMP10-EK(D), and assayed for pSMAD1/5/9 by Western blotting. As expected, this saturating concentration of BMP10 GFD resulted in a robust induction of pSMAD1/5/9 at 45 minutes and 4 hours, with a return to baseline expression by 24 hrs (Figure 15B,C). However, neither furin cleavable proBMP10-F(D) or uncleavable proBMP10-EK(D) induced pSMAD1/5/9 at any time point compared to unstimulated cells. These data suggest that proBMP10 homodimer is not inherently active on ECs.

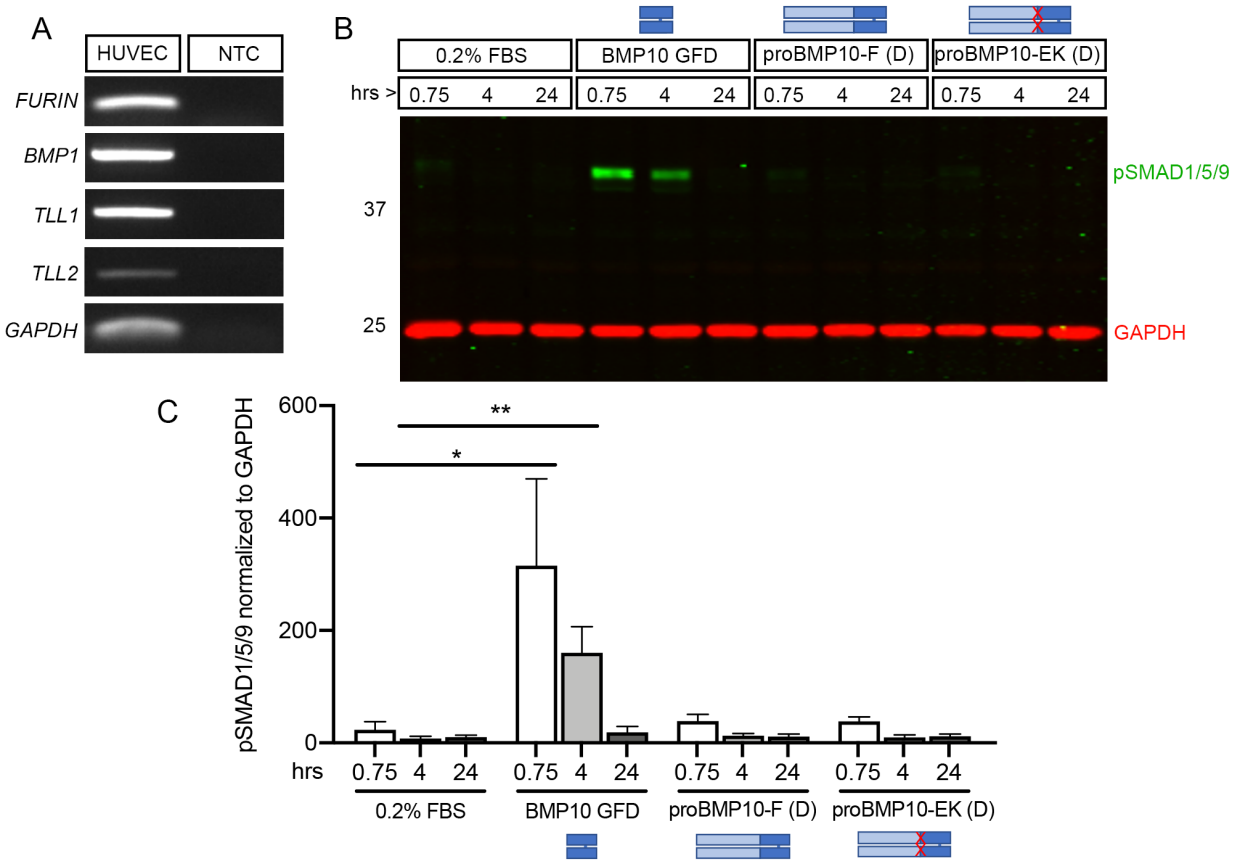

Figure 15 Full-length proBMP10 dimer is not active on HUVECs

A RT-PCR for *FURIN* (161 bp), *BMP1* (424 bp), *TLL1* (424 bp), *TLL2* (376 bp), and *GAPDH* (100 bp), on HUVEC cDNA (1:10 dilution) N = 1. NTC = no template control. **B** Representative western blot for pSMAD1/5/9 (green) and GAPDH (red); HUVEC lysates treated with 0.2% FBS or stimulated with 1 ng/mL BMP10 GFD, full-length proBMP10-F (D), or full-length proBMP10-EK (D) for indicated times. **C** Quantification of western blot, pSMAD1/5/9 normalized to GAPDH. Data analyzed by two-way ANOVA, followed by Tukey's multiple comparisons test; all treatments were compared for each time point. Significant comparisons are indicated in the graph, all other comparisons were not significant: 0.75 hrs: 0.2% FBS vs BMP10 GFD, P = 0.0203; 4 hrs: 0.2% FBS vs BMP10 GFD, P = 0.0017. N = 3 independent experiments each with two experimental replicates.

4.4.5 BMP10 obligate monomer is active in a zebrafish model

The fact that BMP10 is preferentially secreted as a full-length monomer in HEK293 cells may be an artefact of the overexpression system or may have physiological importance. To assess BMP10 processing and activity in a more physiological model, we injected synthetic human *BMP10* mRNA into early zebrafish embryos, which express *furina* [149], *bmp1*, and *tll1* [150]. Injected embryos developed normally until 4 hpf (sphere stage), then arrested development. Therefore, we analyzed embryo lysate by western blotting at 4 hpf using antibodies against pSMAD1/5/9, BMP10 PD, and BMP10 GF domain. We detected robust pSMAD1/5/9 induction at 4 hpf compared to *egfp*-injected controls (Figure 16A,B), demonstrating that human BMP10 can strongly induce signaling in zebrafish embryos and likely explaining the rapid developmental arrest. In these same samples, antibody against human BMP10 PD detected two prominent bands under nonreducing and reducing conditions: a 56 kDa band that is likely glycosylated full-length proBMP10 monomer (Figure 16C-F), and a 45 kDa band is likely glycosylated free PD. The minor 54 kDa band may be an alternatively cleaved or glycosylated proBMP10 monomer. Surprisingly, we could not detect BMP10 using an antibody that detects both BMP10 GFD and GFM under non-reducing conditions (data not shown). Given that PD processing and signaling occurred, we speculate that failed detection may reflect the low level of mature ligand produced and its rapid internalization and degradation after signaling. However, unambiguous identification of all BMP10 bands will require additional studies.

To further probe the ability of BMP10 monomers to signal, we injected a modified *BMP10* mRNA in which the cysteine required for interchain disulfide bond formation was mutated to serine (p.C388S), thereby generating an obligate monomer. The obligate monomer behaved very similarly to the wild type protein, with developmental arrest at 4 hpf accompanied by robust

induction of pSMAD1/5/9 compared to control-injected embryos, although induction was not statistically significant due to variability across experiments (Figure 16C-F). The bands detected by the BMP10 PD antibody were similar in size and relative intensity with injection of wild type and obligate monomer mRNA, suggesting no differences in processing. These data strongly support the hypothesis that BMP10 full-length monomer can generate an active ligand.

.

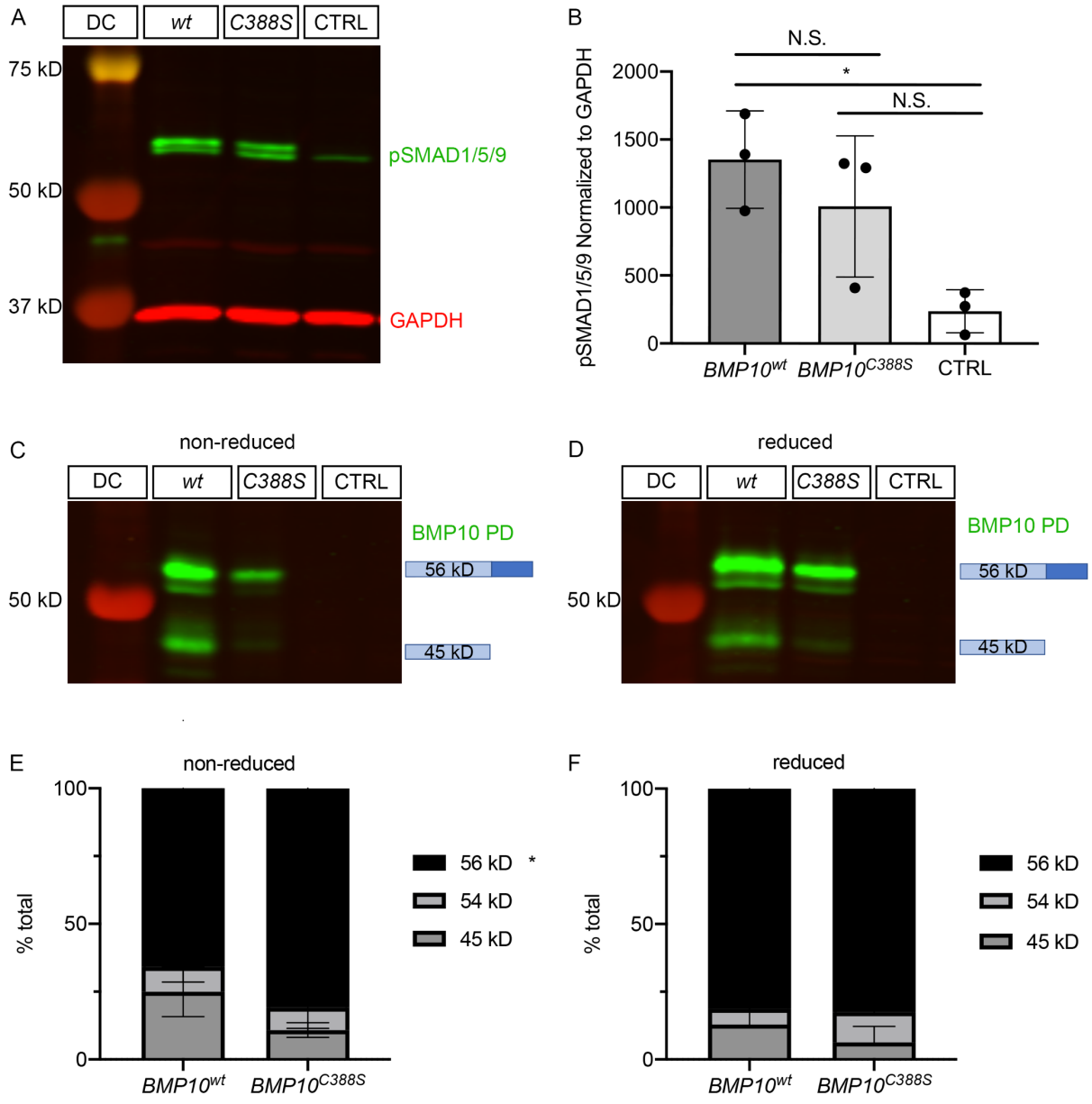

Figure 16 BMP10 obligate monomer is active in zebrafish embryos

Wild type zebrafish embryos were injected at the 2-cell stage with 200 pg *BMP10*^{wt}, 200 pg *BMP10*^{c388s}, or 200 pg control (CTRL: *mCherry* or *eGFP)* mRNA. **A** Reduced samples blotted for pSMAD1/5/9 and GAPDH and **B** quantification. Data analyzed by one-way ANOVA, followed by Tukey's multiple comparisons test. *BMP10* ^{WT} vs CTRL, P = 0.0333. **C** Non-reduced and **D** reduced samples, BMP10 PD western blot. Diagrams to the right of blot represent predicted molecular identity of bands. **E** Non-reduced and **F** reduced BMP10 PD western quantification. Data were analyzed by two-way ANOVA followed by Šídák's multiple comparisons test. Non-reduced 56 kD

BMP10^{wt} vs *BMP10*^{c388s}, P = 0.0438; all other comparisons between *BMP10*^{wt} and *BMP10*^{c388s} were not significant. N = 3 individual experiments, 10 embryos collected per condition. N.S. = not significant, DC = BioRad Dual Color protein ladder.

4.5 Discussion

Although BMP9 and BMP10 GFDs similarly bind to ALK1 and activate signaling, my work demonstrates a clear genetic requirement for *bmp10* in zebrafish. This finding fails to support the idea of ALK1 ligand redundancy and suggests that BMP10 must have some unique characteristic that underlies its strict requirement. Using a battery of sandwich ELISAs on normal human plasma, I found that signal was generated with detection antibodies against BMP9 GF but not BMP9 PD, and with antibodies against BMP10 PD but not BMP10 GF. Together, these data suggest that BMP10 may circulate in a predominantly unprocessed form, whereas BMP9 may circulate in a predominantly processed form. Accordingly, it is possible that the BMP10 PD plays a critical function in ligand stability, solubility, latency, and/or targeting to the endothelium.

Although it is clear that proBMP10 is in circulation, I cannot discern from ELISAs whether this protein exists as a monomer, a homodimer, and/or a heterodimer in complex with BMP9. The fact that full-length proBMP10 homodimer was not active on cultured endothelial cells may reflect the fact that this is not an endogenous circulating ligand. Alternatively, the lack of activity may reflect experimental artefact, as endothelial cells in static culture do not mimic environmental conditions of endothelial cells in a blood vessel. In circulation, endothelial cells experience mechanical forces including wall shear stress and stretch [151], and shear stress has been shown to enhance ALK1 signaling [82]. To determine whether shear stress is required for activation of proBMP10, microfluidic devices can be used to mimic flow conditions in the vasculature [152]. Endothelial cells in the microfluidic chamber can be stimulated with ligands under flow and static conditions, and assayed for pSMAD1/5/9. If flow is required for proBMP10 activity, I would expect signal in response to full-length proBMP10-F dimer but not full-length proBMP10-EK under shear stress but not static conditions. proBMP10 dimer should also be assayed in vivo.

Intravascular injection of recombinant human BMP10 GFD can at least partially rescue *bmp10/bmp10-like* zebrafish double mutants when injected at 30 hpf (data not shown), prior to the formation of the cranial AVM (Figure 4B). Accordingly, if proBMP10 dimer can be activated in circulation or at the endothelial cell surface, then I would expect full-length proBMP10-F but not proBMP10-EK to rescue *bmp10/bmp10-like* double mutants.

A second possibility is that full-length proBMP10 may exist in circulation as a monomer. This idea is supported by the fact that recombinant human BMP10 produced by HEK293 cells is largely monomeric, and human BMP10 produced after mRNA injection into zebrafish is exclusively monomeric. Furthermore, in our zebrafish experiments, we observe strong pSMAD1//5/9 stimulation, even when we express an obligate monomeric form of BMP10. And our BMP10 GF/PD ELISA can detect recombinant full-length proBMP10 monomer (data not shown). We need to evaluate the activity of proBMP10 monomers in HUVEC and in zebrafish as described for proBMP10 dimers. Notably, BMP9 GF monomers can signal in human pulmonary artery endothelial cells, albeit with somewhat lower efficacy than covalent dimers [148], and our preliminary data show that BMP10 GF monomers can also signal on HUVEC (A. Anbalagan and S. Morosky, data not shown).

Finally, my ELISAs strongly suggest the presence of half-processed proBMP10/BMP9 GF, which may account for most, if not all circulating ALK1 ligand. That is, it is possible that all assays that generated a signal in plasma detect proBMP10/BMP9 GF, but with different efficacies. Further experiments using recombinant half-processed proBMP10/BMP9 GF in these ELISAs will help to clarify this hypothesis. It is also necessary to test the activity of this recombinant protein in cell culture and zebrafish assays. We speculate that a half-processed dimer may be more

accessible to furin and BMP1/tolloid enzymes that are required to cleave the BMP10 PD to allow signaling.

Ultimately, it will be necessary to unambiguously define circulating ALK1 ligands using affinity chromatography using ALK1-Fc, ENG, and/or BMP10 PD followed by mass spectrometry. Endogenous ligands that are present in circulation and can activate ALK1 signaling in a controlled manner in vivo may be useful as lead candidates for development of targeted therapeutics for HHT patients.

.

5.0 In search of “hepatic factor”: lack of evidence for ALK1 ligands

The work in this chapter has been published in part in: Capasso, T. L., S. M. Trucco, M. Hindes, T. Schwartze, J. L. Bloch, J. Kreutzer, S. C. Cook, C. S. Hinck, D. Treggiari, B. Feingold, A. P. Hinck and B. L. Roman (2021). "In Search of "Hepatic Factor": Lack of Evidence for ALK1 Ligands BMP9 and BMP10." Am J Respir Crit Care Med **203**(2): 249-251. I performed the ELISAs and data analysis. Samples were collected by Sarah Trucco and prepared by Morgan Hindes.

5.1 Abstract

We explored the role of ALK1 signaling in development of pulmonary AVMs (PAVMs) in pediatric single-ventricle patients after the Glenn procedure, a surgery that rewires the circulation to relieve hemodynamic stress by allowing blood to flow passively to the lungs. The cause of these PAVMs has been hypothesized to be the exclusion of an “hepatic factor” from the pulmonary circulation. Given that BMP9 and BMP10 are produced by the liver and that PAVMs are strongly associated with HHT, I tested the hypothesis that 1) BMP9 and BMP10 concentrations are highest in hepatic effluent, and that 2) the Glenn lowers BMP9 and BMP10 concentrations in the lung vasculature. I found lower concentrations of ALK1 ligands in Glenn cases versus controls, suggesting that ALK1 signaling deficits may contribute to PAVMs in these patients However, I found no evidence for ligand gradient in plasma obtained from five different vessels, failing to support the identity of these ligands as ”hepatic factor.”

5.2 Introduction

Approximately 80% of PAVMs are associated with HHT, a genetic disorder caused primarily by mutations in BMP receptors endoglin and ALK1 [18]. This pathway is active in lung endothelium and ligands include BMP9 and BMP10 homodimers and BMP9/10 heterodimer [31, 153]. Both *BMP9* and *BMP10* are transcribed in hepatic stellate cells [31]. Given the strong relationship between PAVMs and HHT, the hepatic origins of *BMP9* and *BMP10*, and evidence of decreased plasma BMP9 in hepatopulmonary syndrome (HPS) [154], we hypothesized that ALK1 ligands may be the hepatic factor required for PAVM prevention. We expect that hepatic factor is either labile or actively removed from circulation on first pass through the systemic circulation, making it unavailable to the lung vasculature in Glenn cases. Accordingly, in normal circulation, we hypothesized that concentrations of ALK1 ligands would be higher in the right atrium (RA) and pulmonary artery (PA) compared to the aorta (Ao), superior vena cava (SVC) or infrahepatic inferior vena cava (IVC). To test this hypothesis, we applied a battery of ELISAs to plasma samples taken from these sites in Glenn cases and controls.

5.3 Materials and Methods

5.3.1 Plasma samples

This study was approved by the University of Pittsburgh Institutional Review Board. Participants undergoing clinically-indicated cardiac catheterization were recruited between September 2015 and February 2017 and provided informed child assent and/or parental consent. Patients with bidirectional Glenn, prior to Fontan, were compared to two-ventricle controls. Excluded diagnoses among controls included single ventricle physiology, unrepaired complex congenital heart disease, and large shunt lesions. Patients with liver disease, anemia (hemoglobin < 8 g/dL), cardiac surgery within 30 days, or transfusion within 48 hours were excluded from both cohorts. 1 mL blood was collected in K_2EDTA tubes from five sites: the RA, PA, Ao, SVC, and infrahepatic IVC.

5.3.2 ALK1 ligand ELISAs

ELISAs included BMP9 GF/GF; BMP10 GF/PD, BMP10 GF/BMP9 GF, and BMP9 GF/BMP10 PD, as previously described in Table 7. Plasma samples were coded so that identity (case or control, site of plasma collection) was unknown during assay. Samples from each patient were run on a single plate for each assay. A standard curve was run on each plate, and a control adult plasma sample was run to assess interplate and intraplate variation.

5.3.3 Statistical Analysis

Ligand concentrations were analyzed from five vascular sites in Prism. Column tables were generated for each ligand and the interpolated concentrations for RA, PA, Ao, SVC, and IVC were plotted in each column, and each patient was plotted in a separate row. Data were analyzed by repeated measures one-way ANOVA with Geisser-Greenhouse correction.

To determine the correlation between each ligand or between age and ligand, XY tables were generated in Prism. For ligand correlations, concentration of one ligand was plotted on the X axis and another on the Y axis, from the same patient. For age/ligand correlation, age was plotted on the X axis and BMP concentration was plotted on the Y axis. Data were analyzed using simple linear regression to obtain a line of best fit, R^2, and P value.

5.4 Results

5.4.1 Patient Diagnoses

Patient diagnoses for control subjects and Glenn cases are describe in Table 12.

Table 12 Patient diagnoses

	Controls	Cases
Total number of patients	38	9
Male	21 (55.26%)	7 (77.78%)
Female	17 (44.74%)	2 (22.22%)
Age (range)	5.8 years (4 months – 12.6 years)	2.9 years (22 months – 5.1 years)
Cardiac Diagnosis		
Small shunt lesions	21	
Repaired forms of congenital heart disease with two ventricle physiology	11	
Vascular stenosis	5	
Valvar obstructive lesions	2	
Hypertrophic cardiomyopathy	1	
Hypoplastic left heart syndrome		5
Pulmonary atresia with intact ventricular septum		2
Double outlet right ventricle with pulmonary atresia		1
Heterotaxy with right atrial isomerism		1

5.4.2 ALK1 ligands are maintained at a constant concentration in circulation

In control pediatric plasma, ELISAs detect the same ALK1 ligands as in adult plasma (see Chapter 4): BMP9 GFD, proBMP10, BMP9/10 GFD, and proBMP9/10 (Table 11). As in adult

plasma, the BMP9 GF capture/BMP10 PD detection assay reveals the highest signal and may represent a half-processed form of heterodimer consisting of full-length proBMP10 and BMP9 GFD.

To determine if any of these ALK1 ligands are actively removed from circulation as they pass through the lung vasculature, we compared plasma concentrations across five vascular sites in controls. However, we found no differences in plasma concentrations of any ALK1 ligand when comparing within-subject values across the RA, PA, Ao, SVC, and IVC (Figure 17A, B) . This result suggests that these ligands are neither particularly labile nor actively removed on first pass through the systemic or pulmonary circulation, failing to support the hypothesis that they represent the hepatic factor required to prevent PAVMs. Evaluation of plasma from Glenn cases similarly revealed no significant differences in within-subject ligand concentrations across sampling sites (Figure 17C, D).

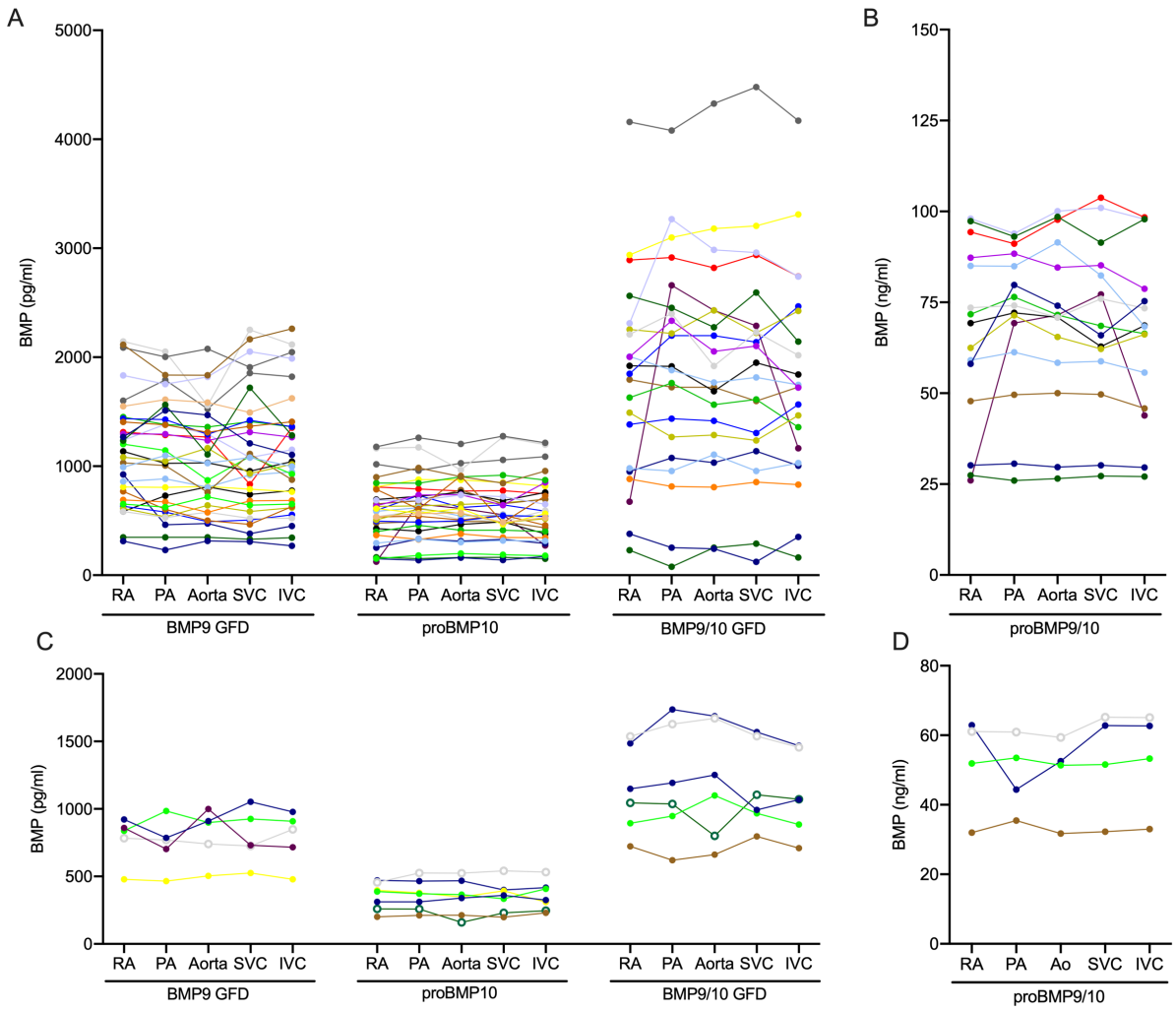

Figure 17 ALK1 ligand concentrations do not differ between pulmonary inflow and systemic venous circulation

Plasma from control subjects (**A, B**) and Glenn cases (**C, D**) was sampled from the right atrium (RA), pulmonary artery (PA), aorta (Ao), superior vena cava (SVC), and infrahepatic inferior vena cava (IVC) and ligands quantified by sandwich ELISA. All values are growth factor dimer equivalents. Lines connect samples from a single patient. There was no significant difference across sampled sites by repeated-measures one-way ANOVA: **A** BMP9 GFD, n = 31, P = 0.13; full-length proBMP10, n = 31, P = 0.17; BMP9/10 GFD, n = 21, P = 0.21; **B** full-length proBMP9/10, n = 15, P = 0.16; **C** BMP9 GFD, n = 5, P = 0.67; full-length proBMP10, n = 7, P = 0.8956; BMP9/10 GFD, n = 6, P = 0.46; and **D** full-length proBMP9/10, n = 4, P = 0.37. Open circle = cases with PAVM.

5.4.3 ALK1 ligands are significantly reduced in Glenn patients

After collapsing data across sites, comparison of grand means revealed significant decreases in plasma concentrations of all ligands in Glenn cases compared to controls (Figure 18A, B), and significance persisted after age-adjustment (multiple linear regression; BMP9 GFD, P = 0.04; full-length proBMP10, P = 0.0002; BMP9/10 GFD, P = 0.002; full-length proBMP9/10, P = 0.0077). Although our sample set is underpowered, we saw no correlation between ligand concentration and PAVMs (Figure 18A, B). This may suggest that ALK1 ligands may play a role in PAVMs in Glenn patients, though further studies are required to support this assertion.

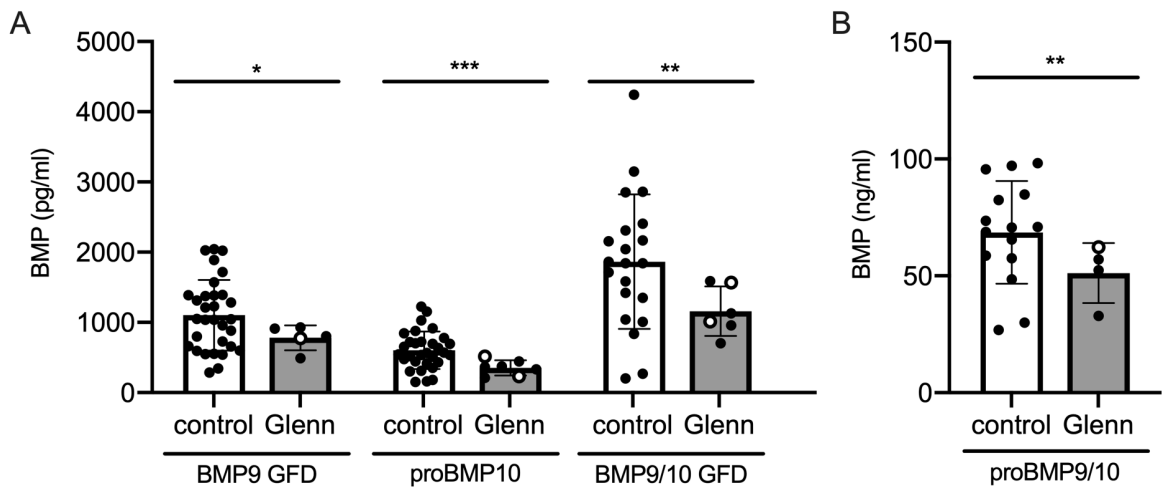

Figure 18 Plasma ligand concentrations are lower in Glenn cases compared with control subjects

A, **B** Within-patient data were averaged across all sampling sites (right atrium, pulmonary artery, aorta, superior vena cava, and inferior vena cava) for control subjects and Glenn cases and evaluated by age-adjusted multiple linear regression. Error bars represent SD. BMP9 GFD: control, n = 31; Glenn, n = 5; P = 0.0400. Full-length proBMP10: control, n = 31; Glenn, n = 7; P = 0.0002. BMP9/10 GFD: control, n = 21; Glenn, n = 6; P = 0.0024. Full-length proBMP9/10: control, n = 15; Glenn, n = 4; P = 0.0077. *P , 0.05; **P, 0.01; ***P , 0.001. Open circles indicate cases with pulmonary arteriovenous malformations.

5.4.4 ALK1 ligands are inversely correlated with age

In mouse, it has been reported that circulating BMP9 and BMP10 levels decrease with age [61]. To determine whether this inverse correlation also exists in human plasma, I plotted mean ligand concentrations (collapsed across all five sites) against age for each control subject and found that each ALK1 ligand is inversely correlated with age.

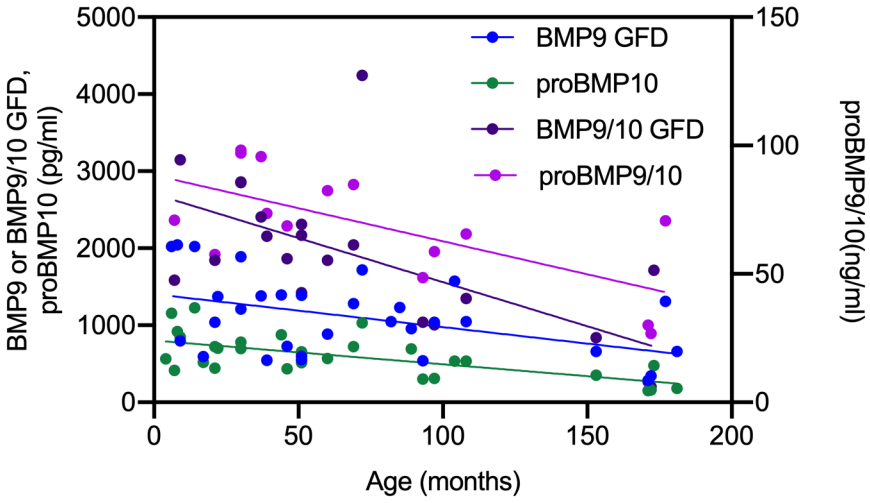

Figure 19 ALK1 ligands are inversely correlated with age

BMP9 GFD, full-length proBMP10, and BMP9/10 GFD means are plotted on the left Y-axis, full-length proBMP9/10 is plotted on the right Y-axis. Data were analyzed using simple linear regression: BMP9 GFD y = -4.277x + 1404, R^2 = 0.2062, P = 0.010, N = 39; full-length proBMP10 y = -3.091x + 803.1, R^2 = 0.4153, P < 0.0001, N = 40; BMP9/10 GFD y = -11.44x + 2704, R^2 = 0.4124, P = 0.0017, N = 40; full-length proBMP9/10 y = -0.2574x + 88.47, R^2 = 0.4533, P = 0.0059, N = 40.

5.4.5 All ALK1 ligand concentrations show correlation in plasma

Previous studies reported that BMP9 GFD and full-length proBMP10 are significantly correlated in human plasma [25, 131]. To validate and extend these findings, I compared the mean ligand concentrations (collapsed across all sites) within each control subject (Figure 20). My results confirmed the correlation between BMP9 GFD and proBMP10 (Figure 20A) and revealed a similar relationship between BMP9 GFD and BMP9/10 GFD or proBMP9/10 (Figure 19B,D), with r^2 values ranging from ~0.4-0.7. Strikingly, the correlations between proBMP10 and BMP9/10 GFD or proBMP9/10 (Figure 20C,E), and the correlation between proBMP9/10 and BMP9/10 GFD (Figure 20F) were remarkably high (r^2 ~0.9) . These results may suggest that BMP9 and BMP10 are co-regulated; however, this is unlikely to occur at the transcriptional level because *bmp9* expression is maintained in *bmp10* zebrafish mutants (Figure 4). An alternative interpretation is that these ALK1 ligand ELISAs may overlap in their ability to detect different forms of ALK1 ligands. For example, the BMP10 GF/PD, BMP9/10 GF, and BMP9 GF/BMP10 PD assays may all detect half-processed proBMP10/BMP9 GFD, with sensitivity highest with the BMP9 GF/BMP10 PD assay.

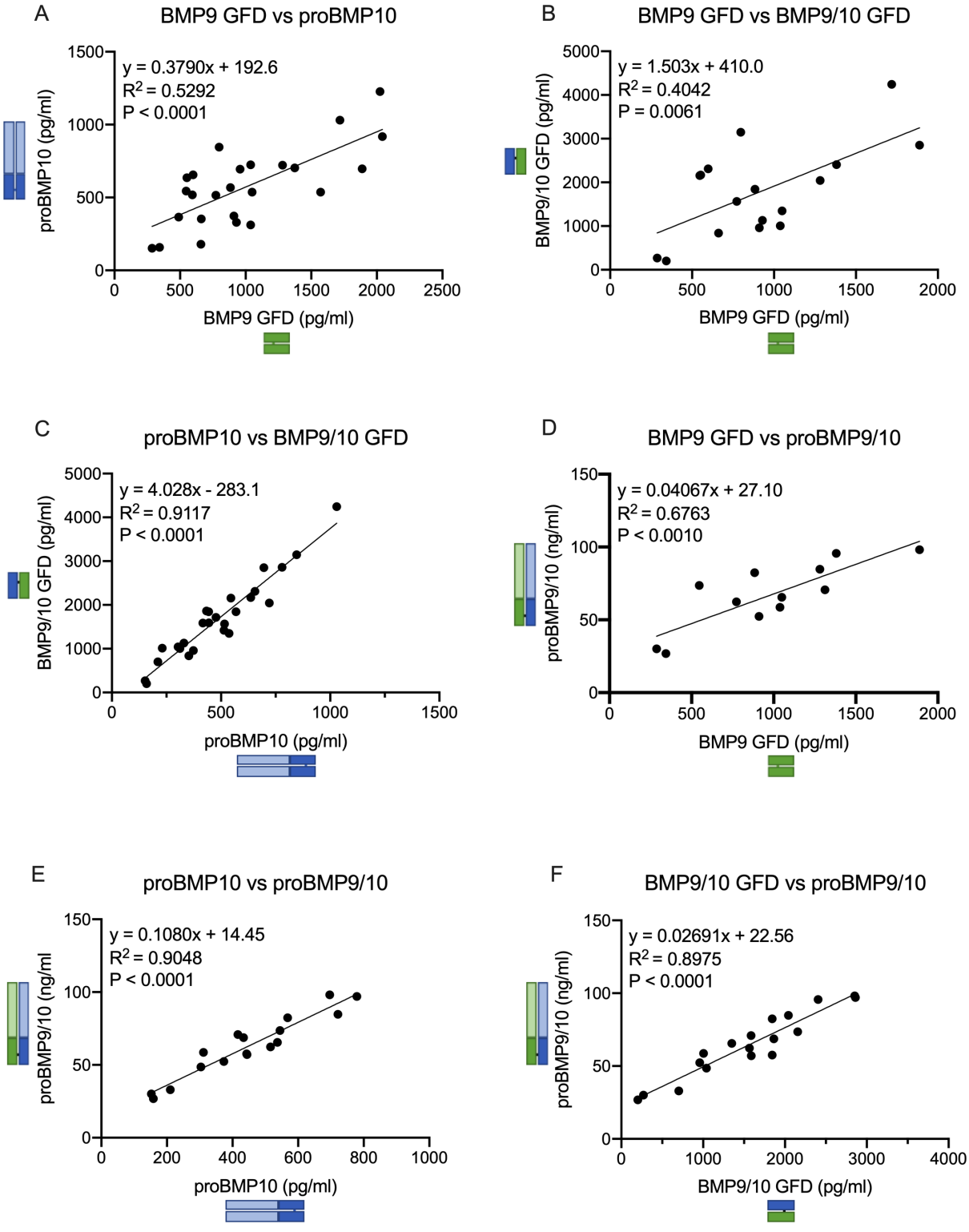

Figure 20 ALK1 ligands are signifcantly correlated

Within-patient data for each ligand concentration was averaged across the five vascular sites. Data for all four assays were plotted against each other. All comparisons show significant correlation. Line of best fit, R^2 value, and P value are indicated in the graphs. **A** full-length proBMP10 vs BMP9 GFD, N = 29. **B** BMP9/10 GFD vs BMP9 GFD, N = 18. **C** BMP9/10 GFD vs full-length proBMP10, N = 27. **D** full-length proBMP9/10 vs BMP9 GFD, N = 13. **E** full-length proBMP9/10 vs full-length proBMP10, N = 20. **F** BMP9/10 GFD vs full-length proBMP9/10, N = 20. FL = full-length.

5.5 Discussion

In control subjects, we found no within-subject differences in plasma concentrations of BMP9 GFD, full-length proBMP10, BMP9/10 GFD or full-length proBMP9/10 across different sampling sites, in agreement with a recent report regarding BMP9 GFD [155] and failing to support the idea that ALK1 ligands are the "hepatic factor" required to prevent PAVMs. However, it remains possible that enzymes required to cleave proproteins and activate ligands are unavailable in the Glenn circulation.

Although we found no ALK1 ligand gradient in any subject, we found that Glenn cases had significantly lower concentrations of all four ligands compared to controls. This finding was unexpected and the implications remain unclear due in part to a very small sample size. Measurement of these ligands in additional Glenn cases and in Fontan cases will be required to determine the biological significance of this finding with respect to the etiology of Glenn-associated PAVMs.

Finally, our ELISA results suggest that all detectable ALK1 ligands are significantly correlated with each other in plasma. While these results may suggest that ALK1 ligands are co-regulated, we favor the interpretation that these assays may have overlapping specificities, detecting the same ligand species with differing efficiency. Specifically, we suggest that at least three of the assays detect a half-processed proBMP10/BMP9 GF ligand that may be by far the predominant circulating ALK1 ligand. Synthesis of this recombinant protein will be necessary to assay this hypothetical ligand in each ELISA, and direct identification of this ligand in blood by affinity chromatography and mass spectrometry will be required to validate this assertion.

Cite: Teresa L. Capasso, Sara M. Trucco, Morgan Hindes, Tristin Schwartze, Jamie L. Bloch, Jacqueline Kreutzer, Stephen C. Cook, Cynthia S. Hinck, Davide Treggiari , Brian Feingold , Andrew P. Hinck , and Beth L. Roman/2021/In Search of “Hepatic Factor”: Lack of Evidence for ALK1 Ligands BMP9 and BMP10/American Journal of Respiratory and Critical Care Medicine/203/249-251.

The American Journal of Respiratory and Critical Care Medicine is an official journal of the American Thoracic Society.

6.0 Conclusions and future directions

HHT is a vascular genetic disorder characterized by the development of AVMs. Though decreased ALK1 signaling has been identified as causal for disease in HHT patients, therapies that specifically target this pathway have not yet been developed. Enhancing ALK1 signaling through administration of ligand may be a targeted approach for HHT patients. In this work, we aimed to characterize the known ALK1 ligands, BMP9 and BMP10. Specifically, our goal was to determine their post-embryonic role in the vasculature and to identify their circulating molecular forms.

We found that although *bmp10* and *bmp10-like* are redundant embryonically, Bmp10 is the only required Alk1 ligand throughout life in the zebrafish: juvenile and adult *bmp10* mutants develop vascular abnormalities with associated high-out heart failure, despite continued expression of *bmp9* and *bmp10-like* in adulthood. In zebrafish, *bmp10* is transcribed in the heart and liver in endocardial cells and presumably hepatic stellate cells, respectively (Figure 4, [31, 66, 156]), whereas the duplicate paralog, *bmp10-like*, is transcribed in cardiomyocytes. Together with the genetic requirement for *bmp10*, this observation suggests that endocardial and/or stellate cell-derived ligand may play a key role in vascular maintenance. This hypothesis is supported by observations in mice, in which *Bmp10* is expressed in both cardiomyocytes and hepatic stellate cells, but conditional deletion in cardiomyocytes fails to generate a vascular phenotype [130].

Although *bmp10* is the only required Alk1 ligand in zebrafish, both BMP9 and BMP10 are found in human plasma. Based on ELISA data, one key difference has emerged that distinguishes circulating forms of BMP9 and BMP10: whereas BMP9 seems to circulate in a cleaved form, the BMP10 PD remains covalently attached to the GF domain. Yet, both have canonical furin cleavage sites, and both are expressed by hepatic stellate cells; as such, one might expect that both would

be secreted from these cells in cleaved form if furin is present, or in uncleaved form if furin is not present. However, some TGF-β family ligands, such as GDNF, are highly resistant to intracellular cleavage by furin and are secreted in unprocessed form. In such cases, cleavage may be dictated by prodomain sequence outside of the furin cleavage site, which may differentially traffic ligands through alternative pathways that do not allow interaction with intracellular furin [39]. We speculate that the BMP10 PD may traffic it along a route that is different from BMP9 and that does not intersect with furin trafficking.

Given the genetic requirement for *bmp10* and the detection of proBMP10 in human plasma, we hypothesized that proBMP10 may be an important circulating ALK1 ligand that requires activation at the endothelial cell surface. However, we found that proBMP10 homodimer fails to signal when applied to HUVECs. It is possible that failed signaling reflects the non-physiological environment of static cell culture. Though we found that HUVECs express mRNAs encoding FURIN, BMP1, TLL1, and TLL2, which may be necessary for the removal of BMP10 PD, the subcellular localization of these enzymes is unknown. Localization to the membrane or secretion into the extracellular space would be necessary for activation of externally-supplied BMP10. Moreover, these enzymes are zymogens, so mRNA expression in no way equates with activity [39]. It will be interesting to determine whether shear stress may activate and/or alter subcellular localization of these enzymes to allow proBMP10 processing and ALK1 signaling.

The fact that proBMP10 homodimer failed to signal in HUVECs may reflect the artificial environment in which this ligand was tested, as just discussed. However, ELISA results suggest that the majority of full-length proBMP10 in plasma forms a heterodimer with BMP9 GF to form "half-processed" proBMP10/BMP9 GF (Figure 21), an ALK1 ligand that has not been previously described. Because BMP10 is the only required ALK1 ligand in zebrafish, it is difficult to reconcile

with the fact that proBMP10/BMP9 GF may be the predominant circulating ligand. We can only speculate on why this form of the ligand predominates in blood. Perhaps proBMP10/BMP9 GF is more stable or soluble in blood than a fully cleaved ligand, and/or the BMP10 PD may help to target this ligand to the endothelial cell surface. Another possibility is that the free BMP9 GF half of the protein may allow for increased accessibility of the ligand to ENG or ALK1, or increase accessibility of the furin cleavage site in BMP10, facilitating post-secretory cleavage between the BMP10 PD and GF. While this ligand may form within stellate cells (Figure 21), it is also possible that it may form post-secretion from proBMP10 and BMP9 GF monomers. Future studies on half-processed proBMP10/BMP9 GF will focus on isolating this ligand from human plasma and assessing its activity in vitro, as described below.

Isolating proBMP10/BMP9 GF from plasma. Although the battery of ELISAs presented in this work has lent valuable insight into circulating forms of ALK1 ligands, their inability to fully distinguish monomers, dimers, and heterodimers prevents accurate interpretation. To unambiguously define BMP10 PD-containing ligands in plasma, we plan to immunoprecipitate these ligands from plasma using biotinylated-BMP10 PD antibody (R&D; BAF3956) conjugated to streptavidin coated magnetic beads. Since our ALK1 ligand ELISAs suggest that most circulating ligands contain at least one BMP10 PD, this antibody should precipitate a majority of circulating ligands. The captured ligands will then be analyzed by mass-spectrometry and N-terminal sequencing. If the half-processed ligand does exist in circulation, we expect to detect peptides corresponding to BMP10 GF, BMP10 PD and BMP9 GF, but not BMP9 PD, and to capture the N-terminal sequences corresponding to the BMP10 PD and the BMP9 GFD.

Assessing proBMP10/BMP9 GF activity in vitro. Recombinant half-processed proBMP10/BMP9 GF covalent heterodimer will be generated using Factor Xa-cleavable BMP9

and furin-cleavable BMP10, and ALK1 stimulating activity will be assessed in HUVECs as already described for proBMP10 dimer (Figure 15). In TGF-β signaling, although receptor complexes are generally thought to be heterotetrameric, one type I and one type II receptor is minimally required for signaling [157], whereas in BMP signaling, one type I and two type II receptors are minimally required for signaling [158-160]. Since the PD and the type II receptor have overlapping binding sites, we expect that release of BMP10 PD via furin cleavage will be required for signaling to occur [18]. The BMP10 PD also contains a validated BMP1 site [44] that may be an important secondary cleavage site for the release of active BMP10 GF, as has been shown for other ligands such as GDF8 and GDF11 [39] (Figure 22). To determine whether membrane-associated or secreted furin and BMP1 cleavage of the BMP10 PD are required for ALK1 stimulation, we will use our HUVEC ALK1 signaling assay, in static conditions or in the presence of shear stress, to assess proBMP10/BMP9 GF activity in the presence of furin or BMP1 inhibitors, and to evaluate activity of half-processed proBMP10/BMP9 GF variants in which the furin or BMP1 cleavage sites have been mutated. Together these experiments will be essential for determining whether half-processed proBMP10/BMP9 GF may be a good candidate for biopharmaceutical development for HHT.

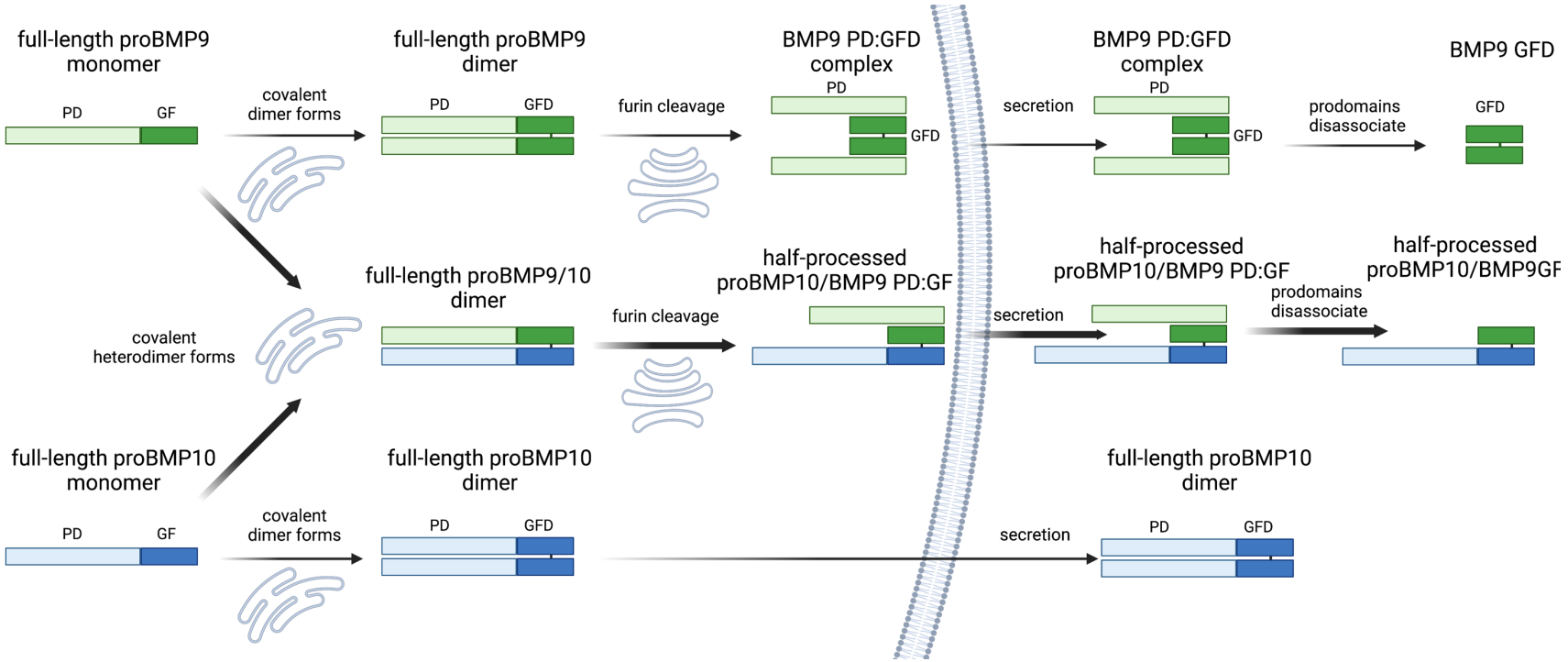

Figure 21 Hypothesis 1: full-length proBMP9 and full-length proBMP10 monomers preferentially heterodimerize in hepatic stellate cells

TOP: Minor BMP9 processing and secretion pathway. BMP9 forms a homodimer in the endoplasmic reticulum and follows canonical BMP processing and secretion from hepatic stellate cells. **MIDDLE:** Major processing and secretion pathway for BMP9 and BMP10. Full-length proBMP9 and full-length proBMP10 monomers preferentially heterodimerize in the endoplasmic reticulum, BMP9 is cleaved by furin in the golgi and half-processed proBMP10/BMP9 PD:GF is secreted as the predominant circulating ALK1 ligand. **BOTTOM:** minor BMP10 processing and secretion pathway. BMP10 forms a homodimer in the endoplasmic reticulum.

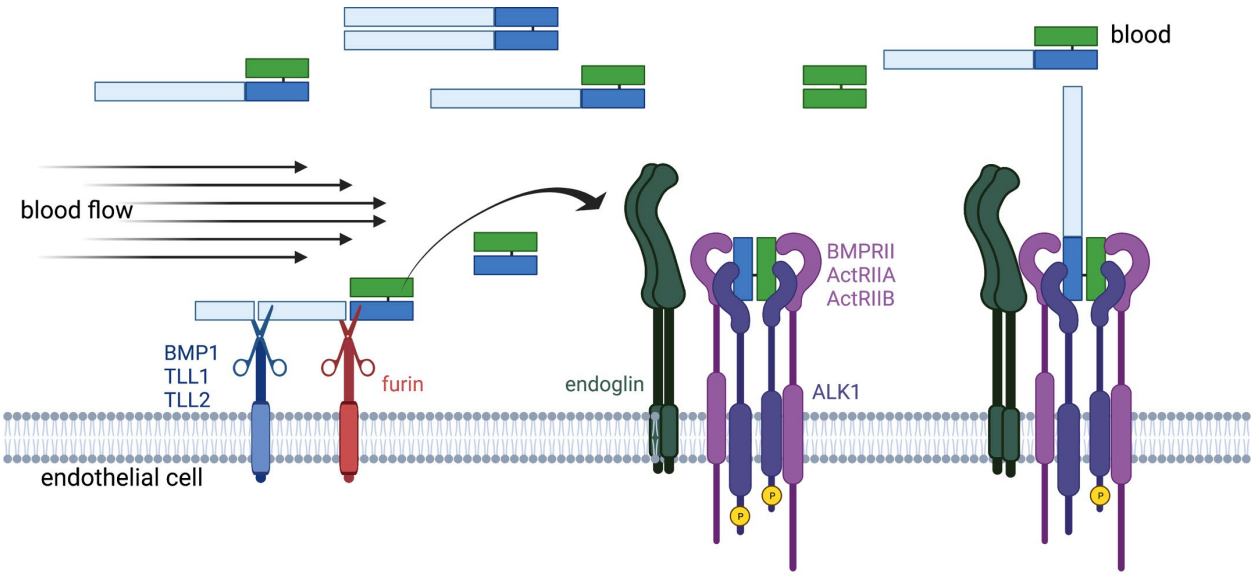

Figure 22 Hypothesis 2: full-length proBMP10 is cleaved at the endothelial cell surface

Hypothesis 2: Circulating half-processed proBMP10/BMP9 GF may require activation by both furin and metalloproteinases (BMP1, TLL1, or TLL2) at the endothelial cell surface. This would allow for release of the BMP9/10 GF heterodimer to signal through ALK1. Alternatively, the BMP9 half of half-processed proBMP10/BMP9 GF may allow receptor binding and removal of the BMP10 PD may not be required for ALK1 stimulation. Created with BioRender.com

Bibliography

1. Larrivee, B., et al., *Guidance of vascular development: lessons from the nervous system.* Circ Res, 2009. **104**(4): p. 428-41.

2. Marcelo, K.L., L.C. Goldie, and K.K. Hirschi, *Regulation of endothelial cell differentiation and specification.* Circ Res, 2013. **112**(9): p. 1272-87.

3. Majesky, M.W., *Vascular Development.* Arterioscler Thromb Vasc Biol, 2018. **38**(3): p. e17-e24.

4. Potente, M. and T. Makinen, *Vascular heterogeneity and specialization in development and disease.* Nat Rev Mol Cell Biol, 2017. **18**(8): p. 477-494.

5. Gao, Y., *Architecture of the Blood Vessels*, in *Biology of Vascular Smooth Muscle: Vasoconstriction and Dilatation*. 2017, Springer Singapore: Singapore. p. 3-12.

6. Tucker, W.D., Y. Arora, and K. Mahajan, *Anatomy, Blood Vessels*, in *StatPearls*. 2021: Treasure Island (FL).

7. Lantz, K.E., et al., *Arteriovenous Malformations in the Setting of Osler-Weber-Rendu: What the Radiologist Needs to Know.* Curr Probl Diagn Radiol, 2021.

8. Guest, W. and T. Krings, *Brain Arteriovenous Malformations: The Role of Imaging in Treatment Planning and Monitoring Response.* Neuroimaging Clin N Am, 2021. **31**(2): p. 205-222.

9. Bofarid, S., et al., *Pulmonary Vascular Complications in Hereditary Hemorrhagic Telangiectasia and the Underlying Pathophysiology.* Int J Mol Sci, 2021. **22**(7).

10. Ginon, I., et al., *Hereditary hemorrhagic telangiectasia, liver vascular malformations and cardiac consequences.* Eur J Intern Med, 2013. **24**(3): p. e35-9.

11. Droege, F., et al., *Life expectancy and comorbidities in patients with hereditary hemorrhagic telangiectasia.* Vasc Med, 2018: p. 1358863X18767761.

12. Zarrabeitia, R., et al., *Quality of life in patients with hereditary haemorrhagic telangiectasia (HHT).* Health Qual Life Outcomes, 2017. **15**(1): p. 19.

13. de Gussem, E.M., et al., *Life expextancy of parents with Hereditary Haemorrhagic Telangiectasia.* Orphanet J Rare Dis, 2016. **11**: p. 46.

14. Faughnan, M.E., et al., *International guidelines for the diagnosis and management of hereditary haemorrhagic telangiectasia.* J Med Genet, 2011. **48**(2): p. 73-87.

15. Halderman, A.A., et al., *Bevacizumab for Epistaxis in Hereditary Hemorrhagic Telangiectasia: An Evidence-based Review.* Am J Rhinol Allergy, 2018: p. 1945892418768588.

16. Mitchell, A., et al., *Bevacizumab reverses need for liver transplantation in hereditary hemorrhagic telangiectasia.* Liver Transpl, 2008. **14**(2): p. 210-3.

17. Dupuis-Girod, S., et al., *Bevacizumab in patients with hereditary hemorrhagic telangiectasia and severe hepatic vascular malformations and high cardiac output.* JAMA, 2012. **307**(9): p. 948-55.

18. Roman, B.L. and A.P. Hinck, *ALK1 signaling in development and disease: new paradigms.* Cell Mol Life Sci, 2017. **74**(24): p. 4539-4560.

19. Gallione, C.J., et al., *A combined syndrome of juvenile polyposis and hereditary haemorrhagic telangiectasia associated with mutations in MADH4 (SMAD4).* Lancet, 2004. **363**(9412): p. 852-9.

20. Johnson, D.W., et al., *Mutations in the activin receptor-like kinase 1 gene in hereditary haemorrhagic telangiectasia type 2.* Nature Genet., 1996. **13**(2): p. 189-95.

21. McAllister, K.A., et al., *Endoglin, a TGF-b binding protein of endothelial cells, is the gene for hereditary haemorrhagic telangiectasia type 1.* Nature Genet., 1994. **8**(4): p. 345-51.

22. Snellings, D.A., et al., *Somatic Mutations in Vascular Malformations of Hereditary Hemorrhagic Telangiectasia Result in Bi-allelic Loss of ENG or ACVRL1.* Am J Hum Genet, 2019. **105**(5): p. 894-906.

23. McDonald, J., et al., *Hereditary hemorrhagic telangiectasia: genetics and molecular diagnostics in a new era.* Front Genet, 2015. **6**: p. 1.

24. Wooderchak-Donahue, W.L., et al., *BMP9 mutations cause a vascular-anomaly syndrome with phenotypic overlap with hereditary hemorrhagic telangiectasia.* Am J Hum Genet, 2013. **93**(3): p. 530-7.

25. Hodgson, J., et al., *Homozygous GDF2 nonsense mutations result in a loss of circulating BMP9 and BMP10 and are associated with either PAH or an "HHT-like" syndrome in children.* Mol Genet Genomic Med, 2021: p. e1685.

26. Bayrak-Toydemir, P., et al., *Genotype-phenotype correlation in hereditary hemorrhagic telangiectasia: mutations and manifestations.* Am J Med Genet A, 2006. **140**(5): p. 463-70.

27. Letteboer, T.G., et al., *Genotype-phenotype relationship in hereditary haemorrhagic telangiectasia.* J Med Genet, 2006. **43**(4): p. 371-7.

28. Sabba, C., et al., *Hereditary hemorrhagic telangiectasia: clinical features in ENG and ALK1 mutation carriers.* J Thromb Haemost, 2007. **5**(6): p. 1149-57.

29. ten Dijke, P., et al., *Activin receptor-like kinases: a novel subclass of cell-surface receptors with predicted serine/threonine kinase activity.* Oncogene, 1993. **8**(10): p. 2879-87.

30. David, L., et al., *Identification of BMP9 and BMP10 as functional activators of the orphan activin receptor-like kinase 1 (ALK1) in endothelial cells.* Blood, 2007. **109**(5): p. 1953-61.

31. Tillet, E., et al., *A heterodimer formed by bone morphogenetic protein 9 (BMP9) and BMP10 provides most BMP biological activity in plasma.* J Biol Chem, 2018. **293**(28): p. 10963-10974.

32. Franzen, P., C.H. Heldin, and K. Miyazono, *The GS domain of the transforming growth factor-beta type I receptor is important in signal transduction.* Biochem Biophys Res Commun, 1995. **207**(2): p. 682-9.

33. Gougos, A. and M. Letarte, *Primary structure of endoglin, an RGD-containing glycoprotein of human endothelial cells.* J Biol Chem, 1990. **265**(15): p. 8361-4.

34. Castonguay, R., et al., *Soluble endoglin specifically binds bone morphogenetic proteins 9 and 10 via its orphan domain, inhibits blood vessel formation, and suppresses tumor growth.* J Biol Chem, 2011. **286**(34): p. 30034-46.

35. Alt, A., et al., *Structural and functional insights into endoglin ligand recognition and binding.* PLoS One, 2012. **7**(2): p. e29948.

36. Lebrin, F., et al., *Endoglin promotes endothelial cell proliferation and TGF-beta/ALK1 signal transduction.* EMBO J, 2004. **23**(20): p. 4018-28.

37. Mi, L.Z., et al., *Structure of bone morphogenetic protein 9 procomplex.* Proc Natl Acad Sci U S A, 2015. **112**(12): p. 3710-5.

38. Le, V.Q., et al., *Protection of the prodomain α1-helix correlates with latency in the transforming growth factor-β family.* bioRxiv, 2021: p. 2021.06.24.449816.

39. Constam, D.B., *Regulation of TGFbeta and related signals by precursor processing.* Semin Cell Dev Biol, 2014. **32**: p. 85-97.

40. Brown, M.A., et al., *Crystal structure of BMP-9 and functional interactions with pro-region and receptors.* J Biol Chem, 2005. **280**(26): p. 25111-8.

41. Mitchell, D., et al., *ALK1-Fc inhibits multiple mediators of angiogenesis and suppresses tumor growth.* Mol Cancer Ther, 2010. **9**(2): p. 379-88.

42. Townson, S.A., et al., *Specificity and structure of a high affinity activin receptor-like kinase 1 (ALK1) signaling complex.* J Biol Chem, 2012. **287**(33): p. 27313-25.

43. Scharpfenecker, M., et al., *BMP-9 signals via ALK1 and inhibits bFGF-induced endothelial cell proliferation and VEGF-stimulated angiogenesis.* J Cell Sci, 2007. **120**(Pt 6): p. 964-72.

44. Sengle, G., et al., *Prodomains of transforming growth factor beta (TGFbeta) superfamily members specify different functions: extracellular matrix interactions and growth factor bioavailability.* J Biol Chem, 2011. **286**(7): p. 5087-99.

45. Kienast, Y., et al., *Rapid Activation of Bone Morphogenic Protein 9 by Receptor-mediated Displacement of Pro-domains.* J Biol Chem, 2016. **291**(7): p. 3395-410.

46. Salmon, R.M., et al., *Molecular basis of ALK1-mediated signalling by BMP9/BMP10 and their prodomain-bound forms.* Nat Commun, 2020. **11**(1): p. 1621.

47. Jiang, H., et al., *The Prodomain-bound Form of Bone Morphogenetic Protein 10 Is Biologically Active on Endothelial Cells.* J Biol Chem, 2016. **291**(6): p. 2954-66.

48. Urness, L.D., L.K. Sorensen, and D.Y. Li, *Arteriovenous malformations in mice lacking activin receptor-like kinase-1.* Nat Genet, 2000. **26**(3): p. 328-31.

49. Corti, P., et al., *Interaction between alk1 and blood flow in the development of arteriovenous malformations.* Development, 2011. **138**(8): p. 1573-82.

50. Park, S.O., et al., *Real-time imaging of de novo arteriovenous malformation in a mouse model of hereditary hemorrhagic telangiectasia.* J Clin Invest, 2009. **119**(11): p. 3487-96.

51. Tual-Chalot, S., et al., *Endothelial depletion of Acvrl1 in mice leads to arteriovenous malformations associated with reduced endoglin expression.* PLoS One, 2014. **9**(6): p. e98646.

52. Park, H., et al., *Defective Flow-Migration Coupling Causes Arteriovenous Malformations in Hereditary Hemorrhagic Telangiectasia.* Circulation, 2021. **144**(10): p. 805-822.

53. Srinivasan, S., et al., *A mouse model for hereditary hemorrhagic telangiectasia (HHT) type 2.* Hum Mol Genet, 2003. **12**(5): p. 473-82.

54. Bourdeau, A., D.J. Dumont, and M. Letarte, *A murine model of hereditary hemorrhagic telangiectasia.* J Clin Invest, 1999. **104**(10): p. 1343-51.

55. Arthur, H.M., et al., *Endoglin, an ancillary TGFbeta receptor, is required for extraembryonic angiogenesis and plays a key role in heart development.* Dev Biol, 2000. **217**(1): p. 42-53.

56. Sugden, W.W., et al., *Endoglin controls blood vessel diameter through endothelial cell shape changes in response to haemodynamic cues.* Nat Cell Biol, 2017. **19**(6): p. 653-665.

57. Mahmoud, M., et al., *Pathogenesis of arteriovenous malformations in the absence of endoglin.* Circ Res, 2010. **106**(8): p. 1425-33.

58. Singh, E., et al., *Arterial endoglin does not protect against arteriovenous malformations.* Angiogenesis, 2020.

59. Garrido-Martin, E.M., et al., *Common and distinctive pathogenetic features of arteriovenous malformations in hereditary hemorrhagic telangiectasia 1 and hereditary hemorrhagic telangiectasia 2 animal models--brief report.* Arterioscler Thromb Vasc Biol, 2014. **34**(10): p. 2232-6.

60. Torsney, E., et al., *Mouse model for hereditary hemorrhagic telangiectasia has a generalized vascular abnormality.* Circulation, 2003. **107**(12): p. 1653-7.

61. Ricard, N., et al., *BMP9 and BMP10 are critical for postnatal retinal vascular remodeling.* Blood, 2012. **119**(25): p. 6162-6171.

62. Levet, S., et al., *Bone morphogenetic protein 9 (BMP9) controls lymphatic vessel maturation and valve formation.* Blood, 2013. **122**(4): p. 598-607.

63. Levet, S., et al., *BMP9 and BMP10 are necessary for proper closure of the ductus arteriosus.* Proc Natl Acad Sci U S A, 2015. **112**(25): p. E3207-15.

64. Laux, D.W., et al., *Circulating Bmp10 acts through endothelial Alk1 to mediate flow-dependent arterial quiescence.* Development, 2013. **140**(16): p. 3403-12.

65. Chen, H., et al., *Context-dependent signaling defines roles of BMP9 and BMP10 in embryonic and postnatal development.* Proc Natl Acad Sci U S A, 2013. **110**(29): p. 11887-92.

66. Chen, H., et al., *BMP10 is essential for maintaining cardiac growth during murine cardiogenesis.* Development, 2004. **131**(9): p. 2219-31.

67. Ruiz, S., et al., *A mouse model of hereditary hemorrhagic telangiectasia generated by transmammary-delivered immunoblocking of BMP9 and BMP10.* Sci Rep, 2016. **5**: p. 37366.

68. Roman, B.L., et al., *Disruption of acvrl1 increases endothelial cell number in zebrafish cranial vessels.* Development, 2002. **129**(12): p. 3009-19.

69. Krowka, M.J., et al., *Hepatopulmonary syndrome with progressive hypoxemia as an indication for liver transplantation: case reports and literature review.* Mayo Clin Proc, 1997. **72**(1): p. 44-53.

70. Newman, B., et al., *Congenital extrahepatic portosystemic shunt associated with heterotaxy and polysplenia.* Pediatr Radiol, 2010. **40**(7): p. 1222-30.

71. Cloutier, A., et al., *Abnormal distribution of pulmonary blood flow after the Glenn shunt or Fontan procedure: risk of development of arteriovenous fistulae.* Circulation, 1985. **72**(3): p. 471-9.

72. Vettukattil, J.J., et al., *Intrapulmonary arteriovenous shunting may be a universal phenomenon in patients with the superior cavopulmonary anastomosis: a radionuclide study.* Heart, 2000. **83**(4): p. 425-8.

73. Srivastava, D., et al., *Hepatic venous blood and the development of pulmonary arteriovenous malformations in congenital heart disease.* Circulation, 1995. **92**(5): p. 1217-22.

74. Shah, M.J., et al., *Pulmonary AV malformations after superior cavopulmonary connection: resolution after inclusion of hepatic veins in the pulmonary circulation.* Ann Thorac Surg, 1997. **63**(4): p. 960-3.

75. Long, L., et al., *Selective enhancement of endothelial BMPR-II with BMP9 reverses pulmonary arterial hypertension.* Nat Med, 2015. **21**(7): p. 777-85.

76. Miller, A.F., et al., *Bone morphogenetic protein-9. An autocrine/paracrine cytokine in the liver.* J Biol Chem, 2000. **275**(24): p. 17937-45.

77. Bidart, M., et al., *BMP9 is produced by hepatocytes and circulates mainly in an active mature form complexed to its prodomain.* Cell Mol Life Sci, 2012. **69**(2): p. 313-24.

78. Breitkopf-Heinlein, K., et al., *BMP-9 interferes with liver regeneration and promotes liver fibrosis.* Gut, 2017. **66**(5): p. 939-954.

79. Neuhaus, H., V. Rosen, and R.S. Thies, *Heart specific expression of mouse BMP-10 a novel member of the TGF-beta superfamily.* Mech Dev, 1999. **80**(2): p. 181-4.

80. van Baardewijk, L.J., et al., *Circulating bone morphogenetic protein levels and delayed fracture healing.* Int Orthop, 2013. **37**(3): p. 523-7.

81. Ola, R., et al., *PI3 kinase inhibition improves vascular malformations in mouse models of hereditary haemorrhagic telangiectasia.* Nat Commun, 2016. **7**: p. 13650.

82. Baeyens, N., et al., *Defective fluid shear stress mechanotransduction mediates hereditary hemorrhagic telangiectasia.* J Cell Biol, 2016. **214**(7): p. 807-16.

83. Westerfield, M., *The zebrafish book*. 3 ed. 1995, Eugene: University of Oregon Press.

84. Choi, J., et al., *FoxH1 negatively modulates flk1 gene expression and vascular formation in zebrafish.* Dev Biol, 2007. **304**(2): p. 735-44.

85. Whitesell, T.R., et al., *An alpha-smooth muscle actin (acta2/alphasma) zebrafish transgenic line marking vascular mural cells and visceral smooth muscle cells.* PLoS One, 2014. **9**(3): p. e90590.

86. Bussmann, J., et al., *Arteries provide essential guidance cues for lymphatic endothelial cells in the zebrafish trunk.* Development, 2010. **137**(16): p. 2653-7.

87. Gordon, K., et al., *Mutation in vascular endothelial growth factor-C, a ligand for vascular endothelial growth factor receptor-3, is associated with autosomal dominant milroy-like primary lymphedema.* Circ Res, 2013. **112**(6): p. 956-60.

88. Lin, Y.F., I. Swinburne, and D. Yelon, *Multiple influences of blood flow on cardiomyocyte hypertrophy in the embryonic zebrafish heart.* Dev Biol, 2012. **362**(2): p. 242-53.

89. Huang, C.J., et al., *Germ-line transmission of a myocardium-specific GFP transgene reveals critical regulatory elements in the cardiac myosin light chain 2 promoter of zebrafish.* Dev Dyn, 2003. **228**(1): p. 30-40.

90. Rottbauer, W., et al., *Reptin and pontin antagonistically regulate heart growth in zebrafish embryos.* Cell, 2002. **111**(5): p. 661-72.

91. Kettleborough, R.N., et al., *A systematic genome-wide analysis of zebrafish protein-coding gene function.* Nature, 2013. **496**(7446): p. 494-7.

92. Cade, L., et al., *Highly efficient generation of heritable zebrafish gene mutations using homo- and heterodimeric TALENs.* Nucleic Acids Res, 2012. **40**(16): p. 8001-10.

93. den Dunnen, J.T., et al., *HGVS Recommendations for the Description of Sequence Variants: 2016 Update.* Hum Mutat, 2016. **37**(6): p. 564-9.

94. Isogai, S., M. Horiguchi, and B.M. Weinstein, *The vascular anatomy of the developing zebrafish: an atlas of embryonic and early larval development.* Dev. Biol., 2001. **230**(2): p. 278-301.

95. Wang, L.W., et al., *Standardized echocardiographic assessment of cardiac function in normal adult zebrafish and heart disease models.* Dis Model Mech, 2017. **10**(1): p. 63-76.

96. Spanjaard, B., et al., *Simultaneous lineage tracing and cell-type identification using CRISPR-Cas9-induced genetic scars.* Nat Biotechnol, 2018. **36**(5): p. 469-473.

97. Stuart, T., et al., *Comprehensive Integration of Single-Cell Data.* Cell, 2019. **177**(7): p. 1888-1902 e21.

98. Butler, A., et al., *Integrating single-cell transcriptomic data across different conditions, technologies, and species.* Nat Biotechnol, 2018. **36**(5): p. 411-420.

99. Hafemeister, C. and R. Satija, *Normalization and variance stabilization of single-cell RNA-seq data using regularized negative binomial regression.* bioRxiv, 2019: p. 576827.

100. Becht, E., et al., *Dimensionality reduction for visualizing single-cell data using UMAP.* Nat Biotechnol, 2018.

101. Dowle, M., Srinivasan, A., *data.table:Extension of data.frame. R packaged version 1.12.2*. 2019.

102. Wickham, H., *ggplot2 Elegant Graphics for Data Analysis*. Second ed. useR!, ed. R. Gentleman, Hornik, K., Parmigiani, G. 2016, New York, USA: Springer Nature.

103. Susan-Resiga, D., et al., *Furin is the major processing enzyme of the cardiac-specific growth factor bone morphogenetic protein 10.* J Biol Chem, 2011. **286**(26): p. 22785-94.

104. Rochon, E.R., P.G. Menon, and B.L. Roman, *Alk1 controls arterial endothelial cell migration in lumenized vessels.* Development, 2016. **143**(14): p. 2593-602.

105. El-Brolosy, M.A., et al., *Genetic compensation triggered by mutant mRNA degradation.* Nature, 2019. **568**(7751): p. 193-197.

106. Zhang, W., et al., *Tbx20 transcription factor is a downstream mediator for bone morphogenetic protein-10 in regulating cardiac ventricular wall development and function.* J Biol Chem, 2011. **286**(42): p. 36820-9.

107. Huang, J., et al., *Myocardin regulates BMP10 expression and is required for heart development.* J Clin Invest, 2012. **122**(10): p. 3678-91.

108. Zhou, Y., et al., *Latent TGF-beta binding protein 3 identifies a second heart field in zebrafish.* Nature, 2011. **474**(7353): p. 645-8.

109. Zhang, W., et al., *Molecular mechanism of ventricular trabeculation/compaction and the pathogenesis of the left ventricular noncompaction cardiomyopathy (LVNC).* Am J Med Genet C Semin Med Genet, 2013. **163C**(3): p. 144-56.

110. Chen, H., et al., *Overexpression of bone morphogenetic protein 10 in myocardium disrupts cardiac postnatal hypertrophic growth.* J Biol Chem, 2006. **281**(37): p. 27481-91.

111. Peshkovsky, C., R. Totong, and D. Yelon, *Dependence of cardiac trabeculation on neuregulin signaling and blood flow in zebrafish.* Dev Dyn, 2011. **240**(2): p. 446-56.

112. Liu, J., et al., *A dual role for ErbB2 signaling in cardiac trabeculation.* Development, 2010. **137**(22): p. 3867-75.

113. Shovlin, C.L., et al., *Diagnostic criteria for hereditary hemorrhagic telangiectasia (Rendu-Osler-Weber syndrome).* Am J Med Genet, 2000. **91**(1): p. 66-7.

114. Bussmann, J., S.A. Wolfe, and A.F. Siekmann, *Arterial-venous network formation during brain vascularization involves hemodynamic regulation of chemokine signaling.* Development, 2011. **138**(9): p. 1717-26.

115. Hasan, S.S., et al., *Endothelial Notch signalling limits angiogenesis via control of artery formation.* Nat Cell Biol, 2017. **19**(8): p. 928-940.

116. Weijts, B., et al., *Blood flow-induced Notch activation and endothelial migration enable vascular remodeling in zebrafish embryos.* Nat Commun, 2018. **9**(1): p. 5314.

117. Harrison, M.R., et al., *Chemokine-guided angiogenesis directs coronary vasculature formation in zebrafish.* Dev Cell, 2015. **33**(4): p. 442-54.

118. Rasmussen, J.P., N.T. Vo, and A. Sagasti, *Fish Scales Dictate the Pattern of Adult Skin Innervation and Vascularization.* Dev Cell, 2018. **46**(3): p. 344-359 e4.

119. Xu, C., et al., *Arteries are formed by vein-derived endothelial tip cells.* Nat Commun, 2014. **5**: p. 5758.

120. Korzh, S., et al., *Requirement of vasculogenesis and blood circulation in late stages of liver growth in zebrafish.* BMC Dev Biol, 2008. **8**: p. 84.

121. Yao, Y., et al., *Fine structure, enzyme histochemistry, and immunohistochemistry of liver in zebrafish.* Anat Rec (Hoboken), 2012. **295**(4): p. 567-76.

122. Daly, J.J. and A.L. Schiller, *The liver in hereditary hemorrhagic telangiectasia (Osler-Weber-Rendu disease).* Am J Med, 1976. **60**(5): p. 723-6.

123. Sawabe, M., et al., *Three-dimensional organization of the hepatic microvasculature in hereditary hemorrhagic telangiectasia.* Arch Pathol Lab Med, 2001. **125**(9): p. 1219-23.

124. Garcia-Tsao, G., *Liver involvement in hereditary hemorrhagic telangiectasia (HHT).* J Hepatol, 2007. **46**(3): p. 499-507.

125. Niessen, K., et al., *ALK1 signaling regulates early postnatal lymphatic vessel development.* Blood, 2010. **115**(8): p. 1654-61.

126. Subileau, M., et al., *Bone Morphogenetic Protein 9 Regulates Early Lymphatic-Specified Endothelial Cell Expansion during Mouse Embryonic Stem Cell Differentiation.* Stem Cell Reports, 2019. **12**(1): p. 98-111.

127. Sergeeva, I.A. and V.M. Christoffels, *Regulation of expression of atrial and brain natriuretic peptide, biomarkers for heart development and disease.* Biochim Biophys Acta, 2013. **1832**(12): p. 2403-13.

128. Reddy, Y.N.V., et al., *High-Output Heart Failure: A 15-Year Experience.* J Am Coll Cardiol, 2016. **68**(5): p. 473-482.

129. Bouvard, C., et al., *Different cardiovascular and pulmonary phenotypes for single- and double-knock-out mice deficient in BMP9 and BMP10.* Cardiovasc Res, 2021.

130. Wang, L., et al., *BMP9 and BMP10 Act Directly on Vascular Smooth Muscle Cells for Generation and Maintenance of the Contractile State.* Circulation, 2021. **143**(14): p. 1394-1410.

131. Hodgson, J., et al., *Characterization of GDF2 Mutations and Levels of BMP9 and BMP10 in Pulmonary Arterial Hypertension.* Am J Respir Crit Care Med, 2020. **201**(5): p. 575-585.

132. Wang, X.J., et al., *Germline BMP9 mutation causes idiopathic pulmonary arterial hypertension.* Eur Respir J, 2019. **53**(3).

133. Eyries, M., et al., *Widening the landscape of heritable pulmonary hypertension mutations in paediatric and adult cases.* Eur Respir J, 2019. **53**(3).

134. Balachandar, S., et al., *Identification and validation of a novel pathogenic variant in GDF2 (BMP9) responsible for hereditary hemorrhagic telangiectasia and pulmonary arteriovenous malformations.* Am J Med Genet A, 2021.

135. Lek, M., et al., *Analysis of protein-coding genetic variation in 60,706 humans.* Nature, 2016. **536**(7616): p. 285-91.

136. Kang, Q., et al., *Characterization of the distinct orthotopic bone-forming activity of 14 BMPs using recombinant adenovirus-mediated gene delivery.* Gene Ther, 2004. **11**(17): p. 1312-20.

137. Snellings, D.A., et al., *Somatic Mutations in Vascular Malformations of Hereditary Hemorrhagic Telangiectasia Result in Bi-allelic Loss of ENG or ACVRL1.* Am J Hum Genet, 2019.

138. Little, S.C. and M.C. Mullins, *Bone morphogenetic protein heterodimers assemble heteromeric type I receptor complexes to pattern the dorsoventral axis.* Nat Cell Biol, 2009. **11**(5): p. 637-43.

139. Montague, T.G. and A.F. Schier, *Vg1-Nodal heterodimers are the endogenous inducers of mesendoderm.* Elife, 2017. **6**.

140. Pashmforoush, M., et al., *Nkx2-5 pathways and congenital heart disease; loss of ventricular myocyte lineage specification leads to progressive cardiomyopathy and complete heart block.* Cell, 2004. **117**(3): p. 373-86.

141. Grego-Bessa, J., et al., *Notch signaling is essential for ventricular chamber development.* Dev Cell, 2007. **12**(3): p. 415-29.

142. Lee, J., et al., *4-Dimensional light-sheet microscopy to elucidate shear stress modulation of cardiac trabeculation.* J Clin Invest, 2016. **126**(5): p. 1679-90.

143. Morine, K.J., et al., *Conditional knockout of activin like kinase-1 (ALK-1) leads to heart failure without maladaptive remodeling.* Heart Vessels, 2017. **32**(5): p. 628-636.

144. Iyer, V.N., et al., *Liver Transplantation Trends and Outcomes for Hereditary Hemorrhagic Telangiectasia In the United States.* Transplantation, 2018.

145. Mehta, P.A. and S.W. Dubrey, *High output heart failure.* QJM, 2009. **102**(4): p. 235-41.

146. Dumortier, J., et al., *Recurrence of Hereditary Hemorrhagic Telangiectasia After Liver Transplantation: Clinical Implications and Physiopathological Insights.* Hepatology, 2019. **69**(5): p. 2232-2240.

147. Jean, F., et al., *alpha1-Antitrypsin Portland, a bioengineered serpin highly selective for furin: application as an antipathogenic agent.* Proc Natl Acad Sci U S A, 1998. **95**(13): p. 7293-8.

148. Wei, Z., et al., *Regulation of bone morphogenetic protein 9 (BMP9) by redox-dependent proteolysis.* J Biol Chem, 2014. **289**(45): p. 31150-9.

149. Tessadori, F., et al., *Nodal signaling range is regulated by proprotein convertase-mediated maturation.* Dev Cell, 2015. **32**(5): p. 631-9.

150. Jasuja, R., et al., *bmp1 and mini fin are functionally redundant in regulating formation of the zebrafish dorsoventral axis.* Mech Dev, 2006. **123**(7): p. 548-58.

151. Gordon, E., L. Schimmel, and M. Frye, *The Importance of Mechanical Forces for in vitro Endothelial Cell Biology.* Front Physiol, 2020. **11**: p. 684.

152. Sonmez, U.M., et al., *Endothelial cell polarization and orientation to flow in a novel microfluidic multimodal shear stress generator.* Lab Chip, 2020. **20**(23): p. 4373-4390.

153. Mahmoud, M., et al., *Endoglin and activin receptor-like-kinase 1 are co-expressed in the distal vessels of the lung: implications for two familial vascular dysplasias, HHT and PAH.* Lab Invest, 2009. **89**(1): p. 15-25.

154. Rochon, E.R., et al., *BMP 9/10 in Pulmonary Vascular Complications of Liver Disease.* Am J Respir Crit Care Med, 2020.

155. Shirali, A.S., et al., *Angiopoietin-2 predicts morbidity in adults with Fontan physiology.* Sci Rep, 2019. **9**(1): p. 18328.

156. Zhao, D., et al., *ALK1 signaling is required for the homeostasis of Kupffer cells and prevention of bacterial infection.* J Clin Invest, 2021.

157. Huang, T., et al., *TGF-beta signalling is mediated by two autonomously functioning TbetaRI:TbetaRII pairs.* EMBO J, 2011. **30**(7): p. 1263-76.

158. Knaus, P. and W. Sebald, *Cooperativity of binding epitopes and receptor chains in the BMP/TGFbeta superfamily.* Biol Chem, 2001. **382**(8): p. 1189-95.

159. Isaacs, M.J., et al., *Bone morphogenetic protein-2 and -6 heterodimer illustrates the nature of ligand-receptor assembly.* Mol Endocrinol, 2010. **24**(7): p. 1469-77.

160. Yadin, D., P. Knaus, and T.D. Mueller, *Structural insights into BMP receptors: Specificity, activation and inhibition.* Cytokine Growth Factor Rev, 2016. **27**: p. 13-34.